Nanoscale

REVIEW

View Article Online
View Journal | View Issue

Cite this: *Nanoscale*, 2016, **8**, 4799

Highly energetic compositions based on functionalized carbon nanomaterials

Qi-Long Yan,[a] Michael Gozin,*[a] Feng-Qi Zhao,[b] Adva Cohen[a] and Si-Ping Pang[c]

In recent years, research in the field of carbon nanomaterials (CNMs), such as fullerenes, expanded graphite (EG), carbon nanotubes (CNTs), graphene, and graphene oxide (GO), has been widely used in energy storage, electronics, catalysts, and biomaterials, as well as medical applications. Regarding energy storage, one of the most important research directions is the development of CNMs as carriers of energetic components by coating or encapsulation, thus forming safer advanced nanostructures with better performances. Moreover, some CNMs can also be functionalized to become energetic additives. This review article covers updated preparation methods for the aforementioned CNMs, with a more specific orientation towards the use of these nanomaterials in energetic compositions. The effects of these functionalized CNMs on thermal decomposition, ignition, combustion and the reactivity properties of energetic compositions are significant and are discussed in detail. It has been shown that the use of functionalized CNMs in energetic compositions greatly improves their combustion performances, thermal stability and sensitivity. In particular, functionalized fullerenes, CNTs and GO are the most appropriate candidate components in nanothermites, solid propellants and gas generators, due to their superior catalytic properties as well as facile preparation methods.

Received 8th November 2015,
Accepted 27th January 2016

DOI: 10.1039/c5nr07855e

www.rsc.org/nanoscale

[a]*Center for Nanoscience and Nanotechnology, Faculty of Exact Science, Tel Aviv University, Tel Aviv 69978, Israel. E-mail: cogozin@gmail.com, qilonyan@post.tau.ac.il; Tel: +972-3-640-5878*
[b]*Science and Technology on Combustion and Explosion Laboratory, Xi'an Modern Chemistry Research Institute, Xi'an 710065, China*
[c]*School of Materials Science & Engineering, Beijing Institute of Technology, Beijing 100081, China*

Introduction

Energetic materials (EMs) are a class of materials with a large amount of stored chemical energy, which can be rapidly released; typical subclasses of EMs include explosives, pyrotechnics and propellants. Gunpowder (GP), which was

Qi-Long Yan

Dr Qi-Long Yan is a Postdoctoral Fellow in the team of Prof. Michael Gozin at the School of Chemistry, Faculty of Exact Sciences, Tel Aviv University (Israel). He is working in the field of carbon nanomaterial-based energetic composites. He obtained his PhD in 2015 from the University of Pardubice (Czech Republic), focusing research on the preparation and thermal analysis of polymer-bonded energetic compositions. Prior to his PhD studies, he worked for 4 years as an Associate Researcher at the Xi'an Modern Chemistry Research Institute (China), dealing with the thermal analysis and combustion of composite energetic materials.

Michael Gozin

Prof. Michael Gozin is an Associate Professor at the School of Chemistry, Faculty of Exact Sciences, Tel Aviv University (Israel). He is working in the field of synthesis and characterization of organic materials and nanomaterials. He obtained his PhD from the Weizmann Institute of Science (Israel), working on the synthesis of organometallic complexes and the development of novel homogeneous catalytic systems. He also held positions at the PeproTech (NJ, USA) and Clinical Microsensors (CA, USA). He also worked as a Visiting Assistant Professor in Stanford University. He is currently a member of the Israeli Chemical Society.

invented in ancient China, is considered as the first EM in human history. It is a mixture of sulfur, charcoal, and potassium nitrate (saltpeter). Charcoal as a form of carbon together with sulfur is a fuel, while the saltpeter is an oxidizer.[1,2] Due to its ability to rapidly generate heat and gas, GP has been widely used as a firearm propellant and in pyrotechnics. As a primitive energetic composition, GP is no longer widely in use and has been replaced by more advanced energetic systems, both in civil and military applications, which are still undergoing fast development. During the past few decades, researchers have been seeking safer energetic materials that are highly energetic, insensitive, nontoxic, and environmentally friendly.[3] In newly developed propellants and explosives, carbon-rich materials are gradually being replaced by high-nitrogen materials (HNMs) with a higher energy content and a better oxygen balance.[4] However, these HNMs are in most cases not safe enough for practical applications. Recently, a variety of carbon nanomaterials (CNMs) have been developed as carriers of EMs, combining to form advanced structures with higher performances. Some of them, as coating or encapsulating materials, are also very effective in improving the safety of energetic systems.[5]

It is well known that solid carbon materials (SCMs) can be found in different forms of bulk phases (*e.g.* diamonds) as well as molecular forms (*e.g.* fullerenes).[6] In fact, CNMs have a unique place in nanoscience owing to their exceptional electrical, thermal, chemical and mechanical properties. They have found application in such diverse areas as composite materials, energy storage and conversion, sensors, drug delivery, field emission devices and nanoscale electronic components, due to their strong adsorption capacity, chemical stability, and high mechanical strength as well as easy modification.[7] Currently, several types of SCMs are used in the field of EMs, which can be divided into two groups. One group is nano-powdered carbon, such as carbon black (CB) and nanodiamond, where the latter can be used as a reducing agent in energetic compositions.[8] The other is CNMs with a rich pore structure and a large surface area, including fullerenes, expanded graphite (EG), carbon nanotubes (CNTs), graphene, and graphene oxide (GO). The application of these materials in the field of energetic compositions has been recently summarized.[9] To further expand the scope of their applications in EMs, nano-sized carbon materials with a large surface area can be functionalized with energetic groups or coupled with binders, energetic compounds, metal fuels or combustion catalysts to form novel advanced functional nanostructures with better properties that can be used in propellants, explosives and pyrotechnics.[10] In recent years, extensive research has been carried out on the preparation and application of carbon nanomaterials in EMs,[11] especially graphene, GO, and CNTs and their composites, as combustion catalysts or energetic components.[12,13] In addition, activated carbon fiber and graphite have also been investigated with respect to propellant manufacture and waste treatment. Relevant research topics include design, synthesis, characterization and properties of carbon-based nanomaterials; potential usage of nano-sized carbon materials in rocket propulsion; catalytic effect and mechanisms of carbon-based nano-sized catalysts on decomposition and combustion of energetic materials; and application and characterization of carbon nanomaterials in the purification of waste water in the explosive industry.[14]

In the past few decades, a large number of papers have been published regarding the preparation and applications of CNMs, based on which several review papers are available, mainly in Chinese literature.[8,12,15–18] Experimental and theoretical data on new carbon nanostructures using fullerenes and nanotubes as well as monolithic diamond-like nanoparticles, nanofibers and various nanocomposites as starting materials are summarized in a Russian journal.[15] Their atomic and

Feng-Qi Zhao

Prof. Feng-Qi Zhao is a Full Professor and the Head of one National Key Laboratory at the Xi'an Modern Chemistry Research Institute (China). He is working in the field of thermal analysis and combustion of energetic materials, including evaluation of nano-sized combustion catalysts. He obtained his PhD from the Nanjing University of Science and Technology (China), where his research topic was the synthesis of energetic materials. He serves as an Associate Editor of the Chinese Journal of Explosives and Propellants and as a Member of the Editorial Boards of the Chinese Journal of Energetic Materials and Acta Armamentarii.

Adva Cohen

Mrs Adva Cohen is a PhD in the team of Prof. Michael Gozin at the School of Chemistry, Faculty of Exact Sciences, Tel Aviv University (Israel). She is working in the field of carbon nanomaterial-based energetic composites. She obtained her MSc degree from the Hebrew University in Israel, where she did research in the field of laser-induced breakdown spectroscopy. Prior to her PhD studies, Mrs Cohen worked as a Research Associate in Analytical Chemistry in the field of chromatography. For her achievements, she won several awards and scholarships including Teva Best Student National Award.

electronic structures and the nature of their chemical bonds and their physicochemical properties are compared. The applications of fullerene materials in catalytic reactions, including hydrogen transfer and hydrosilylation, pyrolysis of alkanes, H_2–D_2 exchange, coupling and alkyl transfer reactions are reviewed.[16] Recent advances in the application of graphene-based catalysts in energetic materials are also introduced, revealing that they have a significant catalytic effect on the combustion of solid propellants.[17,18] Graphene-based EMs usually have larger energy release rates; moreover, the burning rate and mechanical properties, as well as the sensitivity of propellants can be improved using graphene or GO.[19] However, these review papers are not accessible for most Western researchers due to language barriers. Besides, many other papers reporting CNTs, EG and CB materials and their applications in the field of EMs have still not been reviewed and summarized. To make such a large amount of data on CNMs, especially that published in Chinese journals, available to all readers, this review aims to summarize preparation methods of CNM-based EMs as well as their effects on the performance and sensitivity of the corresponding energetic compositions.

Classification of carbon nanomaterials

Carbon is one of the most important natural elements and it has sp^3, sp^2, and sp hybridized orbitals. The anisotropic sp^2 in molecular carbon atoms may lead to anisotropy in some crystals of these materials (Table 1). Therefore, carbon materials have widely extended properties. In fact, more and more new carbon materials continue to be discovered and artificially prepared. There is no other element like carbon that can form such diverse and completely different substances as a single element, in terms of structures and properties, such as 3-D diamond crystal and graphite, 2-D graphite sheets, 1-D CNTs and 0-D fullerene molecules. It has been discovered that carbon materials are mostly superior in terms of their hardness, optical properties, heat resistance, radiation characteristics, chemical resistance, electrical insulation, electrical conductivity, and surface and interface properties to many other materials. Carbon materials can probably cover the characteristics of all the substances on the planet, such as "the hardest to the softest", "insulator to semiconductor to super conductor", "thermal insulator to thermal conductor" and "fully light-absorbing to completely transparent", so these materials have a wide range of applications, as listed in Table 2. In general, CNMs have attracted more and more attention in recent years due to the possibility of specific preparation of a wide range of variously-shaped nano-carbon crystals in the form of needles, tubes, spheres and many other morphologies.[20] For example, the three key conjugated CNMs are graphene, CNTs and fullerenes. These materials have very different morphologies with unique chemical properties but they still have much in common, especially in terms of basic building units (Fig. 1).

These CNMs can transform to each other under certain experimental conditions; hence, initial study on CNTs has origins in fullerene research. There are many types of fullerene derivatives (*e.g.* C_{20}, C_{32}, C_{60}, C_{70}, and C_{84}), where buckminsterfullerene (C_{60}) is a typical and well-known example.[21] Each fullerene molecule possesses the characteristic of being a pure carbon cage, each atom bonded to three others, as in graphite (Fig. 2).

Table 2 shows examples of various typical carbon materials. As mentioned in the Introduction, current CNMs, including fullerene, graphene, CNTs and other carbon materials, have many excellent physical and chemical properties, and some of them are widely used in the field of EMs. Unlike graphene, every fullerene has exactly 12 pentagonal faces with a different number of hexagonal faces (*e.g.*, C_{60} has 20). CNTs can be viewed as graphene sheets rolled into hollow tubes, which can be classified into single-walled, double-walled and multi-walled nanotubes. As a special cylindrical form of fullerene, CNTs were discovered more than 30 years before fullerenes but this discovery was not fully appreciated at that time. Recently, the production of CNTs exceeded several thousand tons per year, and these materials are used for applications in energy storage, automotive parts, boat hulls, sporting goods, filters, electronics, coatings, carriers of catalysts and electromagnetic shields.[22] CNT-related publications were more than triple during the past decade, while the rate of patent applications also dramatically increased. Although most of the CNM production output was of unorganized structures, organized CNT architectures such as "forests", yarns and regular sheets were manufactured in smaller volumes.[23] In addition to fullerenes and CNTs, other CNMs, including graphene and GO, are currently under intensive investigation.[24–28] In the following sections, newly developed preparation methods for several mentioned CNMs, together with functionalized EMs and energetic compositions based on these materials, are summarized in more detail.

Si-Ping Pang

Prof. Si-Ping Pang is a Full Professor at the Beijing Institute of Technology (BIT, China). He is working on the syntheses and characterization of highly energetic materials, guided by theoretical calculations. He obtained his PhD from the BIT, where his research was focused on the synthesis of HNIW. Since 2011, he has been the Vice Dean of the School of Material Sciences and Engineering at BIT and he also serves as a member of the Editorial Boards of the Chinese Journal of Energetic Materials and Acta Armamentarii. He is a member of the Chinese Chemical Society.

Table 1 Carbon compounds, carbon chemical bonds and phase formations

	Hybridization type			
Bond types	sp	sp^2	sp^3	Mixed
Coordination	2	3	4	Variable
Average C–C length (nm)	0.121	0.133 0.142	0.154	—
Binding energy	46 kJ mol^{-1}	35 kJ mol^{-1}	20 kJ mol^{-1}	—
Typical examples	Acetylene	Ethylene Benzene	Adamantane, cyclododecane $(CF)_n$, SiC, B_4C	—
Identified carbon phases	Carbene (hexagonal facets bulk crystal C60)	Graphite (in-plane) (a cubic, hexagonal)	Diamonds	C_{60}
Undetermined carbon phases	C_2 to C_{20} Carbon molecules	1-Graphite 3d-sp^2 bct-4 polystyrene	6H-Diamonds-BC-8	Carbophene Graphyenes

Table 2 The types of carbon materials

	Fullerenes 0-Dimensional	CNTs 1-Dimensional	Graphite 2-Dimensional	Diamond 3-Dimensional	Amorphous C Amorphous
Preparation methods	CVD, ablation, discharge	Discharge, DoH, fluoride, CVD and ablation	CVD, evaporation, ablation	High-pressure synthesis, CVD	CVD, PVD, sputtering, plasma
Morphology	Single crystal, amorphous	Fibers	FM, crystalline, DC	Crystalline	Amorphous, fiber
Characteristics	Semi-conductive, catalytic, FM, SC	Conductive, high strength, catalytic, high TC	Conductive, catalytic, intercalating	High hardness, high TC, HR, AR	High hardness, conductive, CR
Applications	ULM, nonlinear OM	SLM, USM, ERM, CC	Electronic, X-ray OM, CC	ULM, EEM, coating, CC	ULM, electronic, coating, CC

DoH, decomposition of hydrogen; MF, molecular fiber; DC, directional crystallization; FM, ferromagnetic; SC, superconductive; TC, thermal conductivity; HR, heat resistance; AR, abrasion resistance; CR, corrosion resistance; ULM, ultra-lubricating materials; OM, optical material; SLM, super lightweight material; USM, ultra-high strength material; PVD, Physical vapor deposition; CVD, chemical vapor deposition; ERM, energy raw materials; EEM, electricity–electronic materials; CC, catalyst carrier.

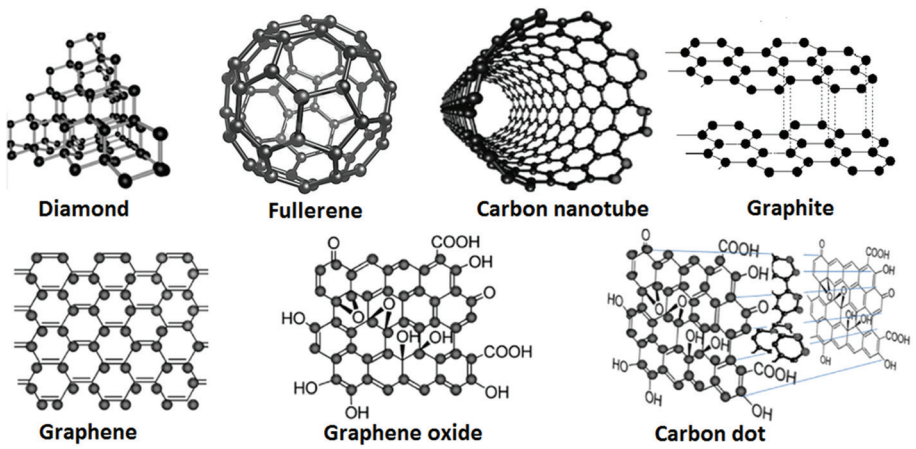

Fig. 1 Various forms of carbon nanomaterials.

CNM-based energetic nanomaterials

Energetic composites containing carbon black

Manufacturing processes of CB. Carbon black (CB) is composed mostly of fine particles of amorphous carbon. Various features of CB are controlled during its production.[29,30] It is widely used in various applications from black coloring pigment (resin coloring, dyes and printing inks) to electric conductive agents for high-technology materials, including antistatic films, fibers and magnetic media. A large amount of CB is used in automobile tires as an excellent rubber reinforcement agent.[31,32]

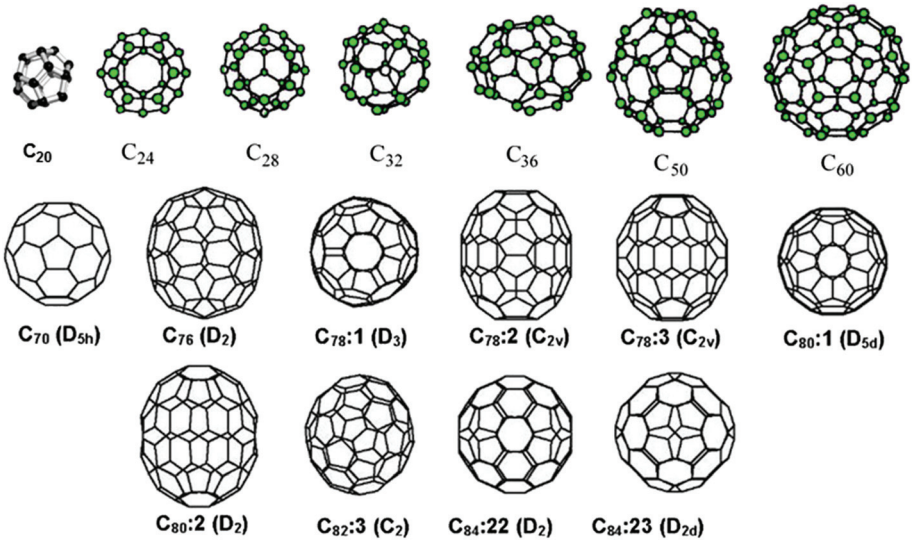

Fig. 2 Fullerene structures and their symmetry.

CB can be produced by thermal decomposition or partial combustion of hydrocarbons, such as oil and natural gas.[33] The characteristics of a particular type of CB vary depending on the manufacturing process. The material produced by the furnace process, currently the most widely used method, is called "furnace black", distinguishing it from CB manufactured by other processes. The latter is usually used in energetic compositions. Furnace black is obtained by blowing an aerosol of petroleum or coal into a high-temperature chamber. This method is efficient for mass production of CB due to high yields as well as better particle size and structure control. Other preparation methods include the channel process (partially combusting fuel), the acetylene black process (thermally decomposing acetylene gas) and the lampblack process (collecting soot from fumes generated by burning oils or pine wood). Recently, a new method has been developed to produce CB from the hydrolysis, carbonization and pyrolysis of rice husk.[34] The specific surface area (SSA) of CB obtained from rice husk was increased from 389 (that of the starting materials) to 1034 $cm^2\ g^{-1}$ and the pore volume was increased from 0.258 to 0.487 $cm^3\ g^{-1}$. This method is also applicable to the preparation of CB from other types of biomass. For better application of CB in different industrial products, it needs to be dispersed in different solvents. For example, stable high-load dispersions of CB in PMA (propyleneglycol methylether acetate) can be prepared by a ball-milling process. Another type of CB is graphitized carbon black (GCB), which is a non-porous form of amorphous carbon. The GCB powder is made up of highly agglomerated nanoparticles with a spherical morphology, and it has been observed from high-resolution TEM images that it has a core–shell structure. A 5 nm graphitic shell covers an amorphous carbon core (Fig. 3).

Highly graphitized CB has been used to evaluate the isosteric heat of adsorption to determine the differences in the adsorption mechanisms of strong polar and non-polar

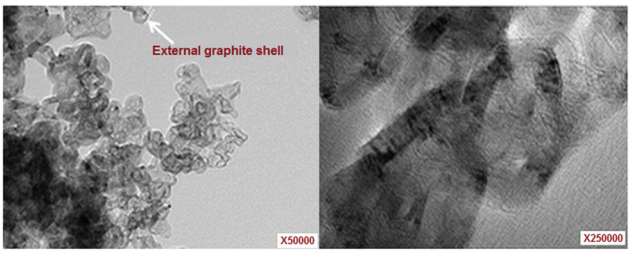

Fig. 3 TEM images of GCB material (crystallized in a 3H graphitic structure with a d_{002} interlayer space of 0.346 nm, which is slightly larger than that of an ideal graphitic structure, 0.335 nm). Reprinted from ref. 37 published in *J. AOAC Int.* (2009) with permission of Publishing Technology.

fluids,[35–38] allowing its use in chemical residue analysis.[39] GCB materials are hydrophobic and are frequently used to effectively trap organic compounds from water or water vapour.

As a super adsorbent, CB can be easily combined with nano-sized EMs,[36] forming new types of energetic mixtures with better performances, which are described in the following sections.

Energetic compositions containing CB. CB is usually used as an additive in solid rocket propellants to modify their combustion properties, due to its large surface area with a strong adsorption capacity.[39] CB is considered as an important additive in energetic compositions and its effect on the performances of EMs is significant even with a content of less than 5 wt%. In fact, graphite, CB and fullerene differ in their structures as well as surface properties in terms of defects and surface groups, which affect their surface free energy characteristics and surface energetic heterogeneity.[40] Therefore, these CNMs have different effects on the performance of solid rocket propellants. As mentioned above, GCB has a larger SSA and

commercial GCB has SSAs from 6 to 225 $m^2 g^{-1}$. It was shown that the GCBs with lower SSAs exhibited a higher degree of graphite crystallinity, resulting in a higher average adsorption energy for N_2.[41] Before adding CB to solid propellants, it must be homogeneously mixed with polymer binders. The homogeneity of CB dispersion in several polymers has been evaluated by measuring the electrical conductivity of the resultant mixture. It has been shown that the minimum viscosity during curing is critical to the CB dispersion morphology.[42] However, no data is available regarding mixtures of CB with polymers, such as hydroxyl-terminated polybutadiene (HTPB) and glycidyl azide polymer (GAP), that are used in propellants. CB may also be used as a flame retardant for interpenetrating polymer networks based on unsaturated polyester/epoxy, where CB maintains the mechanical properties of the polymer more effectively, compared with other additives.[43] To achieve better mechanical strength, CB is usually used together with carbon fiber (CF) in polymer blends. It was indicated that the surface roughness of CB and CF strongly affect carbon–polymer interactions and the entropy penalty plays a determining role in the competitive adsorption of polymers on rough carbon surfaces.[44] This may also be the case for energetic polymer binders, such as poly-BAMMO and poly-NIMMO. It has been found that the surface of CB is energetically heterogeneous. The level of roughness (or heterogeneity) of CB can be evaluated theoretically using lattice density functional theory (DFT), where two lattice DFT models have been developed and experimentally verified.[45] The surface activity of commercial and lab-produced CBs varies according to their particle size. This involves at least four different adsorption sites, the fraction of which depends on the production process of CB and its particle sizes.[46] The fraction of high-energy sites largely decreases with the particle sizes and completely disappears during graphitisation.

The reinforcing potential of CB is closely related to the number of high energy sites. Therefore, it can be used as an active filler in the rubber industry, including in rubber-based propellants to improve their physical and dynamic properties. The surface energy difference between rubbers and CB is large, which has a negative influence on the stability of a CB dispersion in a rubber matrix and on its distribution in blends of different rubbers. It was suggested that plasma polymerization could be used to modify the surface of CB by depositing a thin film of polymer over it.[47] Fullerene soot, as a by-product of fullerene production, can be used in this plasma modification process.[48] In this case, both the CB and the polymer matrix had a comparable surface energy, where the polymer matrix could be an elastomer, such as styrene-butadiene rubber (SBR), butadiene rubber (BR) or ethylene–propylene diene rubber (EPDR), which are widely used in polymer bonded explosives (PBXs) and propellants.[49] There are alternative ways to improve the mechanical strength of CB-containing polymer blends, such as ball-mill mixing, annealing and quenching heat treatment.[50] The first process can break down highly structured CB into finer particles, while the latter two induce CB to form a coagulation structure in the polymers.

The shock wave generated from the detonation of EMs may in turn cause phase transition in CB, due to extreme pressure and high temperature. Such phase transitions provide a route for the preparation of nanodiamond from CBs, where a cubic crystal diamond structure is obtained. This method is significantly different from the preparation of diamonds using graphite as a carbon source.[51] In the past, CB was commonly used in solid propellants but recently it was also used in primary explosives to improve their ignition delays as well as to reduce sensitivity. For example, a primary explosive, bis-(5-nitrotetrazole) tetraammine-cobalt(III) perchlorate (BNCP) has been combined with CB.[52] It was proved that CB can decrease the laser initiation threshold of BNCP, the detailed mechanism of which will be discussed in a later section. CB can also be combined with potassium nitrate (KN) to obtain a new type of propellant (CBKN) for special application in blasting valves.[53] Such blasting valves are used in nuclear power stations in pressurized water reactors. Comparing black powder (HY6) and sulfur-free black powder (WHY6) to CBKN propellant, it was shown that the latter has a higher auto-ignition temperature (over 321 °C) and a lower burn rate, indicating that CBKN has better thermal stability. In addition to the above-mentioned application, CB may have further applications in EMs. For instance, they may be used in the development of nanothermites, for which the requirements for their mechanical and electrostatic sensitivities are high. Such sensitivities may be modulated using pristine or chemically modified CB as additives, as has already shown for the performance improvement of WO_3/Al nanothermite.[54]

Energetic mixtures based on nanodiamonds (nD)

New preparation methods for nD. Diamond has a variety of promising physico-chemical properties, such as high density (among carbon-based materials) and low thermal sensitivity.[55] Nanodiamonds (nDs) are diamonds with sizes in the range of several nanometers. They have been found inside meteorites and can be easily produced by explosion methodology. In past decades, a variety of techniques have been developed for the production of nD,[56] including radio-frequency plasma-aided decomposition of hydrocarbon,[57] plasma-assisted CVD, using hydrocarbons,[58] transformation of graphite under shock compression (SCP),[59] transformation of C_{60} films under SCP,[60] transformation of graphite at high pressure and temperature,[61] plasma-based chemical synthesis using a carbon plasma jet, treatment of the diamond surface in hydrogen plasma and annealing of silica wafers embedded with carbon atoms.[62,63] Furthermore, nD can be synthesized by catalysing CB at ambient pressure and a temperature of 1100 °C.[64–66] As mentioned earlier, CB is composed of fragments of carbon network, either single layers (bent, curved or flat) or small, assembled packs.[67–71] Because nDs can be synthesized from CB as a carbon source, one could speculate that it is also possible to prepare nDs from CNTs. In fact, a unique experimental procedure was designed to synthesize nDs using CNTs as a raw material.[72] It was suggested, on the basis of ultradispersed diamond optical analysis, that the chemical part of detonation

processes could be considered as a superposition of three basic processes: destruction of "explosophoric groups", and endothermic and exothermic reactions.[73] Trinitrotoluene (TNT) and RDX are the explosives primarily used to synthesize nDs by detonation. It was shown that the use of nanostructured explosive charges leads to the formation of detonation nDs (DnDs) with smaller particle sizes, which provides a new understanding of nanodiamond formation-mechanisms.[74] The discontinuity of the explosive at a nanoscale level plays a key role in modifying the particle size of DnDs. Upon using a TNT/RDX mixture as the shock wave source, nD particles with an initial diameter of 2–12 nm were obtained.[75] These nD particles agglomerated during storage with a significant decrease in SSA from 360 to 255 $m^2 g^{-1}$ due to aging. An updated mechanism for the formation of nD particles during TNT detonation synthesis has recently been proposed.[76] This mechanism includes the following steps: (a) decomposition of TNT into radicals, such as dimer C_2 and CO_3; (b) formation of cyclohexane from C_2 or radicals of molecules; (c) interaction of diamond-like core (adamantane radical) with methyl; and (d) growth of DnD particles as in the CVD process. The nD particles can be formed during detonation of EMs and they can also be used as an ingredient of energetic compositions.

Energetic mixtures based on nD. The thermal decomposition of chlorate-based mixtures is initiated by the decomposition of the reducing components. This mechanism was observed in saccharose (Sa)- and thiourea-based compositions.[77,78] This decomposition is initiated by melting of chlorate, while the reducing agent is thermally stable. Therefore, the thermal insensitivity of the reducing agent is the key point of desensitization of chlorate-based energetic formulations. It was suggested that nDs should replace Sa to improve the sensitivity of potassium chlorate (KC)-based compositions.[79] It was shown that nDs/KC formulations are much less sensitive to thermal stress. A TEM image and an XRD spectrum of nDs incorporated into a KC matrix are shown in Fig. 4.

It can be seen that the diameter of the nDs is less than 5 nm, with a carbon content of about 80% and an O content of 12.8%. It seems that the Sa content in Sa/KC mixtures has little effect on their impact sensitivity (IS), while the IS of nDs/KC compositions strongly depends on the nD content. However, nDs/KC compositions with a larger content of nDs are very sensitive to friction, due to the hardness of the diamond. The nDs/KC compositions were found to be deflagrating primary explosives with a maximum propagation rate of 3960 m s^{-1} at 12.3 MPa when the content of nDs is 22 wt%. Such compositions are considered as "green" primers. The nDs/KC reactive formulations usually decompose in two possible combustion modes, *i.e.* (i) continuous or (ii) intermittent, depending on the proportion and pressing level of the nDs used to shape the pellets.[80]

In addition to direct use of nDs as an ingredient in energetic compositions, they can also be used to coat particles of high EMs. It was reported that well-dispersed and uniformly shaped DnDs were produced and used to coat of micron-sized RDX particles.[81] SEM images of these materials are shown in Fig. 5. It has been found that the DnDs could reduce the energy barrier of thermal decomposition of RDX and improve its reactivity. However, excessive coating of over 1/3 of nDs hindered decomposition and gas diffusion, acting as an inert shell.

Similar to the other CNMs, in addition to physical combination with energetic components, nDs could be functionalized with energetic or other functional groups. However, this topic is unexplored and no data has been published in open literature on this issue to date. The most important reason for chemical functionalization of nDs is that detailed and unambiguous characterization of the surface structure of nD particles remains an extremely challenging task. In fact, it was shown that treating nD particles in a reduction reaction resulted in enrichment of hydroxyl and hydroxymethyl functional groups, paving the way for a new generation of nD-based EMs.

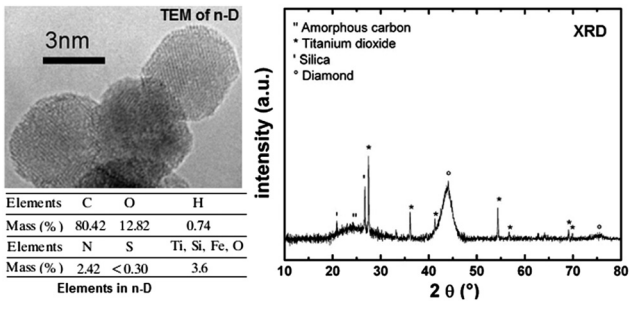

Fig. 4 TEM picture and XRD pattern showing the chemical composition of nDs used to form nD/PC compositions. Reprinted from ref. 79 published in *Propellants, Explos., Pyrotech.* (2009) with permission of John Wiley & Sons, Inc.

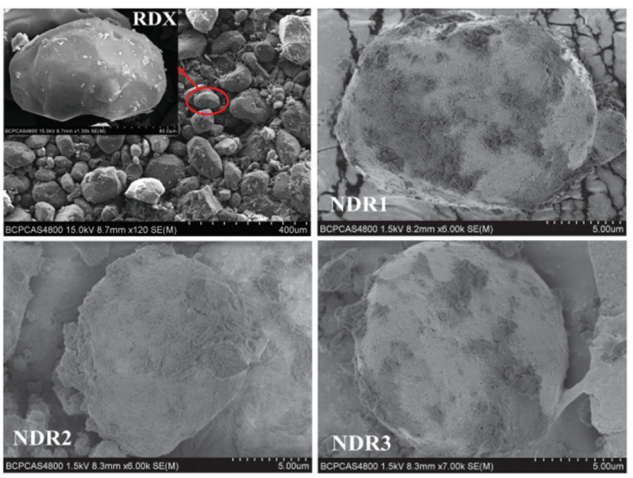

Fig. 5 SEM images of RDX and nDs, where the ratio of nDs to RDX is kept at 1 : 8 (NDR1), 1 : 6 (NDR2), and 1 : 4 (NDR3), which corresponds to increasing the mass proportions of the nD coating to 1/9, 1/7, and 1/5, respectively. Reproduced from ref. 81 with permission from the PCCP Owner Societies.

Energetic composites based on expanded graphite

Development of expanded graphite. Due to the layered structure of graphite, atoms, ions and even small molecules can be inserted (intercalated) between the graphene layers of graphite and this is a relatively easy process in the case of expandable graphite (E_bG). There are several popular ways to prepare E_bG as an excellent halogen-free flame retardant, including liquid phase synthesis, ultrasonic irradiation, and hydrothermal methods.[82,83]

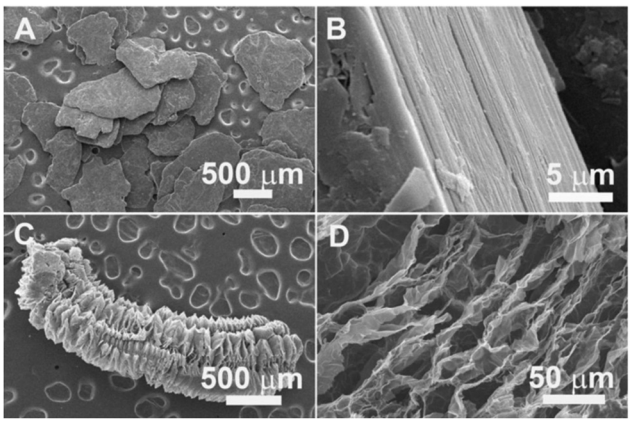

Fig. 6 SEM images of the characteristic structures of flake graphite (A, B) and expanded graphite (C, D). Reproduced from ref. 85 with permission of Copyright 2013, The Electrochemical Society.

Recently, a new preparation procedure was developed, where natural graphite was initially dispersed in H_2O_2 and then introduced into an autoclave to proceed with a hydrothermal process.[84] In all the cases, under the influence of heat, the graphite layers are separated as in an accordion, expanding the graphite flakes (Fig. 6).[85] High-quality E_bG has a large proportion of intercalated layers, where sulphur- or nitrogen-containing compounds are used as intercalating agents. Depending on the nature of the graphite and the intercalating agent, expansion can commence at temperatures as low as 180 °C and can occur suddenly and rapidly. In the case of free expansion, the final volume between the layers can be several hundred times greater than the initial volume. It is well known that electrochemical insertion of Na^+ into graphite is greatly hindered by the insufficient interlayer spacing, while EG could be a good option to replace the graphite used in a Na^+ battery anode (Fig. 7).[86] EG can usually be prepared from fine expandable graphite flakes (160 μm in size), using acetic anhydride as an inserting agent and potassium dichromate as an oxidant.[87] The best known conditions for this process are as follows: mole fractions of graphite, acetic anhydride, concentrated sulfuric acid and potassium dichromate should be 1 : 1 : 3.1 : 0.6, with a reaction time of 50 min and a reaction temperature of 45 °C. Similarly, micron-sized EG is prepared by a chemical oxidation method, using sulfuric and glacial acetic acids as inserting reagents and potassium dichromate as an oxidizing agent.[88] The optimum mass ratio of raw materials $E_bG : H_2SO_4 : CH_3COOH : K_2CrO_7$ for the latter

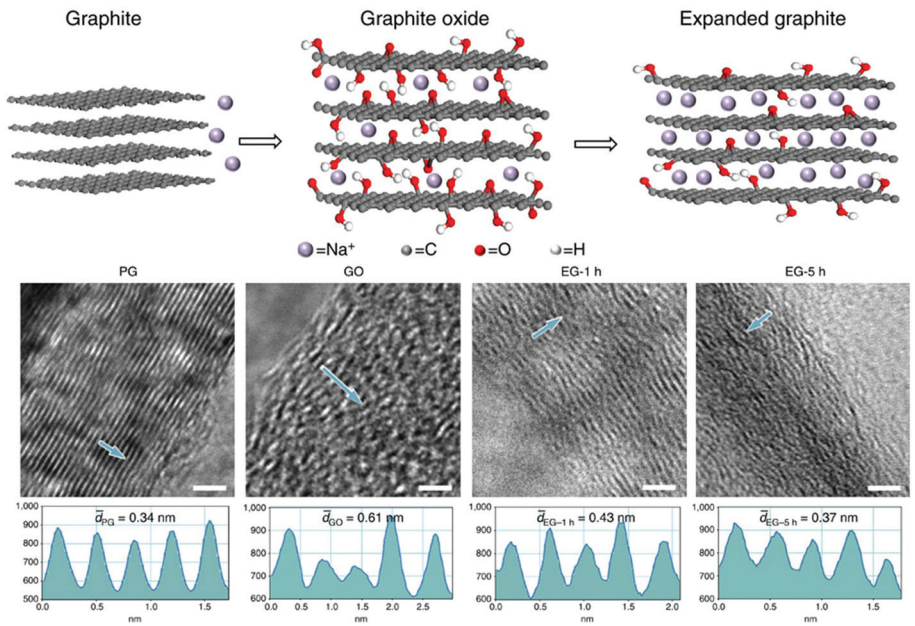

Fig. 7 Above is a schematic diagram: (left) Na^+ cannot be electrochemically intercalated into graphite because of the small interlayer spacing; (middle) electrochemical intercalation of Na^+ into GO is enabled by the enlarged interlayer distance resulting from oxidation; however, the intercalation is limited by steric hindering from large amounts of oxygen-containing groups; (right) a significant amount of Na^+ can be electrochemically intercalated into EG owing to a suitable interlayer distance and reduced oxygen-containing groups in the interlayers. Below are high-resolution TEM images showing cross-sectional layered structures for PG, GO, EG-1 h and EG-5 h. Reprinted from ref. 79 with permission. Copyright © 2014, Nature Publishing Group.

Table 3 The preparation methods and application of expanded graphite-based energetic materials

Materials	Preparation methods	Application fields	Contributors
EG	1. Using natural graphite flakes as raw material, acetic anhydride as inserting agent and potassium dichromate as oxidant	Antistatic and anti-electromagnetic materials, Electronic devices, flame retardants, energetic materials	Ji-Hui *et al.* (2006)[87]
	2. By dispersing natural graphite in H_2O_2 with subsequent hydrothermal treatment in autoclave		Kuan *et al.* (2012)[84]
	3. Micron-sized EG can be prepared by chemical oxidation, using sulfuric acid and glacial acetic acid as inserting reagents and potassium dichromate as oxidizing agent.		Ba *et al.* (2011)[88]
Porous carbon	Prepared from energetic carbon precursors, alkali propiolates, *via* ultrasonic spray pyrolysis	Purification, catalysts	Xu *et al.* (2012)[332]
EG/PP	EG/polypropylene (PP) nanocomposites are prepared by solid-state ball-milling followed by low-temperature melt mixing.	Engineering materials, binders	Mohammad *et al.* (2013)[90]
EG/$Mg(OH)_2$	By mixing $Mg(OH)_2$ powder and EG.	Chemical heat pumps	Zamengo *et al.* (2014)[91]
γ-Fe_2O_3/EG	Nano γ-Fe_2O_3/EG is prepared by a sol–gel and low temperature self-combustion technique.	Magnetic materials	Zhang *et al.* (2011)[93]
$CaCl_2/CH_3NH_2$/EG	Mixed using a cylindrical solid–gas reactor.	Chemical heat pumps	Balat *et al.* (1993)[90]

process is 1 : 5 : 3 : 0.5, while the reaction time is 60 min at room temperature. The micron-sized EG has a larger infrared extinction coefficient than the raw graphite, due to inclusion of some open or semi-open small holes that can absorb infrared radiation. The expansion usually occurs at the very beginning of the reaction and extension of the reaction time has little effect on the microstructure of the final EG.[89] After its preparation, the EG is ready for application in various fields, including preparation of advanced EMs.

Preparation of EG-containing materials. EG can be used in heat-generating energetic compositions to enhance thermal conductivity in packed bed reactors (PBR) or chemical heat pumps (CHP).[90,91] The PBR is fabricated using a certain energetic mixture. The corresponding CHP is based on reversible solid–gas reactions, where the energetic density and energy content are the key factors that determine its performance, depending on the reactive medium implementation. It has been shown that the solid–gas pair, $CaCl_2/CH_3NH_2$, can be optimized by adding EG as a filling material, which can improve the heat and mass transfer.[90] This is also the case for packed bed reactor system, MgO–H_2O.[91] For both dehydration and hydration, EG/MgO–H_2O pellets have higher reaction rates and reactivity than pure $Mg(OH)_2$ pellets. The temperature distribution is also more homogeneous in the packed bed. As mentioned above, EG is currently widely used as a flame-retardant in many types of polymers. Moreover, a novel flame-retardant EVA/IFR/synergist composite containing $CaCO_3$, EG and graphite was developed.[92] Because of its properties, this composite material has a great potential application in solid propellant cladding materials. In addition to its flame-retardancy, EG also found application in electromagnetic materials. Recently, a nano γ-Fe_2O_3/EG magnetic composite was prepared by sol–gel and low temperature self-combustion techniques.[93] This magnetic composite may also be very useful as a combustion catalyst in solid propellants. To make a mutual comparison, the preparation methods of EG and its composites are summarized in Table 3.

EMs based on functionalized C_{60} fullerene

Introduction of functional materials based on C_{60}. C_{60} has been very extensively investigated in terms of its functionalization and corresponding applications.[94] The application field depends on functionalization reactions, which can be one of the following: hydrogenation reduction by electron addition, reaction of fullerene radical anions with electrophiles, nucleophilic addition, nucleophilic substitution, and forming its organometallic derivatives, polymers, dendrimers and related structures.[95] The applications of fullerene materials in catalytic reactions include singlet oxygen oxidation, non-metal nitrogen-fixation, graphite-diamond transition and EMs combustion processes. Several new functionalization reactions have been developed using molecular catalysis, such as (a) organoboron addition to fullerenes, (b) C–H bond allylation and arylation of hydroxyfullerenes, (c) C–H/C–C bond cleavage of alkynyl-hydroxyfullerenes, (d) regioselective tetraallylation of fullerenes, (e) nucleophilic substitution of aziridinofullerene, and (f) cycloaddition of alkynes to aziridinofullerene.[96] A new interdisciplinary field was created when the fields of supramolecular chemistry and fullerenes were overlapped, whereby many unprecedented fullerene-based supramolecular architectures have been designed and constructed.[97] For example, rotaxanes,[98] catenanes,[99] self-assembled coordination compounds,[100] liquid crystalline inclusion complexes,[101] and photoactive supramolecular devices[102] were prepared and characterized. Later on, a stable supramolecular complex was synthesized from a bis-crown ether receptor and a bis-ammonium fullerene ligand.[103] Fullerenes have extraordinary capabilities to coordinate metal atoms, both inside (endohedral) and outside (exohedral) the carbon cage.[104] Many exohedral compounds have been synthesized, such as Pd and Ir

complexes. The fullerene ligands in these cases are acting in a manner similar to olefins (Fig. 8).[105,106]

Exohedral metallofullerenes may open a new way to prepare a variety of novel energetic materials and combustion catalysts. Some functionalized fullerenes can be heated to their ignition temperature with low-intensity, continuous-wave (c.w.) laser irradiation.[107] Laser-induced ignition was demonstrated with various types of laser radiation at intensities as low as 100 W cm^{-2}. As shown in Fig. 9, process (a) is the laser-induced cleavage of functional groups, which induces acoustic shock-waves

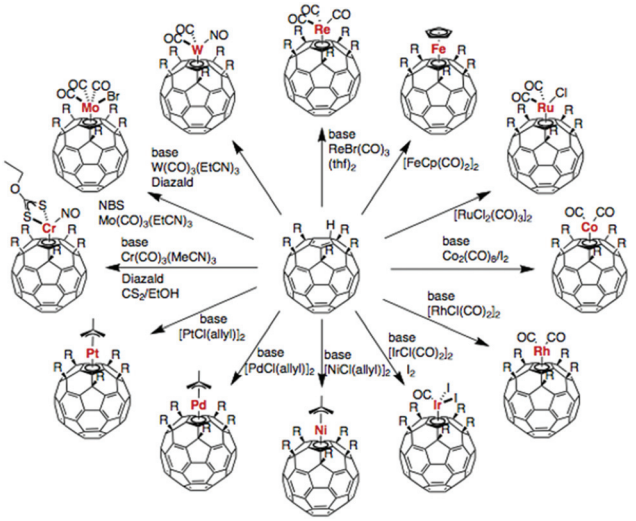

Fig. 8 Synthesis paths for exohedral metal fullerene complexes. Reprinted from ref. 106 with permission from Copyright © 2011, Royal Society of Chemistry.

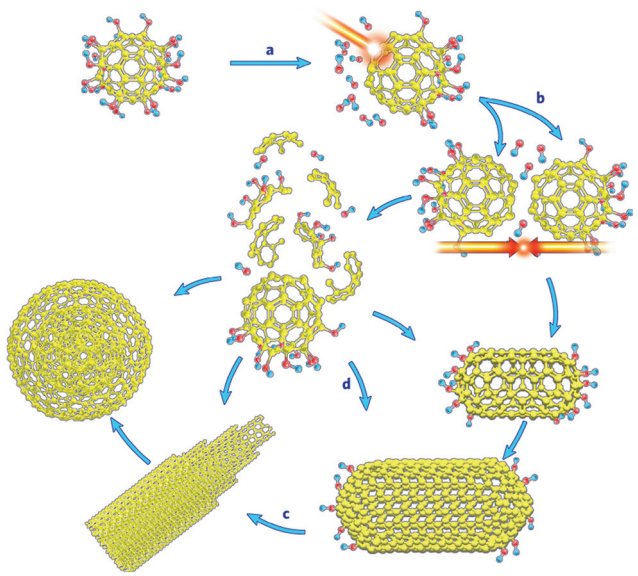

Fig. 9 Proposed mechanism for laser-induced transformation of functionalized fullerenes. Reprinted from ref. 107 with permission. Copyright © 2008, American Chemical Society.

or otherwise imparts kinetic energy to the fullerene cages; (b) energetic fullerene cages collide, leading to coalescence or disintegration; (c) coalescence of SWCNTs into larger SWCNTs, MWCNTs and carbon onions is promoted by the heat generated by the incident laser, cleavage of the functional groups and the exothermic coalescence processes, together with the catalytic action of cleaved functional groups and defects in the nanostructures; (d) alternatively, disintegration of fullerene cages supplies carbon for the simultaneous formation of SWCNTs, MWCNTs and carbon onions, with intact fullerene cages acting as nucleation sites. The simultaneous formation of various carbon nanostructures can be catalysed by cleaved functional groups and the defects present in intact fullerene cages. The energetic fullerene cages collide, leading to coalescence or disintegration.

Functionalization of fullerenes by energetic moieties. The preparation of energetic fullerene can be traced back to the 1990s in China, while the first compound of this type mentioned in the literature might be a trinitrophenyl C_{60} derivative (Cp-1, TNPF), obtained by reacting trinitrochlorobenzene with sodium azide.[108] There were no further reports on this issue until 2006, when a new fullerene derivative containing an energetic moiety, *N*-methyl-2-(1,3-dinitrophenyl) fulleropyrrolidine (MDFP), was prepared by the Prato reaction (Scheme 1).

The optimum molar ratio of C_{60}, 2,4-dinitrobenzaldehyde and *N*-methylglycine reactants was 1 : 2 : 6, while the reaction was conducted at 95 °C for 40 h.[109] After the latter publication, the preparation of energetic fullerene derivatives became a popular topic and many new compounds were synthesized. Typical representatives of this family of compounds are nitrofulleropyrrolidine derivatives, which are synthesized by 1,3-dipolar cycloaddition reactions of C_{60} and the nucleophilic substitution reaction of *N*-unsubstituted fulleropyrrolidine[110] (Scheme 2). In particular, Cp-1 to Cp-4 compounds are prepared by 1,3-dipolar cycloaddition, while Cp-6 and Cp-7 are prepared from Cp-2 *via* nucleophilic substitution.

It was found that the mechanical sensitivity of HMX was greatly reduced when it was mixed with 1% of *N*-methyl-2-(3-nitrophenyl) fulleropyrrolidine (Cp-3, MNPFP). Moreover, *N*-methyl-2-(*N*-ethylcarbazole)-fulleropyrrolidine (Cp-8, MECFP) and *N*-methyl-2-(4′-*N*,*N*-diphenylaminophenyl)-fulleropyrrolidine (Cp-9, MDPAFP) were synthesized *via* microwave irradiation (MR; Scheme 3).[111] A photoinduced intramolecular electron transfer process from a C_{60} moiety to a carbazole moiety has been studied by nanosecond laser flash photolysis. The performance of *N*-methyl-3-(2′,4′,6′-trinitrobenzene)-fulleropyrrolidine (Cp-5, MTNBFP) has been estimated using a self-consistent field calculation method based on the following overall isodesmic reaction (Scheme 4).

It has been calculated that the enthalpy of formation of Cp-5 is 2782.2 kJ mol^{-1}, while its detonation velocity and pressure are 3282 km s^{-1} and 4.443 GPa, respectively.[112] Upon complete combustion, the total heat of combustion for Cp-5 is 2.17 × 10^5 kJ mol^{-1} due to its high carbon content. It seems that this compound may not be useful as the main ingredient of an explosive or a propellant but it might be a good additive for

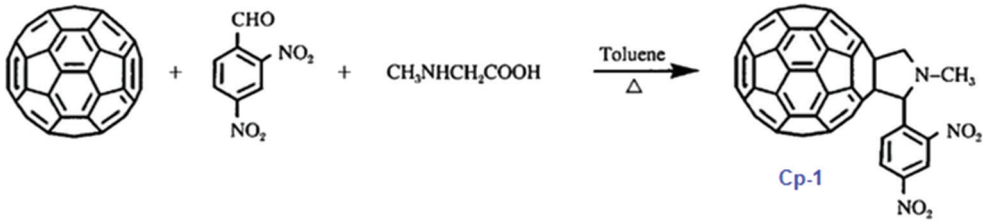

Scheme 1 Preparation procedure of MDFP.[108]

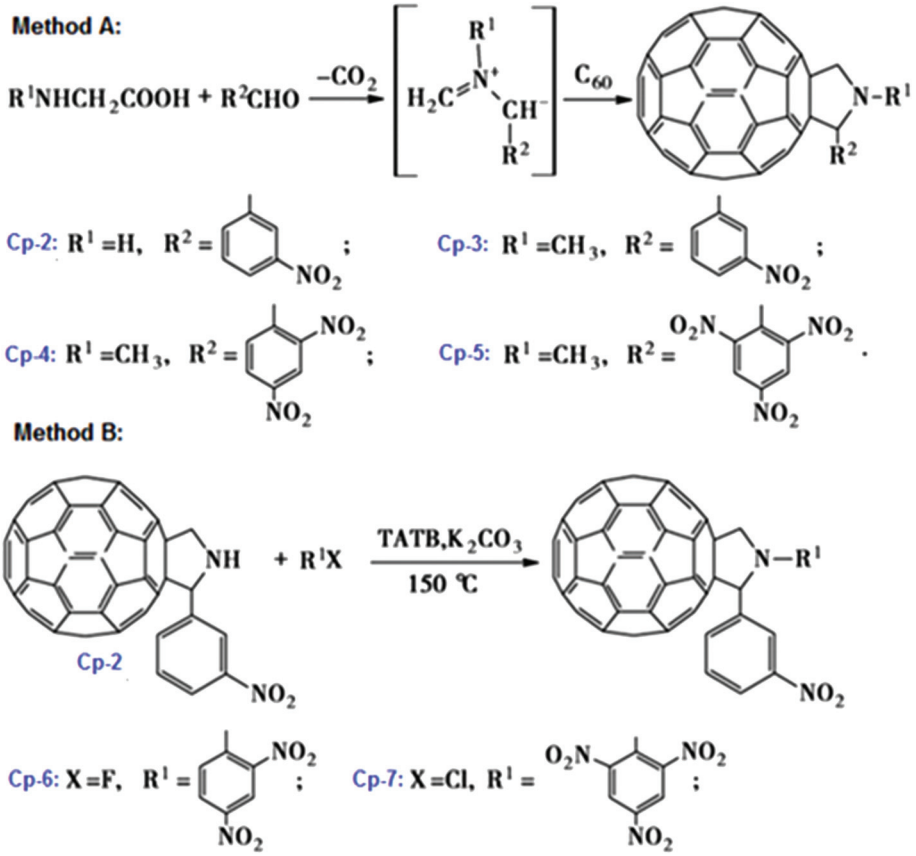

Scheme 2 Preparation methods of *N*-unsubstituted fulleropyrrolidine. Reprinted from ref. 110 published in *Chin. J. Energet. Mater.* (2009) with permission.

heat-generating energetic compositions. To improve the energetic content of fullerene derivatives, more nitro groups can be introduced on the fullerene skeleton. Such a strategy has been recently attempted, where a high-nitrogen-content derivative, $C_{60}(NO_2)_{14}$ (FP, CP-10), was prepared and characterized,[113] using a prolonged treatment of C_{60} in benzene with very high concentrations of N_2O_4. However, Cp-10 is not so thermally stable and it deflagrates when heated above 170 °C in nitrogen or air, releasing a considerable amount of heat. This compound may be used as a powerful explosive, depending on its sensitivity, which has not been reported. In addition to the nitro-derivatives of fullerene, fullerene nitrates have also been reported that can be used in propellant compositions as energetic burn rate modifiers. As a typical example, fullerene ethylenediamine nitrate (Cp-11, FEDN) was synthesized by reacting fullerene and ethylenediamine in diluted nitric acid (Scheme 5).[114]

Cp-11 can undergo a three-step decomposition process starting at about 100 °C. The details of its decomposition mechanism will be described in a later section. Energetic fullerene catalysts improve the specific impulse of solid propellants, while decrease their pressure exponents. There is another type of polymeric catalyst based on fullerene, the so-called fullerene itaconic acid copolymer lead salt (FIAL, Cp-12), which may have a better effect on combustion.[115] This was prepared *via* a two-step reaction using C_{60}, itaconic acid and lead nitrate as starting materials (Scheme 6).

As shown in Scheme 6, the reaction time and temperature had little effect on the final content of lead. However, the

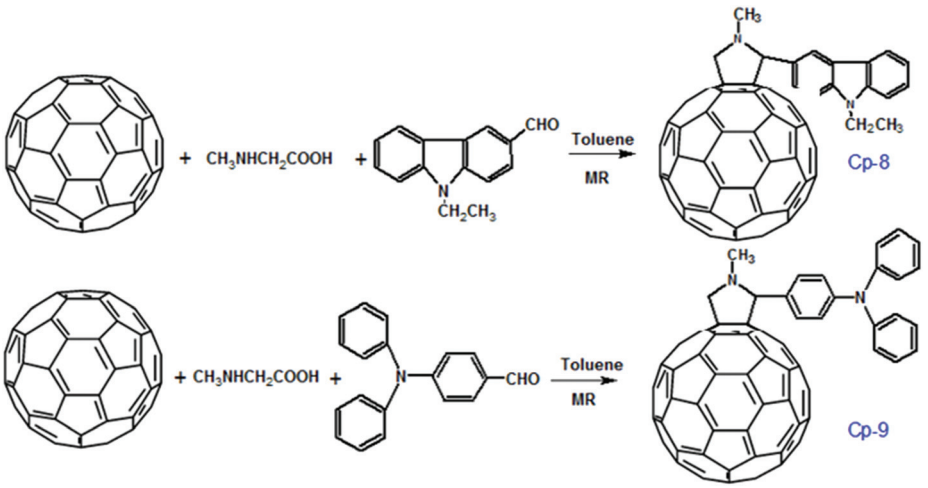

Scheme 3 Preparation method of *N*-methyl-2-(4′-*N*,*N*-diphenylaminophenyl)-fulleropyrrolidine under microwave irradiation.

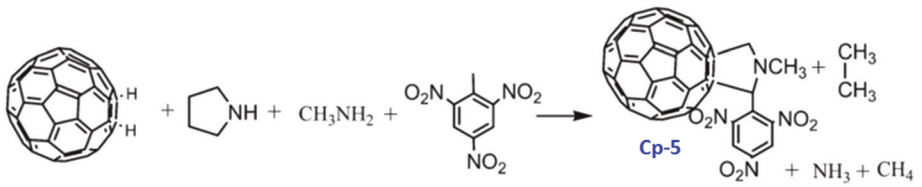

Scheme 4 Preparation of Cp-5.

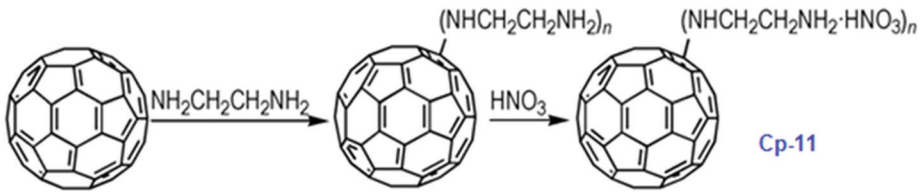

Scheme 5 Synthesis of Cp-11.

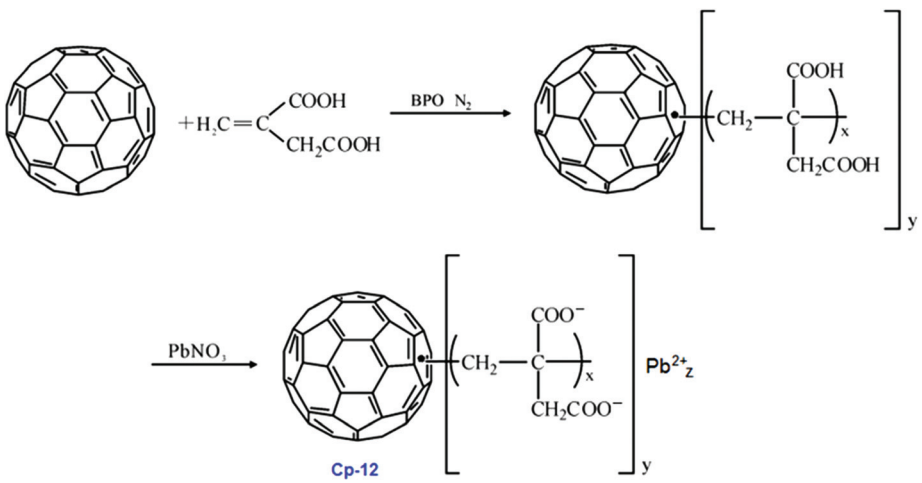

Scheme 6 Synthesis of Cp-12.

optimum reaction conditions for the preparation of Cp-12 were found to be 25 °C with a pH of 6.9. The resulting catalyst, Cp-12, is quite thermally stable, with a decomposition temperature peak at 304 °C. Based on the aforementioned fullerene nitrate (FN, Cp-11), a more energetic derivate, fullerene ethylenediamine dinitramide (FED, Cp-13) could be obtained *via* an ion exchange reaction with ammonium dinitramide in 84% yield (ADN; Scheme 7).[116]

The Cp-13 product has the appearance of a yellowish solid and its structure was analyzed by UV-vis, FT-IR, elemental analysis and XPS techniques. Based on these analyses, Cp-13 was found to have a formula of $H_{12}C_{60}(HNCH_2CH_2NH_2 \cdot HN(NO_2)_2)_{12}$ and it was proposed for use as an oxidizer in solid propellants like ADN. To combine the advantages of fullerene and lead salts as propellant catalysts, another lead salt based on fullerene phenylalanine (FPL, Cp-14) was prepared. Analogously to Cp-12, Cp-14 can be prepared using the same strategy, where the Pb cation comes from $Pb(NO_3)_2$ (Scheme 8).[117,118]

FPL was found to have a significant catalytic effect on the decomposition of 1,3,5-trinitroperhydro-1,3,5-triazine (RDX) and it may be used as an efficient combustion catalyst in solid propellants. On the basis of the above-mentioned synthetic method, a new potential energetic combustion catalyst, fullerene hydrazine nitrate (FHN, Cp-15) was designed and prepared in a two-step process. Fullerene hydrazine (FH) was first prepared in 84% yield from fullerene and hydrazine hydrate, and then the obtained FH was reacted with concentrated nitric acid to form the FHN salt (Scheme 9).[119]

Elemental and other chemical analyses of FH showed a composition of C, 69.38%, N, 26.86% and H, 3.76%, strongly indicating that the formula of FH, obtained under these reaction conditions, is $C_{60}(NHNH_2)_{10}H_{10}$. The corresponding formula of the FHN salt was found to be $C_{60}(NHNH_2)_{10}H_{10} \cdot 4HNO_3$, with an oxygen content of 14.9%. In general, C_{60} can either be combined with energetic moieties, as shown above, or be functionalized with energetic polymers.

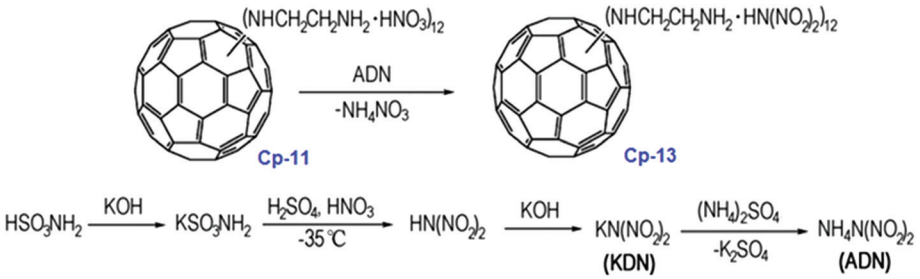

Scheme 7 Synthesis of Cp-13 and ADN.

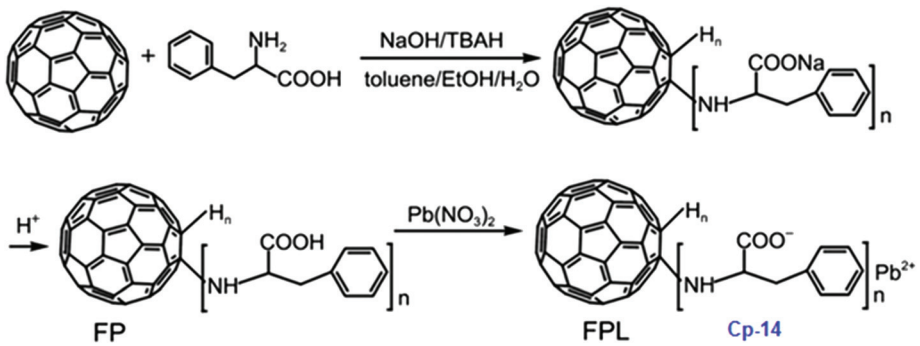

Scheme 8 Synthesis of Cp-14.

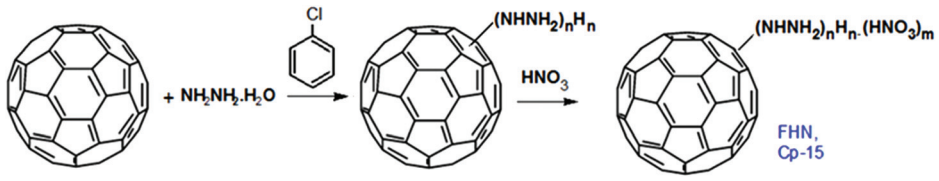

Scheme 9 Synthesis of Cp-15.

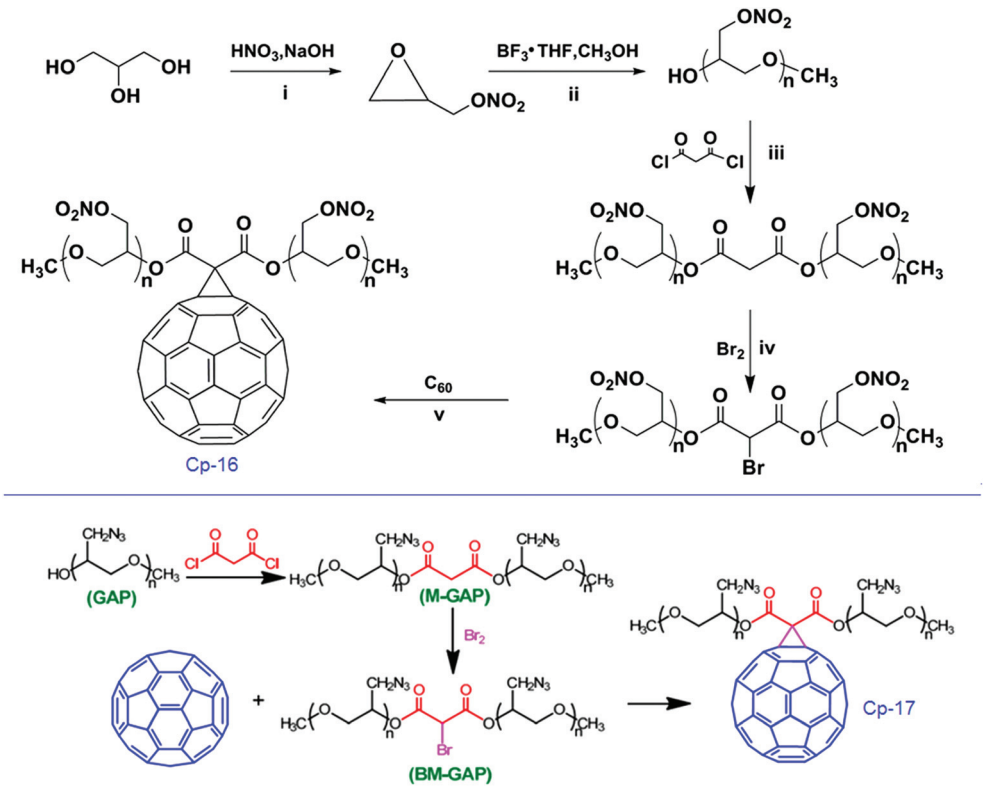

Scheme 10 Synthesis of C_{60}-PGN and C_{60}-GAP.

Two novel fullerene-based energetic polymers have been prepared recently, including C_{60}-poly(glycidyl nitrate) (C_{60}-PGN, Cp-16)[120] and C_{60}-glycidyl azide polymer (C_{60}-GAP, Cp-17).[121] The former polymer was synthesized through a modified Bingel reaction of C_{60} with bromomalonic acid PGN ester, in the presence of amino acid in dimethyl sulfoxide, while the latter was prepared using the same reaction between C_{60} and bromomalonic acid glycidyl azide polymer ester (Scheme 10). Both Cp-16 and Cp-17 have excellent thermal stability over 200 °C and can be used as energetic binders for solid propellants.

For better comparisons, the preparation methods and applications of the above-mentioned energetic fullerene derivatives are summarized in Table 4.

As shown in Table 4, it is clear that most of the energetic fullerene derivatives were obtained directly by reacting C_{60} with the corresponding energetic precursors. Almost all the studies have been reported during the past 5 years, strongly indicating that this research field is in its infancy. These energetic fullerene derivatives could either be used as combustion catalysts or as energetic binders. However, the compatibility and sensitivity have not yet been systematically investigated for all these materials; this is very important with respect to their practical applications.

EMs based on graphene, GO or reduced GO

Improved methods of graphene, GO and rGO preparation. Graphene is a carbon-based material that is typically a one-atom-thick sheet of graphite. It has been widely investigated in past decades, starting with a report by Novoselov *et al.*, on its isolation and unique electronic properties.[122] Soon after its discovery, graphene was mainly applied in electronic devices.[123,124] High-quality graphene sheets are usually prepared by a CVD process,[125,126] requiring very expensive facilities, hence new alternative methods for graphene preparation need to be developed. The exfoliation of alkali metal graphite intercalation compound (GIC), as a promising alternative method, is therefore designed to prepare non-functionalized and functionalized graphene sheets, retaining the sp^2 network. For example, alkali metal-based GICs readily exfoliate in *N*-methylpyrrolidone (NMP), giving stable solutions of negatively charged graphene sheets,[127] and soluble functionalized graphenes with minimum sp^2 disruption were synthesized by reacting exfoliated alkali metal-based GICs with electrophiles.[128]

GO is another form of graphene that is also very attractive for preparation of graphene-based materials.[129–131] In fact, thin films of GO could be reduced in solution under various reducing conditions and the reduction converts GO into a reduced-GO (rGO) material, which exhibits better electrical conductivity.[131,132] In addition to its use in making rGO for electronic devices, GO has been used in catalytic oxidation,[133–135] biotechnology[136–139] and as a surfactant.[140]

Recently, a facile and scalable liquid-phase preparation method for aqueous solutions of isolated graphene sheets from low-temperature EG, was reported.[141] It has been shown

Table 4 The preparation methods and application of fullerene-based energetic materials

Materials	Preparation method	Application field	Contributors
FPGN	Through a modified Bingel reaction of C_{60} and bromomalonic acid PGN ester in the presence of amino acid and dimethyl sulfoxide	Energetic binder	Gong *et al.* (2015)[120]
FFGAP	Using a modified Bingel reaction of [60]fullerene (C_{60}) and bromomalonic acid glycidyl azide polymer ester (BM-GAP)	Energetic binder	Huang *et al.* (2015)[121]
FPL	Fullerene phenylalanine (FP) was dissolved in 10 mL water, then the pH of the FP water solution was adjusted to 6.96 using 1 mol L^{-1} HNO_3 by adding $Pb(NO_3)_2$ (0.01 mol) and the mixture was stirred at 30 °C for 3 h	Propellant catalyst	Guan *et al.* (2014)[117]
FHN	Fullerene hydrazine is synthesized from fullerene and hydrazine hydrate and then it reacts with concentrated nitric acid to form fullerene hydrazine nitrate	Energetic combustion catalyst	Guan *et al.* (2014)[119]
FEN	Using fullerene, ethylenediamine and dilute nitric acid as raw materials	Propellant catalysts	Chen *et al.* (2014)[116]
FED	*Via* ion exchange reaction of fullerene ethylenediamine nitrate and ammonium dinitramide (ADN)	Energetic components	Chen *et al.* (2014)[114]
mPF	Glycyl-porphyrin (20 mg) and C_{60} (42 mg) are dissolved in 45 ml of anhydrous toluene under stirring, then three-fold excess of benzaldehyde was added	Catalyst for explosives	Jin *et al.* (2014)[114]
FIA-Pb	Prepared *via* a two-step reaction using C_{60}, itaconic acid and lead nitrate as raw materials	Propellant catalyst	Liu *et al.* (2013)[115]
PF	Prolonged treatment of C_{60} in benzene with very high concentrations of N_2O_4	Magnetic material	Cataldo *et al.* (2013)[113]
MTNBFP	Not available in the literature	Primary explosive	Tan *et al.* (2010)[112]
NFD	Synthesized by 1,3-dipolar cycloaddition reactions of C_{60} and a nucleophilic substitution reaction of *N*-unsubstituted fulleropyrrolidine	Propellant catalyst	Jin *et al.* (2009)[110]
FDFP	Prepared by the Prato reaction with a reactant molar ratio of C_{60}, 2,4-dinitrobenzaldehyde and *N*-methylglycine 1 : 2 : 6	Energetic catalyst	Jin *et al.* (2006)[109]
NPF	Prepared *via* C_{60} reaction with trinitrochlorobenzene and sodium azide	Energetic components	Wang *et al.* (1996)[108]

FEN, fullerene ethylenediamine nitrate; FED, fullerene ethylenediamine dinitramide $H_{12}C_{60}(HNCH_2\ CH_2NH_2{\cdot}HN(NO_2)_2)_{12}$; mNPF, *N*-methyl-2-(3-nitrophenyl) pyrrolidino-[3′,4′:1,2] fullerene; NFD, nitro fulleropyrrolidine derivatives; PF, polynitro[60]fullerene, $C_{60}(NO_2)_{14}$; MTNBFP, *N*-methyl-3-(2′,4′,6′-trinitrobenzene)-fulleropyrrolidine; FPGN, [60]Fullerene-poly(glycidyl nitrate); MDFP, *N*-methyl-2-(1,3-dinitrophenyl) fulleropyrrolidine; FIA-Pb, fullerene itaconic acid copolymer lead salt; FFGAP, functionalized [60]fullerene-glycidyl azide polymer; FPL, fullerene phenylalanine lead salt; FHN, fullerene hydrazine nitrate; NPF, trinitrophenyl C_{60} derivative.

that graphene sheets exfoliated from EG could be restored to an extended conjugated sp^2 network. Later on, novel single- and multi-layer graphene quantum dots (GQDs) were prepared from CX-72 CB by chemical oxidation (Fig. 10).[142] Single-layer GQDs were demonstrated to be excellent probes for cellular imaging, while multi-layer GQDs may offer great applications in optoelectronic devices.

Preparation of GO was first reported more than a century ago and it could be achieved by several approaches. In general, the conversion of graphite to GO is conducted in two steps: (1) the oxidation of graphite to GO; (2) the removal of impurities (*e.g.* acids and manganese salts). Brodie's method, reported in 1859, was the pioneering one, where he used fuming HNO_3 and $KClO_3$ as the intercalatant and oxidant.[143] Nevertheless, this method has several flaws, including a long reaction time and the generation of toxic gases during the reaction. In 1958, Hummers and Offeman developed another method, which is currently the most widely employed way for the synthesis of GO.[144] They used H_2SO_4 to intercalate graphite in the presence of $NaNO_3$, while using $KMnO_4$ as an oxidizer. Recently, Tour *et al.*[145] improved the Hummers method by excluding $NaNO_3$, while increasing the amount of $KMnO_4$ and performing the reaction in a 9 : 1 mixture of H_2SO_4/H_3PO_4. However, there are still several problems with this method. To solve these problems, an improved Hummers method has recently been developed.[146] In the latter method, GO is prepared using a simple purification process in a high yield, using small graphite flakes as a raw material. In fact, GO in the solid state gets gradually "reduced" and becomes darker in colour upon prolonged storage in air at room temperature. Such disproportionation reactions are highly exothermic.[147] In the past, thermal reduction/exfoliation of GO was a typical method for rGO production, which, however, has the drawback of requiring specialized equipment for rapid thermal shock absorption. Currently, a new alternative method is available, based on vacuum and microwave-assisted exfoliation, which has solved the problem of poor reduction of GO with a low C/O ratio.[148] Microwave irradiation of GO under vacuum leads to outgassing from GO and the creation of plasma, which aids temperature distribution and hydrogenation. As mentioned earlier, graphene, GO and rGO derivatives are well-known in the field of

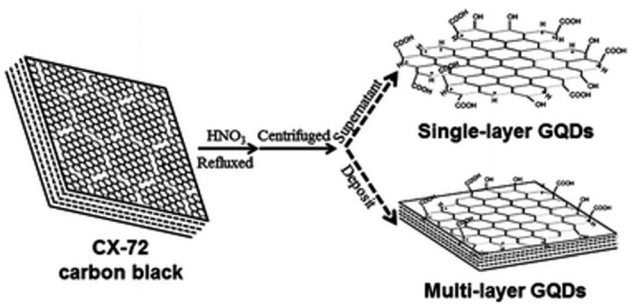

Fig. 10 The preparation procedures for single- and multi-layer GQDs. Reprinted with permission from ref. 141 with permission of © 2009 IOP Publishing Ltd.

electronic technology and biotechnology. Although many of these functionalized carbonaceous nanomaterials have been used in various energetic compositions, the number of publications in this field is limited.[149] For instance, GO itself is a highly energetic material, is thermally unstable and can readily undergo exothermic disproportionation reactions to produce chemically modified graphene under mild heating conditions.

EMs based on graphene. Functionalized graphene can be a multidentate ligand to coordinate many metals or metal ions on its surface.[150] Structures of graphene ligands are similar to metal–porphyrin, metal–phthalocyanine, and metal–phenanthroline complexes. The most commonly used metal ions for coordination with functionalized graphene ligands include copper and nickel.[151,152] Graphene can be combined with EMs or functionalized with energetic groups. The first reported case showed that graphene can be a good carrier for laying molecular monolayers of an insensitive explosive, 1,3,5-triamino-2,4,6-trinitrobenzene (TATB), which was attributed to the strong π–π attraction between the TATB and graphene sheets (Fig. 11).[153]

The calculated detonation enthalpy of the TATB/graphene complex is 1.61 kJ g^{-1} with a density of 2.1 g cm^{-3}, while the detonation pressure and detonation velocity are 10.5 GPa and 2.40 km s^{-1}, respectively. The lubricating properties of graphene are better than those of graphite, and a series of complexes with adjustable properties could be obtained by adjusting the proportion and the order of overlaying layers.

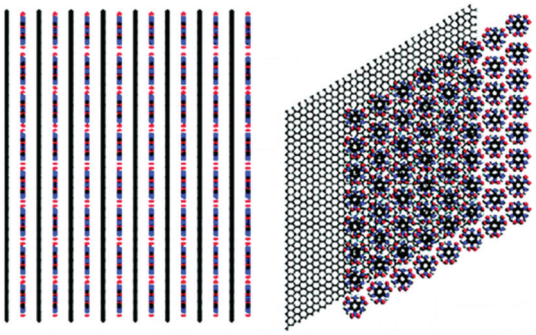

Fig. 11 Structure of sandwich complex of TATB/Graphene layer formed due to strong π–π attraction. Reprinted from ref. 153 with permission. Copyright © 2010, American Chemical Society.

However, this type of material is still in a design stage. In common practice, EMs should be safe enough to be handled even in the case of primary explosives. To improve the electrostatic sensitivity of lead styphnate (LS), graphene nanoplatelet-lead styphnate composites (GLS) were prepared either by adding graphene nanoplatelets (GNP) to the reaction solution or by coating normal LS with GNPs. The composites showed an excellent anti-electrostatic performance with depressed electrostatic spark sensitivity and static electricity accumulation.[154]

Although potassium picrate (KPA) is a less powerful explosive than LS, it has many important applications. KPA is somewhat shock-sensitive and even more sensitive than the parent picric acid. If ignited in a confined space, KPA will detonate. Ultrafine KPA was prepared under the action of a crystalline controlling agent and its thermal sensitivity can be improved by graphene-doping. KPA doped with graphene nanoparticles (having a larger surface area) may partially hinder effective collisions of KPA particles and accelerate the heat dispersion,[155] and hence the mechanical sensitivity of KPA may be decreased. In addition to primary explosives, high-energy solid propellants also need to be safer to allow their use in low vulnerability (LOVA) munitions.

In particular, ammonium perchlorate (AP) is the main ingredient of high-energy composite propellants. However, its surface properties need to be improved for better safety. A nano-composite based on AP and graphene aerogels (AP/GA, Fig. 12) was prepared by a sol–gel method and characterized by scanning electron microscopy (SEM), elemental analysis and X-ray diffraction (XRD) techniques.[156] It can be seen in Fig. 12a and b that (similarly to GA) there are still many voids inside the AP/GA nano-composite material with an SSA of 49.18 m^2 g^{-1}. However, a large number of AP particles, with an average particle size of 69.4 nm, are attached to the skeleton of graphene. Elemental analysis of this material shows that the content of AP can reach to 94%, which is very promising as the main energetic component.[157] Based on AP/GA nanocomposites, a novel GA/Fe_2O_3/AP nanostructured energetic material was prepared by a sol–gel method, which was followed by a supercritical CO_2 drying technique (Fig. 13).[158] It has been demonstrated that Fe_2O_3 and AP are well dispersed in GA layers on a nanometer scale, where Fe_2O_3 exhibits a catalytic effect on the thermal decomposition of AP.

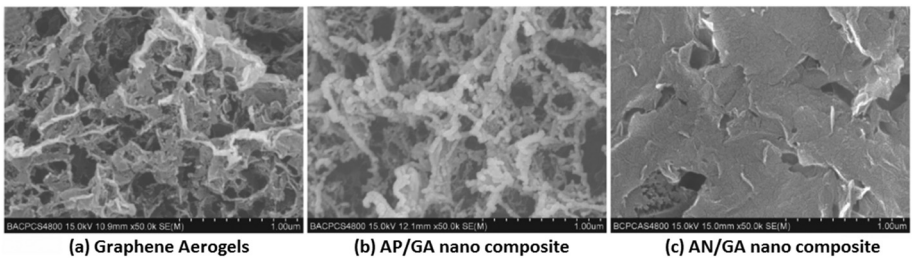

Fig. 12 SEM images of GA (a) and AP/GA (b) and AN/GA (c) nano composites. Reprinted from ref. 156 with permission. Copyright © 2012, *Chin. J. Explos. Propellants*.

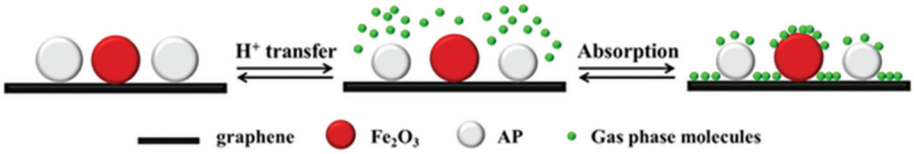

Fig. 13 The principle of GA/Fe_2O_3/AP nanostructured energetic composite formation, where Fe_2O_3 and AP nanoparticles are added and trapped in the porous three-dimensional networks of GA. Reprinted from ref. 158 with permission. Copyright © 2014, Springer Science.

Fig. 14 shows the SEM images of GA and a GA/Fe_2O_3/AP nano-structured energetic composite. It is apparent that the morphology of GA is uniform on a large scale and exhibits a three-dimensional network of randomly oriented sheet-like structures with a wrinkled texture as well as rich hierarchical pores. It is very similar to AP/GA; a large amount of AP crystallizes on the networks of GA and covers the surface. N_2 adsorption–desorption isotherms of GA and the corresponding nanocomposites are shown in Fig. 14c and d.

For GA/Fe_2O_3/AP nano-structured energetic composites and GA, the adsorption–desorption curves indicate an open wedge-shaped meso-porous structure for this material, resulting from the presence of the graphene sheets.[159] The tested SSAs of GA and the nano-composite are 717 and 123 $m^2\ g^{-1}$, respectively, while the total pore volumes (V_{tot}), determined by the Barrett–Joyner–Halenda (BJH) method for GA and the nano-composite, are 3.37 and 0.46 $cm^3\ g^{-1}$, respectively. After filling GA with AP, the nano-composite shows significant decreases in its SSA and V_{tot}, indicating that AP decreases the SSA of the product.

In addition to AP, GA can also be used to prepare nanocomposites of ammonium nitrate (AN), another common oxidant used in propellants and explosives. Similarly, this can be prepared by the sol–gel method followed by a supercritical CO_2 drying process.[160] According to SEM and elemental analysis, nano-sized AN uniformly disperses in the GA, with an average particle size of 71 nm and a mass fraction of 92.7% (Fig. 12c). All the above-mentioned materials are metastable intermolecular composites (MICs), which are among the most attractive EMs in terms of their performance. MICs are generally composed of a fuel and an oxidizer with particle sizes in the nanometer range. The heat and mass transfer are greatly enhanced due to the nanoscale contact of oxidizer and fuel particles. The most promising application for MICs is nanothermites. On the basis of graphene functionalization, long-range electrostatic and short-range covalent interactions could be harnessed to produce multifunctional EMs through hierarchical self-assembly of a nanoscale oxidizer and a fuel into highly reactive macrostructures.

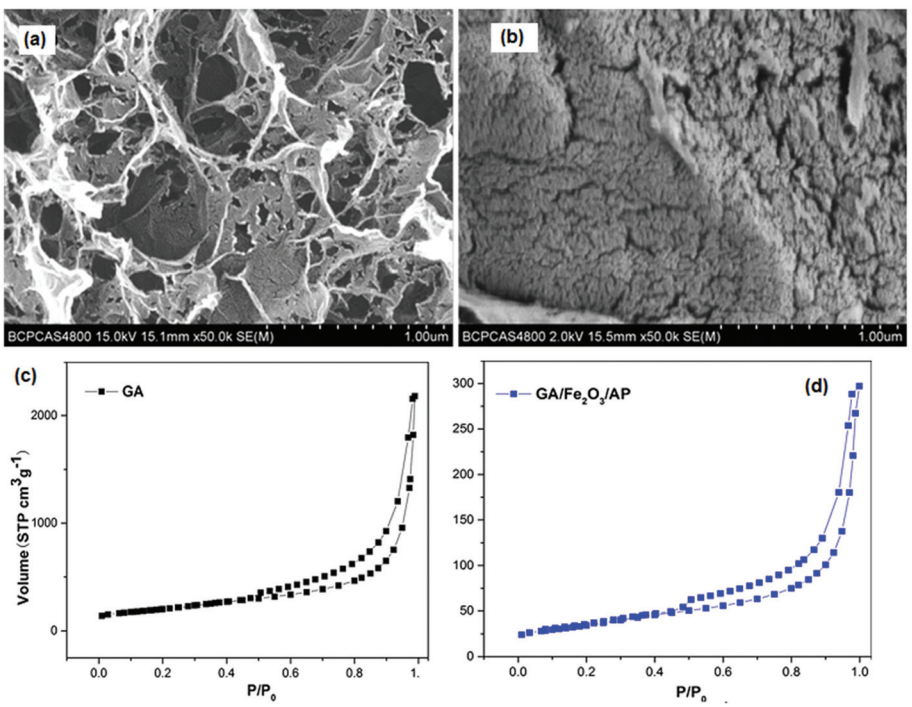

Fig. 14 SEM images of GA (a) and GA/Fe_2O_3/AP nanostructured energetic composite (b); Nitrogen adsorption–desorption isotherms for GA (c) and GA/Fe_2O_3/AP nanostructured energetic composite (d). (reproduced from Lan, *J. Sol-Gel. Sci. Technol.*, 2015, **74**, 161–167.) Reprinted from ref. 158 with permission. Copyright © 2014, Springer Science.

A self-assembly method of Al and Bi_2O_3 nanoparticles on functionalized graphene sheets (FGS) was recently reported.[161] The self-assembly process and the chemical bonds formed are shown in Fig. 15. Such a nanocomposite structure was formed in a colloidal suspension phase that ultimately condenses into ultra-dense macrostructures, which contain 5 wt% of GO. The TEM and SEM photos of GO/Al/Bi_2O_3 composites, as well as Al and Bi_2O_3 nanoparticles are shown in Fig. 15. In this case, the oxygen atom from the OH group on Al is protonated by the hydrogen of the COOH group on GO, which creates a carboxylate anion (GO–COO^-) group on the GO (Fig. 15).

The covalent bonding between Al and GO and the absence of covalent bonding between Bi_2O_3 and GO, were shown by various spectroscopic methods. Fig. 16 shows the orientation of the GO/Al/Bi_2O_3 nanostructures within the larger macrostructures. It is suggested that the formation of this structure is driven by two-particle-size modes, where the smaller sized and less planar GO/Al/Bi_2O_3 forms randomly oriented macrostructures, while the more planar one tends to condense into layered macrostructures for larger-sized assemblies. The layered assembly probably arises from the preference of the larger 2-D GO/Al/Bi_2O_3 and they geometrically align with one another due to van der Waals interactions. Regardless of their structure, the GO/Al/Bi_2O_3 nanocomposites have excellent fuel/oxidizer contact in comparison to randomly mixed Al/Bi_2O_3, resulting in enhanced reactivity.

A remarkable enhancement in measured energy release from 739 to 1421 J g^{-1} was found for this novel composite when it was compared to a normal Al/Bi_2O_3 mechanical mixture. In addition to the aforementioned method, a pyrocarbon (PyC) coating can also be introduced to the Al_2O_3–SiO_2 system, using *in situ* oxidation of PyC by thermolysis of AN.[162] The formation of nitrogen oxides during the decomposition of AN enabled the oxidation of PyC at relatively low temperatures.

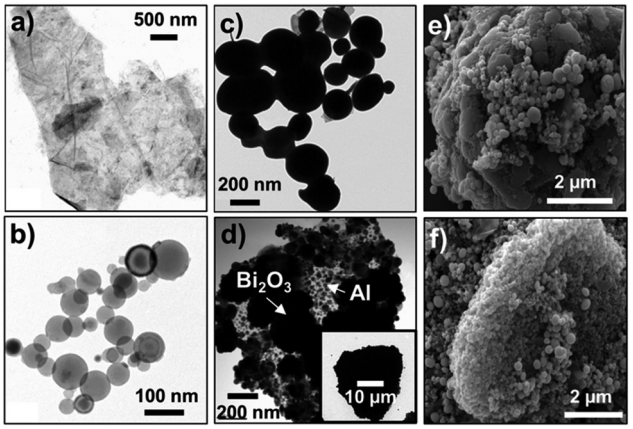

Fig. 16 TEM (a–d) and SEM (e, f) images of GO(5%)/Al/Bi_2O_3 composites self-assembled from nano to macro length scales: (a) a few layered GO sheets, (b) Al nanoparticles with an average diameter of 80 nm, (c) Bi_2O_3 nanoparticles with a size range of 90–210 nm and (d) layered nanoscale building block of a GO densely decorated with Al first and then with Bi_2O_3; The inset in (d) shows a ultradense assembly of Al and Bi_2O_3 on GO; ultradense macro structures self-assembled from GO/Al/Bi_2O_3 nano-composites in layered (e) and random (f) orientations. Reprinted from ref. 161 with permission. Copyright © 2014, American Chemical Society.

In this way, a PyC coating can be easily introduced to the three-dimensional all-oxide fiber-reinforced composite (Fig. 17). For the composites without PyC interphases (Fig. 17a), the fracture surface was very homogeneous and almost devoid of pull-out fibers. As shown in Fig. 17b, the fibers were tightly surrounded by the matrix and no fiber/matrix (F/M) debonding occurred, suggesting strong interfacial bonding. A large number of micro-pores are distributed on the fiber surface due to chemical corrosion of the matrix. Obvious fiber pull-out behaviour is shown for the composites with PyC

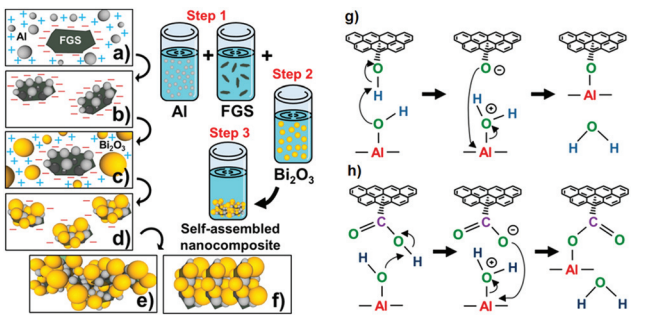

Fig. 15 Schematic of the self-assembly process: (a) electrostatic attraction of Al to GO, (b) covalent bonding of GO/Al existing as a stable GO/Al dispersion, (c) electrostatic attraction of Bi_2O_3 to GO/Al nanostructures, and (d) noncovalent assembly of Bi_2O_3 on GO/Al; the instability of the GO/Al/Bi_2O_3 dispersion continues the self-assembly process to form ultradense macrostructures ((e) and (f)); chemical interactions between (g) hydroxyl groups of GO and surface hydroxyl groups of Al nanoparticles leading to C–O–Al covalent bonding and (h) carboxylic groups of GO and hydroxyl groups of Al nanoparticles leading to O=C–O–Al covalent bonding. Reprinted from ref. 161 with permission. Copyright © 2014, American Chemical Society.

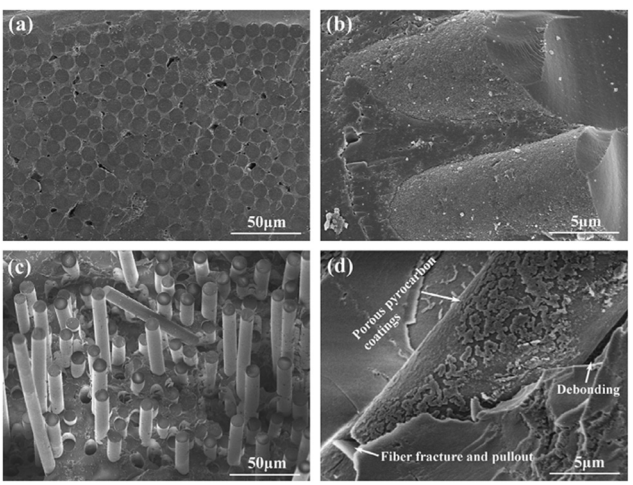

Fig. 17 Fracture surfaces of the N440/AS composites without (a, b) and with (c, d) PyC interphases. Reprinted from ref. 162 with permission. Copyright © 2015, Elsevier Ltd.

interphases (Fig. 17c) due to weak interfacial bonding, which has been confirmed by SEM imaging (Fig. 17d). This indicates that the porous coating is favourable to F/M debonding, thereby improving the performance. As mentioned earlier in this section, insensitive energetic materials are greatly desirable for LOVA ammunition compositions. The capability to control compositions and properties for target EMs is essential to obtain an optimal performance, controlled energy release, and low sensitivity. With these goals in mind, a new study on relatively insensitive explosive 1,1-diamino-2,2-dinitroethylene (FOX-7) has been carried out.[163] The FOX-7 nanocrystals were prepared under confinement of mesoporous carbon FDU-15 *via* a self-assembly process. It has been indicated that complete impregnation can be achieved in *N*-methyl-2-pyrrolidone at 100–110 °C, and the maximum amount of FOX-7 in the FOX-7/FDU-15 composites was 43.8 wt%. There are many other functionalized graphenes that are only used in energy storage such as batteries and fuel cells. One should refer to a comprehensive review on graphene derivatives in energy storage applications for further details.[164]

EMs based on GO and rGO

Compared with graphene, GO seems to be more suitable and more easily functionalized into energetic compounds. GO itself is considered to be a potential EM. Upon heating, GO can readily undergo violent exothermic decomposition due to the extensive oxygenic functional groups on the basal plane (phenol, hydroxyl, and epoxide) and at the edges (carboxylic).[165] This is also the case for rGO, which is shown to retain some oxygenic groups as a result of imperfect reduction. Therefore, rGO is also energetic, yet not as energetic as GO. DSC results suggest that GO takes up to 0.8 kJ g^{-1} of heat to trigger its deoxygenating reaction. Because the heavy addition of inert graphite impaired the energy output of the composite explosives, GO and rGO were promising candidates to replace graphite in insensitive high-energy PBX compositions.

On the one hand, GO and rGO act as space-qualified lubricants, which strongly improve the low-temperature performance of hypergolic ionic liquids by reduction of their viscosity.[166] However, matching the type of graphene to the specific ionic-liquid functionality is very important in achieving the optimum performance. On the other hand, GO and rGO enhance the ignition and burning properties of hypergolic ionic liquids. For example, it has been found that the laser ignition and burn rates of nitrocellulose (NC) microfilms can be enhanced upon doping with GO,[167] where a Nd:YAG (1064 nm, 20 ns) laser was used to ignite GO-doped NC films at low temperatures. The researchers studied several types of NC microfilms doped with different concentrations of GO, (*e.g.* 0.1 wt%, 0.5 wt%, 1 wt% and 2 wt%). Some of the morphologies of these films are shown in Fig. 18. The pure NC films are continuous, smooth, and homogeneous (Fig. 18a). After introducing GO into NC films, the morphology of the latter changes significantly and its surface becomes rough.

Moreover, an increase in the concentration of GO led to the formation of highly porous structures (Fig. 18b and c). AFM imaging and comparison of GO-doped NC containing 0.5 wt% of GO with that containing 1 wt% shows that the latter has larger pores with diameters from 0.5 μm to 3 μm (Fig. 18e).

In addition to burn rate enhancement, GO can also be used to decrease the sensitivity of energetic crystals. For instance, to improve the safety of 1,3,5,7-tetranitro-1,3,5,7-tetrazocine (HMX), GO was introduced by a solvent-antisolvent method (Fig. 19).[168] In a typical procedure, HMX was dissolved in DMF at 40 °C and then GO (about 2 wt%) was added. After GO was completely dispersed in HMX solution in DMF by sonication, the mixture was injected into CH_2Cl_2 (in which GO is much less soluble). After filtration, washing, and dying at 40 °C, the

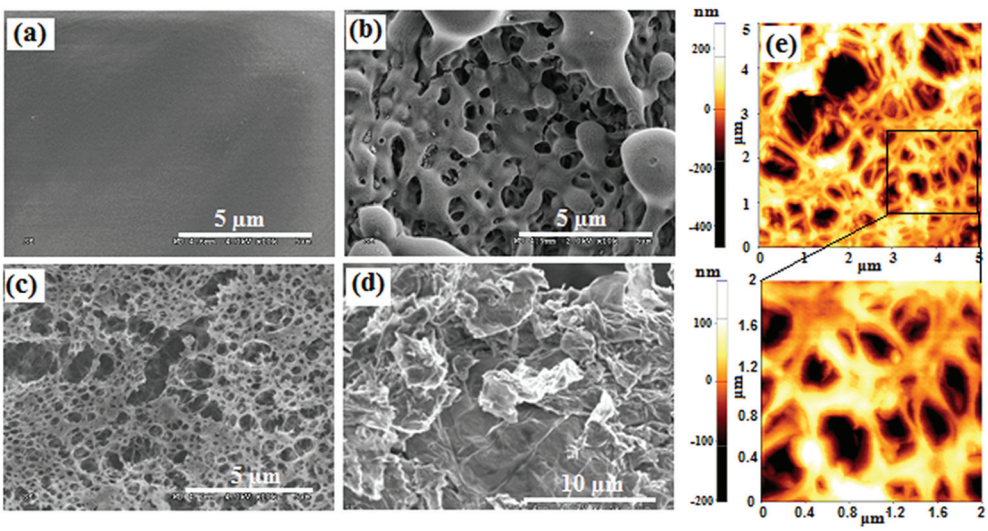

Fig. 18 SEM and AFM images of pure and GO-doped NC films. SEM image of (a) pure NC film, (b) 0.5%, and (c) 2% GO-doped NC film; (d) as-produced GO; and (e) AFM images of 1% GO-doped NC film. (Reproduced from Zhang *et al.*, *Appl. Phys. Lett.*, 2013, **102**, 141905.) Reprinted from ref. 165 with permission. Copyright © 2013, AIP Publishing LLC.

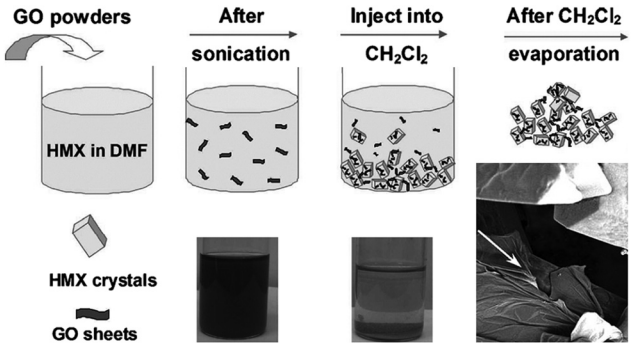

Fig. 19 Procedures for the formation of the HMX/GO composites. Reprinted from ref. 168; published with permission. Copyright © 2013, John Wiley & Sons, Inc.

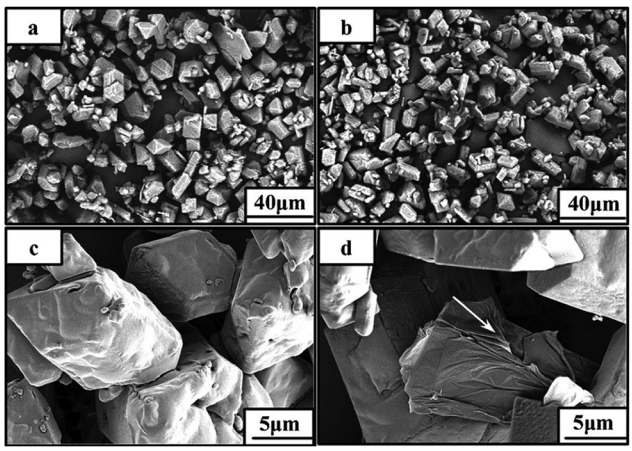

Fig. 20 SEM images of HMX and HMX/GO-2 at low-magnification (a, b) and high-magnification (c, d). Reprinted from ref. 168 with permission. Copyright © 2013, John Wiley & Sons, Inc.

HMX/GO composite was obtained. SEM images of this material are shown in Fig. 20. It can be seen that GO is not capable of changing the shape of HMX crystals. The morphology difference between HMX and HMX/GO was found to be considerable. The surfaces of unmodified HMX crystals are smooth and clean, while some wrinkles are observed in composite HMX/GO, which may significantly improve the safety of HMX. It was also shown that GO sheets exhibited an even better desensitizing effect than C_{60} and CNTs.

As well as simple coating of energetic crystals, GO can also be functionalized with energetic moieties. It has been reported that tetrazine derivatives can be covalently grafted to GO through nucleophilic substitution, forming a new type of material (FGs-Tz).[169] The general synthetic route, leading to the grafting of substituted chlorotetrazines to FGS_2, which is GO with a nominal C/O of 2, is shown in Scheme 11. The reactions of FGS_2 with chlorotetrazines take a long time (48 h) requiring a temperature of 120 °C. The reaction between Tz1 and FGS_2 was found to be unsuccessful and undesirable side reactions took place between the Tz1 and the other components of the suspension. It has been shown by DSC that the unmodified FGS_2 has a strong exothermic peak at ~230 °C due to rapid thermal reduction releasing H_2O vapour and CO_2. This exotherm was not present in thermally reduced FGS and in the FGS-Tz compounds, indicating that the FGS_2 was reduced during the reaction between chlorotetrazines and FGS_2. There might be an exotherm above 300 °C for FGS-Tz3 and FGS-Tz4, because the decomposition was not complete below that temperature.

It is, therefore, not clear whether these functionalized FGS-Tz can be considered as energetic materials. In contrast to the GO grafted with tetrazines, the pure tetrazines are less stable, indicating that GO has a stabilization effect on these tetrazine molecules. All the graphene, GO and rGO-based EMs and their preparation methods, together with their potential applications, are summarized in Table 5.

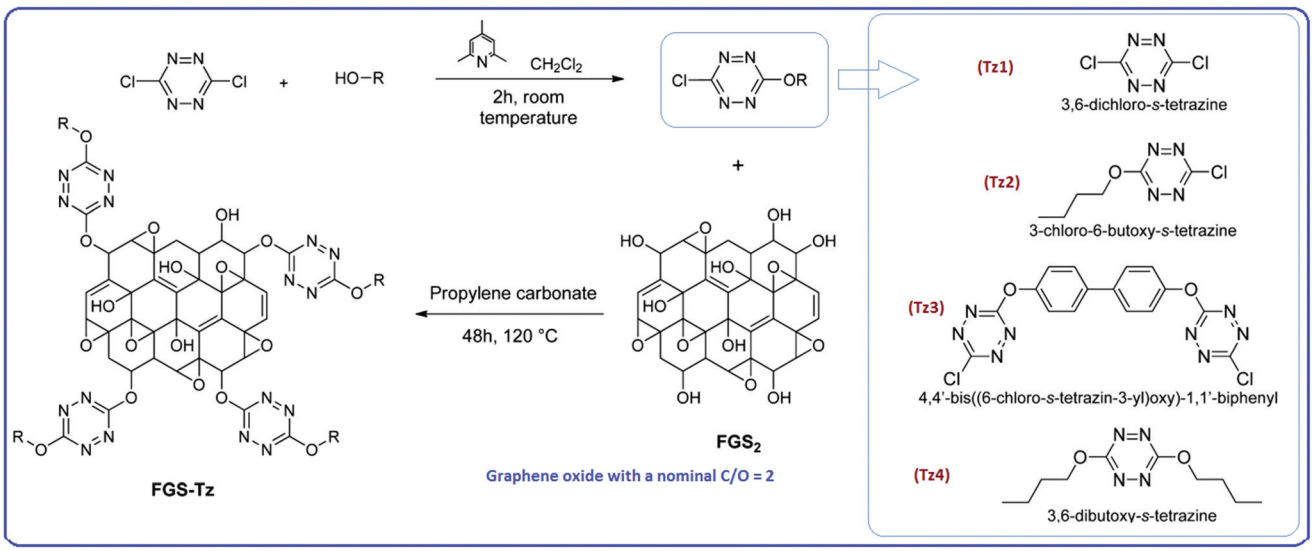

Scheme 11 General synthetic route leading to the grafting of substituted chlorotetrazines to FGS_2.[169]

Table 5 The preparation methods and applications of graphene, GO and reduced GO-based energetic materials

Materials	Preparation method	Applications	Contributors
GA/Fe_2O_3/AP	By a facile sol–gel method and supercritical carbon dioxide drying technique	Propellants	Lan *et al.* (2015)[158]
GA/AN	By a sol–gel and supercritical CO_2 drying method	Propellants	Lan *et al.* (2015)[160]
GO-Tzs	Tetrazine derivatives are covalently grafted to GO through nucleophilic substitution, at 120 °C for 48 h in propylene carbonate	Not clear	Li Y. *et al.* (2015)[169]
CL-20/GL/rGO	Graded CL-20 particles are coated with 551 glue by an emulsion polymerization method and then mixed with reduced GO	Energetic compositions	Yu L. *et al.* (2014)[265]
Al/Bi_2O_3/FGS	Formed in a colloidal suspension phase that ultimately condenses into ultra-dense macrostructures	Energetic devices	Thiruvengadathan *et al.* (2014)[161]
AP/GA	The nanostructured energetic composite is prepared by the sol–gel method	Solid propellants	Wang *et al.* (2014, 2012)[157,158]
GKPA	Prepared under the action of a crystalline controlling agent and modified by graphene	Energetics	Liu *et al.* (2014)[81]
HMX/GO	A two-dimensional GO was introduced to HMX by the solvent–nonsolvent method	Propellants and explosives	Li R. *et al.* (2013)[168]
GLS	Prepared either by adding graphene nanoplatelets (GNP) to the reaction solution or by coating normal lead styphnate (LS) with GNP	Primary explosives	Li Z. M. *et al.* (2013)[154]
GO/NC	Pure and GO-doped NC films are obtained through mixing pure NC–acetone solution and various weight ratios of GO water solution	Propellants	Zhang X. *et al.* (2013)[165]
GO/FOX-7	FOX-7 nanocrystals are synthesized in mesoporous carbon FDU-15 through self-assembly impregnation in *N*-methyl-2-pyrrolidone at 100–110 °C	Explosives and propellants	Cai H. *et al.* (2013)[163]

NdG, N-doped graphene; GA, graphene aerogel; AP, ammonium perchlorate; GKPA, graphene-doped ultrafine potassium picrate; FOX-7, 1,1-diamino-2,2-dinitroethylene; GL, 551 glue; FGS-Tz, tetrazine derivative functionalized GO with a nominal C/O of 2.

According to Table 5, graphene or its aerogels can be combined with either catalysts or oxidizers. The sol–gel method is commonly used for preparation of these materials. Pure GO and rGO are energetic but there are not many energetic nanomaterials or composites based on these yet, except for composites with HMX, NC and FOX-7. These energetic components were either deposited on the skeleton of GO or coated by thin layers of GO or rGO. All the above-mentioned composite materials are novel and were reported very recently. All these materials can be considered as promising candidate components for energetic compositions, as combustion catalysts or main ingredients.

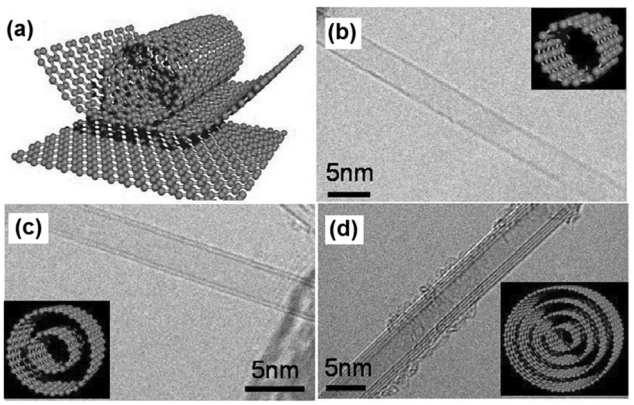

Fig. 21 (a) Schematic diagram of an individual layer of honeycomb-like carbon called graphene and how this can be rolled to form a CNT; (b)–(d) HR-TEM images of single-, double- and multi-walled carbon nanotubes (insets are their corresponding images). Reprinted from ref. 170 with permission. Copyright © 2006, International Union of Pure and Applied Chemistry.

EMs based on functionalized CNTs

New preparation methods for CNTs. CNTs can be visualized as rolled sheets of graphene (sp^2 carbon honeycomb lattice) (Fig. 21a), that are sometimes capped at each end of a tube.[170] They can be either single-walled, with diameters as small as about 0.4 nm (SWCNTs) or multi-walled, consisting of nested tubes (MWCNTs, *e.g.*, 2–30 concentric tubes, positioned one inside another) with outer diameters ranging from 5 to 100 nm (Fig. 21b–d). There are three possible CNT chiralities: zigzag, armchair and chiral, defined by their chiral angle and wrapping integers. For example, MWCNTs can be found in carbon soot on graphite anodes and may have more promising application potential than the SWCNT form. There are many different methods to synthesize CNTs, including electric arc discharge, laser ablation and CVD methods. However, currently the CVD method is the dominant one, which can be used with liquid, solid or gaseous carbon sources. This method should be used in combination with proper catalysts, pre-deposited in the form of thin layers on various substrates[171–175] or through vapor-phase catalyst delivery.[176–181]

CNTs can be endcapped by Cu and Fe nanoparticles for energetic and catalyst applications (Fig. 22). This is essential for large-scale production of high-purity SWCNTs,[182] double-walled CNTs (DWCNTs)[183] and MWCNTs.[184] Preparation of

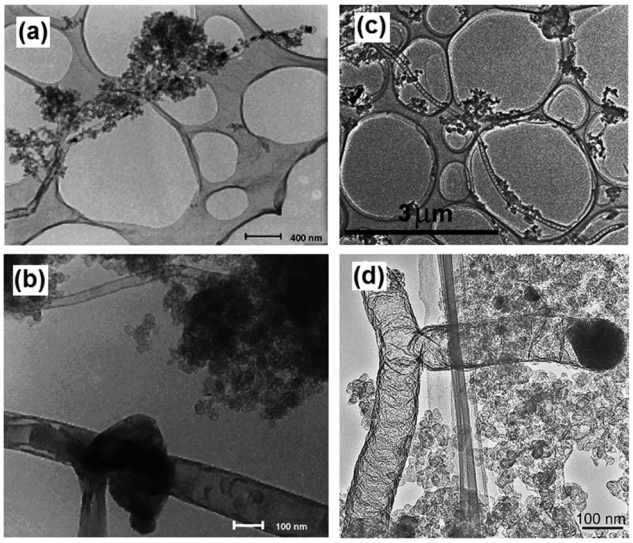

Fig. 22 TEM image of an end-capped CNT with Cu-particles (a), a tube-within-a-tube CNT (b), a segmented CNT with a length of a dozen microns (c) and a CNT–T-junction with a crystalline Fe-particle at its end (d). Reprinted from ref. 188 with permission. Copyright © 2004 Elsevier Ltd.

DWCNTs, with lengths of up to 2.2 mm, were achieved with a selectivity of 85% by precisely controlling the thickness of the iron catalyst.[183] A variety of aligned CNT structures have been prepared predominately on non-conducting substrates, posing limitations on applications where conductive substrates/contacts are required.[172,173,177] To circumvent this problem, aligned MWCNTs can be directly grown on Inconel 600 metallic alloy, using vapor-phase catalyst delivery.[185] Controlled synthesis has endowed SWCNTs with narrow distributions of tube diameter and a large fraction of a predetermined tube type.[186,187]

It is possible that CNTs formed in the detonation processes of the high-nitrogen compound, cyanuric triazide (TAT), contain a small number of nitrogen atoms. Elemental analysis showed that less than 3 wt% nitrogen was present when using a C/N-containing material as the precursor.[188,189] It was reported that the nitrogen atoms in CN_x nanotubes can be inhomogeneously distributed with enrichment of carbon on the external surface.[190] All tubes prepared using nickel, copper or steel cartridges were of a multi-walled type but the morphology and the yield depended on the metal. For Ti-based catalysts, no CNT formation was detected, indicating that this metal has no catalytic effect on nanotube formation. In addition to TAT, polyazidopyrimidines and metal/fluorocarbon pyrolants can also be used to prepare CNTs.[191,192] 2,4,6-Triazidopyrimidine (TAP) was found to be a good precursor for CNTs in the presence of $Ni(ClO_4)_2$. SEM and TEM images of CNTs generated by catalytic detonation of TAP are presented in Fig. 23. It can be seen that hollow-channel CNT structures, with lengths of 3–20 μm and diameters of 60–80 nm are obtained. The yield of CNTs is estimated to be greater than 90%. They have a bamboo-like morphology and these

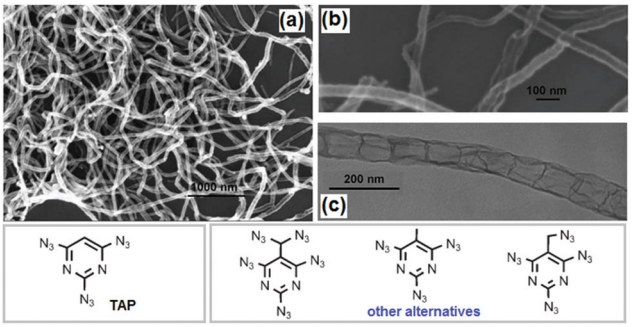

Fig. 23 SEM (a, b) and TEM (c) images of CNTs generated by catalytic detonation of TAP (other polyazidopyrimidines can be used for this purpose) (reproduced from Ye *et al.*, *Angew. Chem., Int. Ed.*, 2006, **45**, 7262–7265). Reprinted from ref. 191 with permission. Copyright © 2006, WILEY-VCH Verlag GmbH & Co. KGaA.

"compartmentalized nanotubes" are segmented with a relatively uniform length of about 90 nm. As well as the detonation synthesis method, SWCNTs and "carbon nano-carpet rolls" (CNCR) were found in the combustion residue of a pyrolant based on poly(carbon-monofluoride) (PMF, $(CF_x)_n$) and were rich in Mg particles.[192] More investigations should be done to clarify the mechanism of CNT formation during combustion of EMs. In addition to organized CNT structures, a variety of tailored structures with enhanced properties have been synthesized for special applications, such as: 1-D yarns, fibers, ropes and brushes, 2D sheets and buckypapers and 3D foams and sponges. 1-D nitrogen-containing CNTs (1-D NCNSs) have emerged in the past two decades as exceptionally promising nanomaterials due to their unique physical and chemical properties, which enable a broad range of applications in various fields of modern technology.[193] All these CNTs or NCNS materials can be used in the field of EMs in the following ways: (1) functionalized with polymeric binders, (2) coupled with pyrotechnics, (3) used as carriers of combustion catalysts, (4) combined with metal fuels and (5) functionalized with energetic moieties/groups.

CNTs functionalized with polymeric binders. Polymeric materials, especially energetic polymers, are very important ingredients in the composition of explosives and propellants. The functionalization of CNTs using energetic polymers may be a promising way to improve the performances of the corresponding energetic compositions. For example, recently, nano-modified energetic binder films were prepared from GAP using hydroxylated CNTs (CNT-OH) as a crosslinking agent and toluene diisocyanate (TDI) as a curing agent.[194] When the content of CNT-OH was 1 wt% and the *R* value (mole ratio of NCO and OH) was 1.4, the obtained binder film exhibited a tensile strength of 7.2 MPa with failure elongation of 375%, which is much higher than that of normal GAP binder film.

The thermal stability was also increased, while its glass transition temperature (T_g) was decreased to below −40 °C. Later on, another similar energetic binder – 3,3′-bisazidomethyloxetane-3-azidomethyl-3′-methyloxetane (BAMO-AMMO), covalently modified with CNTs was synthesized by the same

research group.[195] Their preparation schemes as well as SEM images of the obtained BAMO-AMMO films are shown in Fig. 24. During preparation, BAMO-AMMO random copolymer (or TME) was added to a reactor under a N_2 atmosphere, followed by mixing with TDI and dibutyltin dilaurate (DBD). The reaction mixture was then blended uniformly and cured at 60 °C for 7 days. Similarly to the GAP–CNT composite, upon using 1 wt% of CNT-OH with an R value of 1.4, the elongation ratio of the CNTs/BAMO-AMMO binder was increased to 380% and the tensile strength to 10.4 MPa, which was 82.5% higher than that of the traditional trimethylolethane (TME)/BAMO-AMMO energetic binder. However, the T_g of the CNTs/BAMO-AMMO binder (−34 °C) is slightly higher than that of GAP–CNTs.

In addition to energetic polymers, CNTs can also be used to enhance inert polymers such as fluoropolymer, which is a very important binder for PBXs.[196,197] The mechanical strength of PBXs needs to be improved for application in penetration warheads and nuclear bombs. MWCNT/fluoropolymer (F2314) composites were prepared *via* a melt blending process and the effect of the MWCNT content on the viscoelastic properties of MWCNT/F2314 were explored using a dynamic mechanical analysis (DMA) method.[198] It has been shown that at 80 °C and 0.1 MPa, when the MWCNT content was increased from 2 wt% to 20 wt%, the constant creep strain rate of MWCNT/F2314 composites was decreased by 84.7%.

CNTs coupled with pyrotechnics. It has been mentioned in the former section that one can use GO in pyrotechnic compositions to improve heat generation. For this purpose, CNTs as an analogue of GO could be more suitable. In fact, CNTs were introduced into pyrotechnics based on potassium perchlorate (KP) or potassium nitrate (KN) for the first time in 2009, using water-mixing and acetone-mixing methods.[199] The maximum reaction rate of KP was increased to 8.2 min^{-1}, which is about 4 times faster than that without CNTs. Moreover, its time to maximum rate was decreased to 52.1 min^{-1}, which is 56.4% lower than that of pyrotechnics without CNTs. The improvement for KP was not as significant as for KN. Generally, samples obtained from the water-mixing method are better but neither method is able to achieve contact of CNTs with KN at a molecular level.

In order to achieve the goal of molecular-level mixing, a new wet chemical method was proposed to embed KNO_3 in CNTs, forming uniform novel KNO_3/CNTs nanoenergetic materials.[200,201] The latter material can be integrated into a copper thin-film microbridge (CTFM) positioned on a glass substrate. It has been shown that the hollow cavities of the CNTs were filled with crystalline KNO_3 and that the entire surface of the micro-initiator was well distributed without significant agglomeration. Compared with single-layer CTFMs, the micro-initiator exhibited a more violent electrical explosion process than the micro-initiator without CNTs. Also, the CNT-containing micro-initiator had a longer duration electrical explosion and a higher peak temperature, due to enhancement of heat generation by CNTs. It has been shown that the decomposition heat of CNT-based micro-initiators is about 876.1 J g^{-1} (peak temperature: 386.8 °C). High-speed photography of the ignition process for these micro-initiators showed that fast chemical reaction of CNTs was involved in the electric explosion process, resulting in more heat release. Fig. 25 shows TEM images of KN/CNTs nEMs as well as SEM images of the sectional view and surface morphology of the micro-initiator, after electrophoretic deposition (EPD).

It can be seen in Fig. 25 that the KN nanocrystals homogeneously fill the hollow cavities of CNTs, without impurities attaching on the exterior wall. The average proportion of CNTs : KN is estimated as about 10 : 1 from TEM images. The bulk density of KN is 2.109 $g\ cm^{-3}$ and the density of MWCNTs is typically observed to be around the same as KN. It is clear that the KNO_3/CNTs nEMs tightly covered the CTFM. The whole surface was well distributed without significant agglomeration. The CNT arrays showed excellent electron field emission properties.[202] When KNO_3/CNTs nEMs were integrated with a CTFM deposited onto a ceramic substrate, the electro-explosion performance was greatly improved. This means that, due to the superior electric and thermal conductivities of CNTs, the enhanced chemical reaction of the KNO_3/CNTs nEMs is beneficial for the miniaturization of electro-pyrotechnics. In fact, there are several reported techniques for integrating EMs on an electronics or microelectromechanical system (MEMS) chip. These include modifications to the bulk substrate material, deposition of thin films and growth of nanotubes on the top of the substrate.[203]

The EMs systems involved are nanoporous energetic silicon, energetic CNTs and solution-deposited nitramines (*e.g.* RDX). As well as micro-ignitor applications, CNTs can also be used to stabilize the extremely sensitive new "green" primary explosives. Those that are currently used, such as lead azide (LA) and lead styphnate (LS), are very toxic and harmful to the people who work with them. Nowadays, more and more

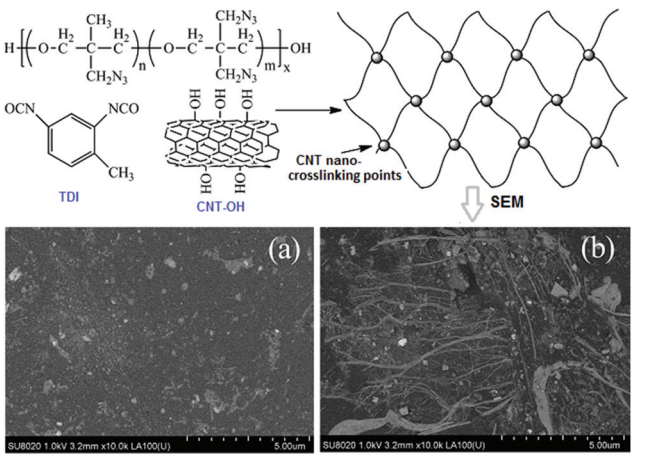

Fig. 24 Synthetic scheme for CNT/BAMO-AMMO thermoset polyurethane elastomer and its SEM images with different CNT mass fractions: (a) 0.5 wt% and (b) 1.0 wt%; (reproduced from Zhang *et al., J. Energet. Mater.*, 2015, **33**, 305–314.) Reprinted from ref. 195 with permission. Copyright © 2015 Taylor & Francis.

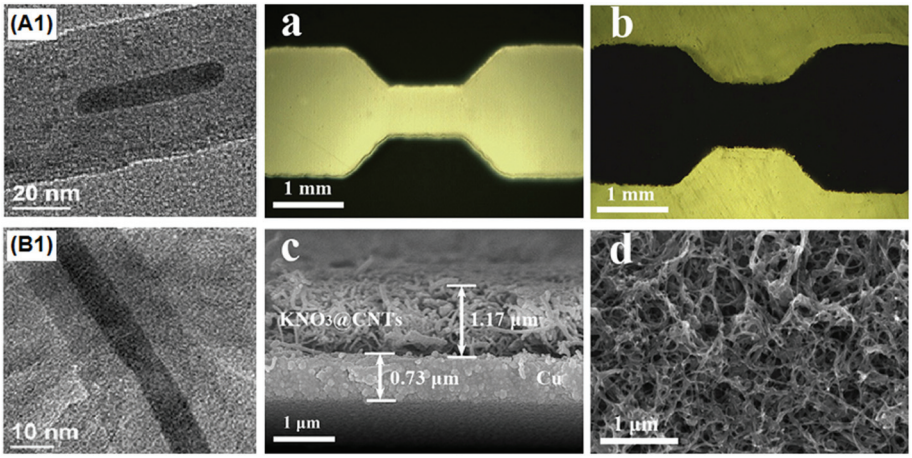

Fig. 25 TEM images of the KN/CNTs nano energetic materials (nEMs) achieved by wet chemical method (A1 and B1), showing the legible lattice stripe (B1); micrographs of the Cu thin-film microbridge (a), the micro-initiator after EPD (b); SEM images of the sectional view (c) and the surface morphology of the micro-initiator after EPD (d). Reprinted from ref. 200 with permission. Copyright © 2012 Elsevier B.V.

novel environmentally friendly EMs have been developed to replace LA and LS but many of the materials are simply too sensitive to handle. Copper azide (CA) is one of these cases and it detonates easily from electrostatic charges during handling. It has been found that the sensitivity of CA can be suppressed when it is encapsulated in conducting containers, such as anodic aluminium oxide (AAO)-templated CNTs.[204] The preparation procedure of CA/AAO–CNT composites and the morphologies of the involved intermediates are shown in Fig. 26.

It can be seen in Fig. 26 that the colloidal copper oxide nanoparticles (nano Cu–O) of ~5 nm are synthesized and fill CNTs with a diameter of ~200 nm, produced by template synthesis. The Cu–O inside the CNTs is reduced by hydrogen to elemental copper and reacts with hydronic acid gas to produce copper azide. It was found that upon ignition, the 60 μm long, straight, open-ended CNTs guide decomposition gases along the tube channels, without fracturing the nanotube walls. These novel materials are potentially useful as nano-detonators and "green" primary explosives. This is also the case for

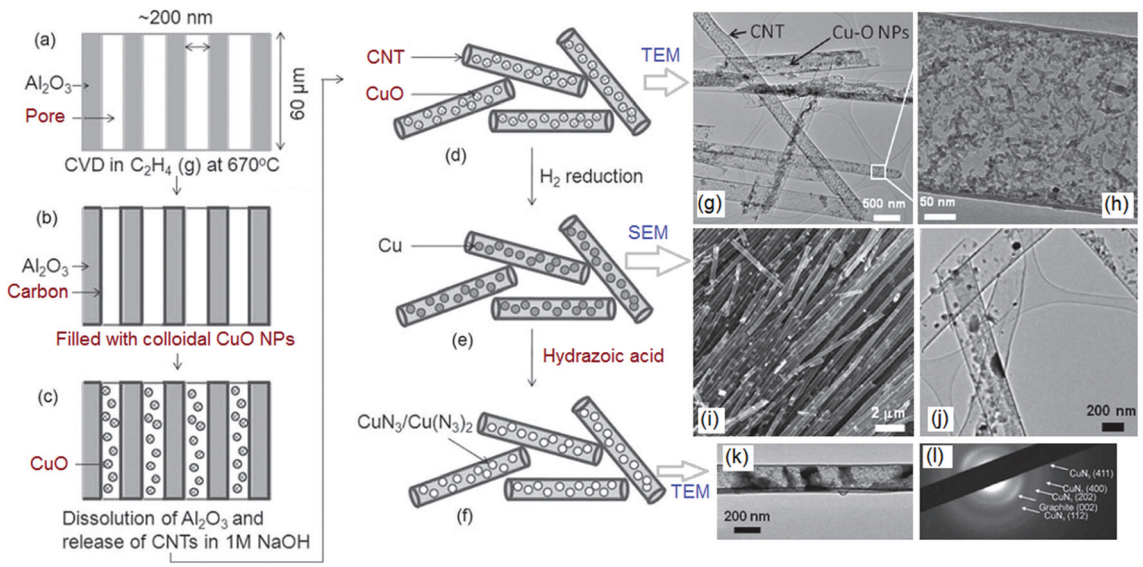

Fig. 26 Schematics of the chronological steps of the synthesis process: (a) commercial alumina membrane; (b) carbon-coated alumina membrane; (c) pores of the carbon-coated membrane filled with colloidal Cu–O NP solution; (d) Cu–O NP-filled CNTs after dissolution of the alumina membrane; (e) Cu NP-filled CNTs after H_2 reduction; (f) CA NPs inside the CNTs. (g) TEM image of Cu–O NP-filled CNTs, (h) an enlarged view showing rod-like NPs inside the CNT framed in (g); TEM micrograph of (i) $CuN_3/Cu(N_3)_2$-filled CNT and (j) SAED pattern of the CuN_3-filled CNTs. Reprinted from ref. 204 with permission. Copyright © 2010 WILEY-VCH Verlag GmbH & Co. KGaA.

BNCP, which can either be coupled with CB or encapsulated by CNTs (Fig. 27).[52]

The encapsulating material should be electrically conducting in order to dissipate electric charges and prevent detonation due to static electricity. If the CNTs are straight and open-ended, nanotube channels can potentially drive the shock waves along their lengths, increasing the efficiency of initiation of the secondary explosives, thus retaining the initiated particles within the nanotubes.[205] In addition to primary explosives, the properties of pyrotechnic compositions used in flashbang or solid state laser pump sources can also be modified by CNTs. To improve the pump efficiency of the $Zr/KClO_4$ pyrotechnic reagent, high strength CNTs with strong adsorption capacity were introduced.[206] It was shown that the inclusion of CNTs had a significant effect on the thermal behavior and light radiation energy. When the content of CNTs is 0.5 wt%, the total radiation energy of the pyrotechnics can reach 1830 J g^{-1}.

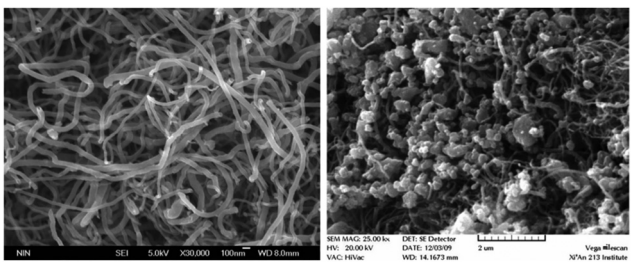

Fig. 27 SEM images of CNTs and BNCP/CNTs. Reprinted from ref. 52 published in *Chin. J. Energet. Mater.* (2013) with permission.

CNTs as carriers of combustion catalysts. Combustion catalysts can influence a radical chemical reaction by changing its mechanism; these are chemical compounds that can change the reaction pathway to products through routes with lower activation energies.[207] As a reagent, the amount of catalyst does not change during combustion. Heterogeneous catalysts catalyse gas-phase chemical reactions that take place on their surfaces. Preferably, to maximize the active surface of such catalysts, they should have a porous or nanoparticulate structure.

Regarding combustion catalysts for propellants, on one hand, they should maintain their activity during production of propellants, which means that the catalyst should be chemically compatible with various ingredients of the propellants.[208,209] On the other hand, the particle size of the catalysts should be as small as possible with a surface structure that can be uniformly dispersed in the propellant matrix. Nano-sized catalysts or additives are highly promising for improving the combustion performance of propellants but they are very active and need to be coated with inert materials. A combination of these nano-sized catalysts with CNTs was a promising solution. For instance, a nano Cu/CNT composite catalyst (see Fig. 28) was prepared by a liquid reductive deposition method, using CNTs as the carrier.[210] The researchers used $CuCl_2{\cdot}2H_2O$ as the source of Cu ions and KBH_4 as a reducing agent. The reaction was conducted at 50 °C with addition of disodium EDTA and PVP as surfactant and complexing agents. It has been shown that Cu/CNTs can remarkably decrease the peak decomposition temperature (T_p) of AP/HTPB propellant.

Similarly, a CuO catalyst can also be carried by CNTs, forming a novel CuO/CNT composite (black powder, Fig. 28).[211] Taking cupric acetate and CNTs as the reactants, CuO/CNTs can also be prepared by a solvent-infusion method

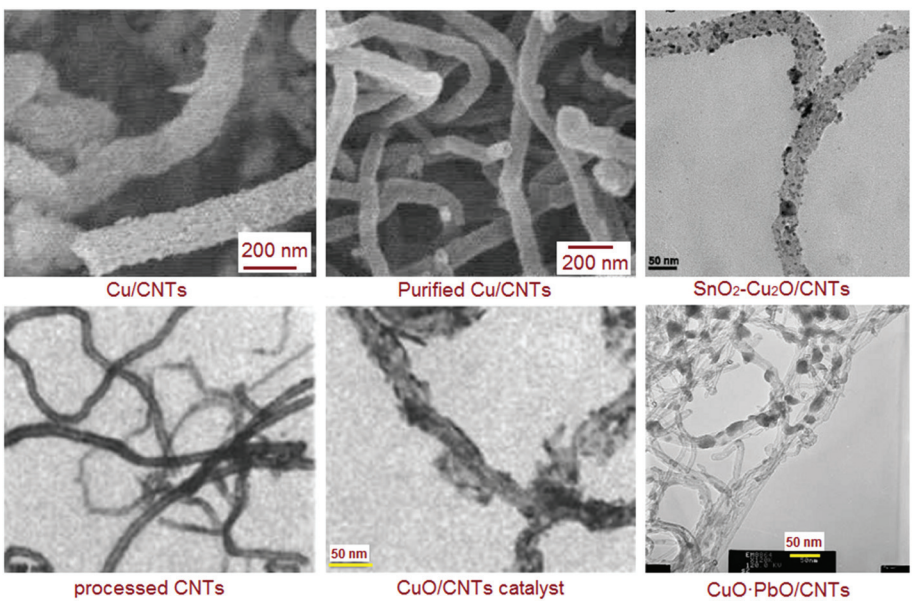

Fig. 28 SEM and TEM images of CNTs, Cu/CNT and CuO/CNT combustion catalysts. Reconstructed from several figures that appeared in ref. 210, 211, 215 and 216 with permission.

at normal pressure and at a temperature of 100 °C. The catalytic effect of this material on *N*-guanylurea-dinitramide (FOX-12 or GUDN) was found to be significant and the resulting composite material had excellent thermal stability and low sensitivity. In addition to the above-mentioned composites, metal fuels or catalysts can also be encapsulated inside CNTs. SWCNTs were proposed to be the best protective coating for energetic metal nanoparticles and as a base for propellant catalysts.[211] An advanced technology has been developed to prepare metalized CNTs using a CO_2 laser for ablation of the composite graphite target[212] or electroless deposition on top of MWCNTs.[213] SEM and TEM images of the resulting product, as well as its XRD spectra are shown in Fig. 29.

It can be seen in Fig. 29 that copper layers with an average thickness of 40 nm have been deposited on the surfaces of MWCNTs. This provides an effective means to fabricate powder metal-coated CNT composites. Based on this principle, Fe_2O_3/MWCNT composite particles were also produced by a mild physical absorption method using molten $Fe(NO_3)_3{\cdot}9H_2O$ as a precursor.[214] It has been shown that a large amount of hematite-phase Fe_2O_3 uniformly fills the MWCNTs, where the fraction of Fe_2O_3 is about 25.8 wt%. In fact, this concept is also applicable to binary catalysts. For instance, an SnO_2–Cu_2O/CNT composite catalyst was prepared by an integrative infusion method based on liquid-phase deposition, using $CuCl_2{\cdot}2H_2O$, $SnCl_4{\cdot}2H_2O$ and CNTs as reactants.[215] It was shown that SnO_2 and Cu_2O nanoparticles were uniformly attached on CNTs with oval morphologies and a layer thickness of 5–10 nm (Fig. 28). This has a positive catalytic effect on the decomposition of FOX-12, which can also be catalyzed by the aforementioned CuO/CNTs. The catalytic effects of these materials will be further discussed in a separate section, in conjunction with the thermal behavior of several other related materials.

Another binary catalyst that is widely used in solid propellants is CuO·PbO. The catalyst can also be modified by addition of CNTs, forming a CuO·PbO/CNT composite material by a microemulsion method.[216] The obtained catalyst has particle sizes below 50 nm (Fig. 28). In addition to copper and lead oxides, cobalt and aluminum oxides can also be deposited on CNTs for better catalytic activity. It was reported that a Co–Al mixed metal oxides/CNTs (CoAl-MMO/CNT) nanocomposite could be synthesized from a Co–Al layered double hydroxide/CNT composite precursor.[217] It has been shown that that in this nanocomposite, the cobalt oxide nanoparticles and Co-containing spinel-type complex metal oxides are well-dispersed on the surface of CNTs, forming a heterostructure of CoAl-MMO and CNTs, which has an excellent catalytic effect on energetic oxidizers such as AP.

CNTs combined with metal fuels. The Metal fuels are very important ingredients in energetic compositions. In solid rocket propellants, the most widely used elemental fuels are aluminium, boron and magnesium.[218,219] For explosives, Al is more effective than the others, especially in thermobaric compositions. The inclusion of CNTs in metal fuels may improve their combustion efficiency. The first attempt to combine metals with CNTs was made by Sylvain *et al.*, who invented novel flash-ignitable EMs based on metal fuels (including Pd, Fe, Ni, Co, Al, Cu, Zn, K, Na and Ti) in combination with CNTs or activated carbon.[220] Recently, Ag and Al particles were deposited on CNTs and the catalytic behavior of the resulting materials was investigated.[221,222] The Ag/CNT composites can be prepared by two methods: a silver mirror reaction and hydrothermal methods, where the former methodology uses $AgNO_3$ in ammonia solution (as the source of Ag) mixed with CNTs and formaldehyde and the latter reacts $AgNO_3$ in ammonia solution with CNTs dispersed in polyvinyl-pyrrolidone (PVP).[221] The contents of carbon in Ag/CNTs obtained from these two methods, were found to be different (Fig. 30); the former has 37.2 wt%, with a particle size of 29.3 nm and the latter has only 8.1 wt% (35.4 nm). A lower amount of CNT in a composition typically results in a higher energy content of the material.

As the most widely used metal fuel, Al has been intensively investigated regarding its oxidation and combustion behavior, which has a significant effect on the final performance of Al-containing propellants and explosives. Controlling the Al oxidation rate and temperature, as well as reaction enthalpy is important for its practical use. CNTs were introduced to Al initially for enhancing its mechanical strength, due to the

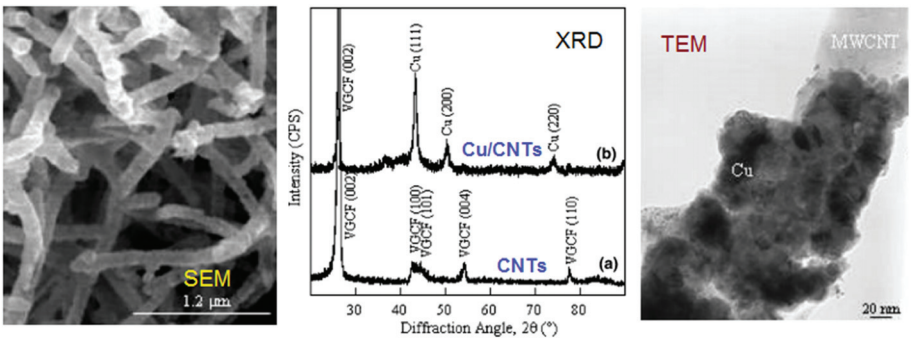

Fig. 29 SEM and TEM images and XRD spectra of CNTs and Cu/CNTs prepared by an electroless deposition method. Reprinted from several figures published in ref. 213 with permission. Copyright © 2004 Elsevier B.V.

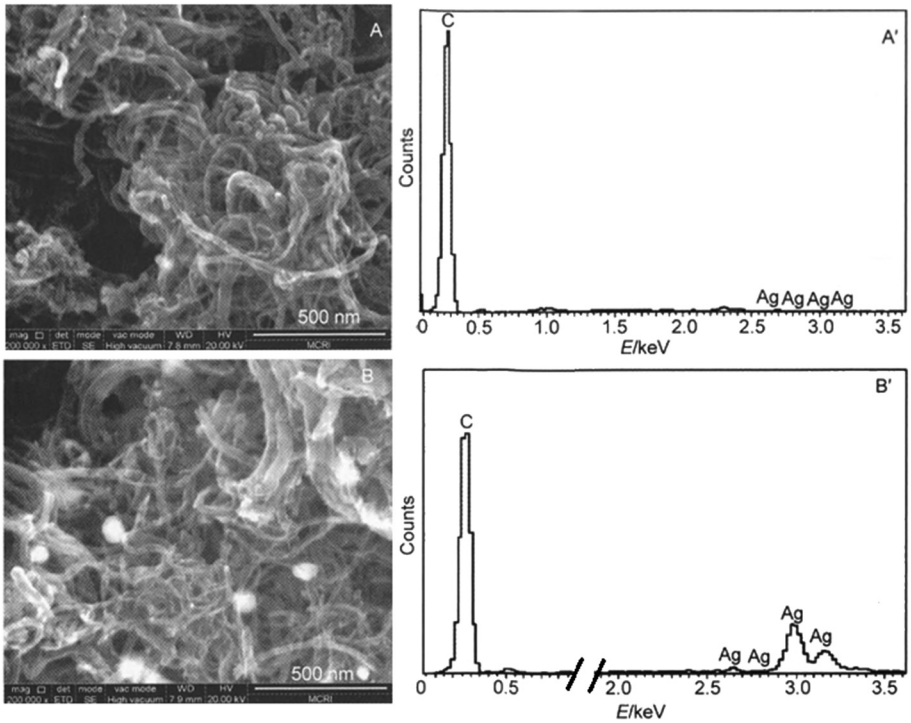

Fig. 30 SEM images (A and B) and EDS spectra (A′ and B′) of Ag/CNTs prepared by two different methods: (A) silver mirror reaction and (B) hydrothermal method. Reprinted from several figures published in ref. 221 with permission of *Acta Phys.-Chim. Sinica*.

large tensile strength of CNTs (150 GPa).[223–225] However, the thermal behavior could also be tailored by CNTs according to a recent report.[222] CNTs have several functions, which can be used to control the sizes and thermal properties of Al particles by changing the CNT content. Morphological modifications of Al/CNT mixtures during different stages of ball-milling of Al particles with CNTs are shown in Fig. 31. This figure shows the morphological changes that Al/CNT mixtures undergo with the progress of milling time. The morphology can be categorized into three types based on milling time: in Stage I, Al particles were coated by CNTs and spherical Al particles were distorted into platelets. In Stage II, Al particles disintegrated into smaller sizes and CNTs were partially embedded inside Al particles, giving them the appearance of sea-urchins, and in Stage III, Al/CNT particles aggregated into larger sizes with CNTs homogeneously dispersed inside the Al matrix.

CNTs functionalized with energetic moieties/groups. As described earlier in this paper, fullerenes can be functiona-

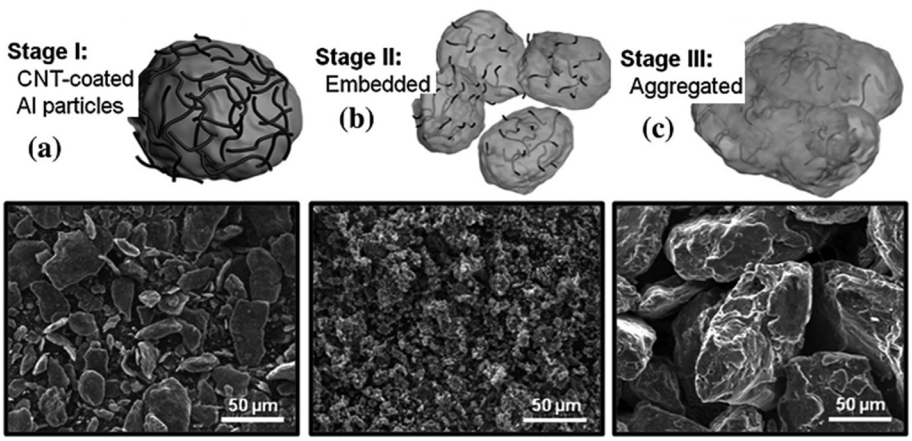

Fig. 31 Morphological modifications of Al/CNT mixtures with ball-milling time: (a) Stage I (30 min); CNTs coated on the surface of Al particles, (b) stage II (120 min); CNTs embedded inside Al particles while a portion of the CNTs remain on the Al surface, and (c) Stage III (180 min); Aggregation of Al particles with embedded CNTs inside. Reprinted from ref. 222 with permission of Crown copyright © 2013, Published by Elsevier Ltd.

lized with various energetic groups to from a new type of EM, which is also the case for CNTs, as another carbon allotrope. In 2003, metallic laser-synthesized SWCNTs were electrochemically functionalized with NO_2 groups. This modification was confirmed by Raman spectroscopy.[226] The nitration process was carried out by acidification of CNTs to form –COOH groups on their surface and was followed by reaction of the resulting material with thionyl chloride and then with 4-nitroaniline.[226,227]

In addition to NO_2 groups, many other energetic groups can be introduced to CNTs. In fact, SWCNTs modified with tetrazolyl groups (SWCNTs-CN_4) were prepared by a diazo-reaction, where covalent bonds were formed to maintain the structure of the five-membered ring.[228] It was confirmed by X-ray photoelectron spectroscopy (XPS) that the nitrogen content in this SWCNTs-CN_4 material was about 14.8%, while the ratio of tetrazolyl groups to carbon atoms was about 4.9%. Similarly, on the basis of diazonium chemistry, SWCNTs can be decorated with nitrobenzenes, *via* microwave irradiation of the reaction mixture.[229] It has been found that even covalent functionalization introduces defects that could reduce conductivity and that thermopower waves rapidly propagate along fuel-coated decorated nanotubes, producing electrical power. A schematic representation of reaction propagation on a SWCNT decorated with trinitrobenzenes and the reaction conditions required to produce different nitrobenzene-functionalized SWCNTs, as well as their Raman spectra and DSC thermograms are shown in Fig. 32. It is clear that the energy from a chemical reaction at one end propagates through the 1-D conductor, initiating reactions in the attached molecules at the wave-front. The energetically decorated SWCNTs appear to generate considerable heat when decomposing at high temperatures. It can be seen from Fig. 32d that MNP-, DNP- and TNP-SWCNTs can undergo exothermic reactions between 300 and 330 °C during linear heating, except for the BrP-SWCNTs (functionalized with a non-energetic 4-bromophenyl group).

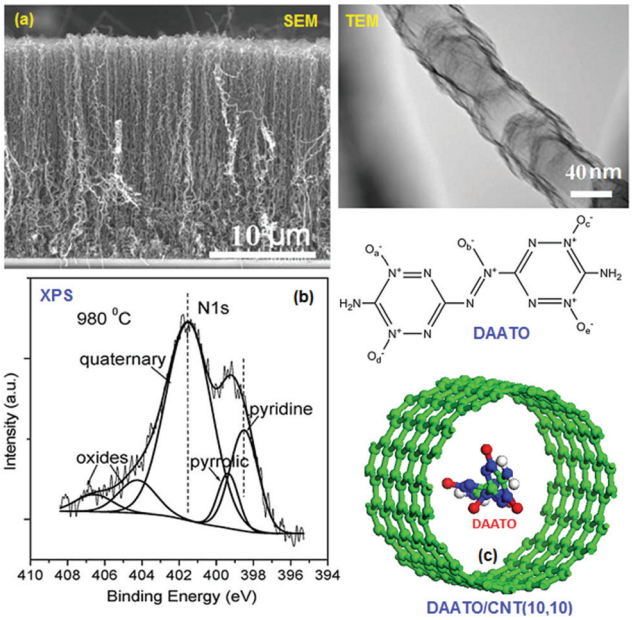

Fig. 33 SEM and TEM images for the morphology (a), N 1s XPS spectra (b) of N-CNTs synthesized at 980 °C and the structural geometry of DAATO/CNT (10, 10) (c). Recombination of several figures from ref. 232 reprinted with permission. Copyright © 2009 Elsevier Ltd.

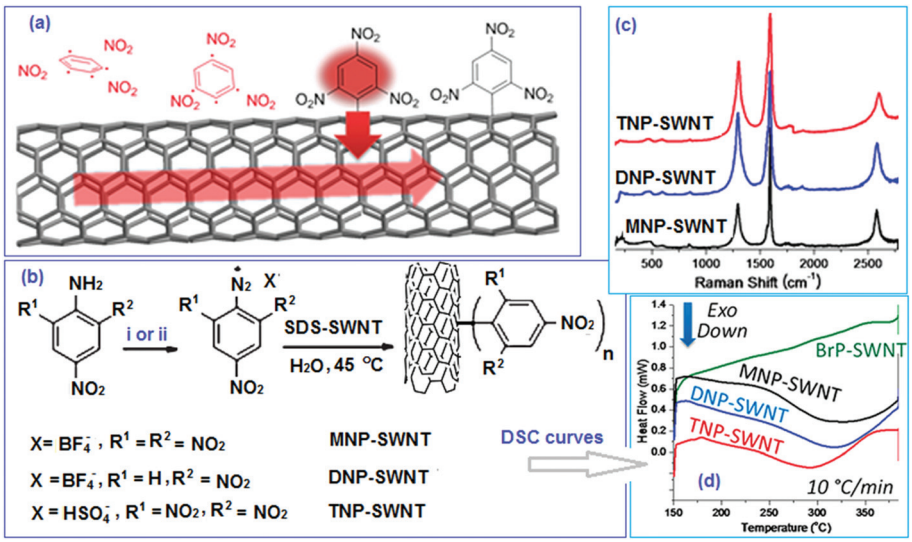

Fig. 32 (a) Schematic representation of reaction propagation on a single-walled carbon nanotube decorated with trinitrobenzenes; (b) synthesis of nitrophenyl-SWCNTs *via* diazonium reactions, where "i" represents $NOBF_4$, acetonitrile, 0 °C, 4 h (for MNP- and DNP-SWNT) and "ii" denotes $NOHSO_4$ ($NaNO_2$ + H_2SO_4), H_2O, room temperature, 3 h (for TNP-SWCNT); (c) Raman spectra of energetically decorated SWCNTs with modes at 1200 cm^{-1} increased in the Raman spectra after covalent functionalization (excited at 785 nm); (d) DSC curves at 10 °C min^{-1} under nitrogen where all the nitrophenyl-SWCNTs decompose with slow heat release, whereas the BrP-SWCNTs do not release heat at all. Recombination of several figures from ref. 229 reprinted with permission. Copyright © 2011, American Chemical Society.

In addition to covalently functionalized CNTs with energetic groups, energetic compounds can non-covalently functionalize CNTs *via* doping or adsorption. For instance, BNCP can be doped with CB or CNTs,[52] whereas TATB can be adsorbed by CNTs.[230] Theoretical calculations show that TATB deforms remarkably when it is non-covalently attached to the surface of CNTs, especially on their inner wall. The diameter of the CNT determines the distortion degree of the TATB molecule inside but it has little effect on the deformation of a TATB molecule bound to the outside of the CNT. Non-covalent combination of TATB with CNTs is exothermic due to the negative adsorption energy. TATB adsorption on the inner wall of CNTs was energetically more favourable than that of adsorption on the outer wall. In both cases, more stable adsorption occurs as the diameter of the nanotube increases. As a comparison, these researchers also theoretically investigated the structure, adsorption energy and initial dissociation reaction of the energetic 3,3′-diamino-4,4′-azofurazan (DAAzF), assembled inside or outside SWCNTs.[231] They found that most of the adsorption processes of SWCNTs with larger diameters are exothermic and thermodynamically favourable, indicating that DAAzF spontaneously assembles inside the CNTs. Based on these theoretical findings, CNTs were successfully used as a host for some high-nitrogen content compounds. For instance, CNTs (10,10) were selected as a nanoscale matrix to host *N*-oxides of 3,3′-azo-bis(6-amino-1,2,4,5-tetrazine) (DAATO) molecules,

Table 6 The preparation methods and application areas of CNT-based energetic materials

CNT based EMs	Preparation methods	Applications	Contributors
SWCNTs-CN_4	Prepared by a diazo-reaction on the wall of SWCNTs	Energetic materials	Ji *et al.* (2015)[228]
MWCNT/F2314	Obtained from the melt blending of fluoropolymer and MWCNT mixture	PBXs, pyrotechnics	Lin *et al.* (2015)[198]
KNO_3/CNTs	By mechanically mixing and grinding to nanosize	Energetic initiator	Guo *et al.* (2012[200] and 2014[202])
Zr/$KClO_4$/CNTs	By grinding a mixture of Zr and $KClO_4$ for 20 min	Pyrotechnic reagent	Liu *et al.* (2015)[206]
CNT/BAMO-AMMO	Using CNT-OH as a crosslinking agent, covalently modified BAMO-AMMO	Energetic binder	Zhang *et al.* (2013[194] and 2015[195])
Fe_2O_3/MWCNTs	By mild and superior physical absorption method using molten $Fe(NO_3)_3{\cdot}9H_2O$ as the precursor	Thermites, pyrophoric substrates	Assovskiy *et al.* (2009)[212] and Wang *et al.* (2014)[214]
GAP/CNTs binder films	Using hydroxylation CNTs as crosslinking agent, GAP as prepolymer, TDI as curing agent	Propellants, PBXs	Zhang *et al.* (2013)[194]
Al/CNT composites	Al/CNT mixture was engineered by mechanical pulverization	Thermites, propellants	Jeong *et al.* (2013)[222]
Nano BNCP/CNT	Prepared from tetraamine BNCP doped with CNTs	Detonators, pyrotechnics	Chen *et al.* (2013)[52]
CoAl–MMO/CNT	Synthesized from Co–Al layered double hydroxide/CNTs precursor	Propellant catalyst	Fan *et al.* (2013)[217]
HMX/CNTs	Prepared with an ultrasonic compositing method	Energetic compositions	Zeng *et al.* (2012)[248]
Ag/CNTs	Using silver mirror reaction and hydrothermal methods	Explosive catalyst	An *et al.* (2012)[221]
Al/Teflon/CNTs	By blending of Al with Teflon and CNTs	Energetic binder	Kappagantula *et al.* (2012)[277,278]
Nitro-SWNTs	Prepared by chemical transformation of the carboxylic acid groups introduced on the wall of CNTs	Energetic materials	Forohar *et al.* (2012)[227]
HMX-P/MCNTs	HMX-polymeric binder system doped with a small mass fraction (1 wt%) multiwalled CNTs or graphite	Microwave materials	Zeng *et al.* (2012)[248]
NB-SWNTs	Single-walled CNTs decorated with mono-, di- and tri-NB *via* diazonium chemistry	Thermopower wave generators	Abrahamson *et al.* (2011)[229]
SnO_2–Cu_2O/CNTs	Prepared by integrate infusioning with liquid phase deposition under normal temperature and pressure using $CuCl_2{\cdot}H_2O$, STP, and CNTs as the reactants	Explosive catalyst	Zhang *et al.* (2011)[215]
AAO/CNTs	AAO is simply mixed with templated CNTs	Nano-detonators	Pelletier *et al.* (2010)[204]
Nd-CNTs	Synthesis from nitrogen-doped CNTs using chemical vapor deposition method	Energetic components	Zhong *et al.* (2010)[232]
PbO·CuO/CNTs	Prepared *via* a microemulsion process	Catalyst for propellants	Ren *et al.* (2010)[216]
MSWCNT	Using a CO_2 laser for ablation of the composite graphite target	Catalyst for propellants	Esawi *et al.* (2010)[225]
CuO/CNTs	Using sol-infusion method under normal pressure and low temperature (at 100 °C)	Catalyst for propellants	Liu *et al.* (2008)[210]
Nano Cu/CNTs	By liquid reductive deposition method and using the carbon nanotubes as the carrier	Catalyst for propellants	Liu *et al.* (2008)[211]
NA/SWNTs	Functionalization is achieved on CVD-produced SWNTs by acidification to –COOH followed by reaction with TC, and then NA	Energetic component	Wang *et al.* (2003)[226]

CNT-OH, hydroxylated CNTs; BAMO-AMMO, 3,3′-bisazido methyloxetane-3-azidomethyl-3′-methyloxetane; TDI, toluene diisocyanate; TNB, trinitrobenzene; STP, stannic tetrachloride pentahydrate; AAO, anodic aluminum oxide; BNCP, bis(5-nitrotetrazolato) cobalt(III) perchlorate; TOC, thionyl chloride; NA, 4-nitroaniline.

using a CVD (chemical vapor deposition) method for obtaining so-called nitrogen-doped CNTs (N-CNTs).[232] Their SEM and TEM images, as well as XPS spectra are shown in Fig. 31. It has been stated that the DAATO contains an average of 3.2–3.6 oxygen atoms per molecule,[233] resulting in five possibilities for positioning and quantifying oxygen atoms per molecule (Fig. 33c).

The diameter and growth rate of these novel hybrid materials are obviously temperature-dependent. It has been found that a single N-CNT has a diameter of 60 nm when its preparation temperature is 980 °C (Fig. 33), while the diameter is only around 30 nm at 800 °C, because as temperature decreases, agglomeration of the catalyst reduces, resulting in thinner N-CNTs. It has also been shown that a lower synthesis temperature usually results in curled and disordered graphitic layers but a higher temperature favours the formation of a better-organized layered graphitic structure.[234] N-CNTs have a nitrogen content of 10.4% when the temperature is 800 °C. As well as tetrazine, triazole moieties can also be used to functionalize MWCNTs using 'click' chemistry.[235] The resulting product was successfully incorporated into a polyurethane (PU) matrix by *in situ* polymerization, where interactions with the PU polymer were enhanced. As a result, the heat of decomposition of the PU/MWCNTs nano-composites was significantly increased due to inclusion of triazole moieties.

In addition to the above-mentioned CNT-based energetic materials, more and more novel EMs are under development. As a comparison, the preparation and applications of existing CNT-based EMs are summarized in Table 6. It can be seen that most functionalized CNTs are used for catalysts or energetic additives of propellants and explosives due to their relatively lower energy content and promising catalytic activity. Several of them can be used as ingredients of pyrotechnics, such as thermites and ignitors. The preparation procedures for these materials are typically facile, including microemulsion, hydrothermal, reductive deposition, ultrasonic and CVD, as well as straightforward chemical reaction methods. Combination of CNTs with sensitive EMs provides a way to improve the sensitivity and performance of the parent EMs. It has been reported that N-doping of CNTs can create well-localized and highly active sites on the CNT surface.[236] When CNTs are filled with highly EMs, *e.g.* a polymeric nitrogen chain, an effective electric field is created between the CNT surface and the nitrogen chain with a minimal C–N distance. This inclusion process stabilizes the highly energetic polynitrogen chain, which is unstable under ambient conditions.[237] This approach helps in the utilization of highly unstable EMs.

Effects of CNMs on performances of EMs

Catalytic decomposition, ignition and combustion

CNMs-promoted thermal decomposition of EMs. It is essential to evaluate the thermal properties of newly developed energetic ingredients of propellants, explosives and pyrotechnics, since these parameters have intrinsic connections to the combustion and detonation performances of the final compounds made from these new materials.[238–242] Several parameters need to be evaluated, including thermal stability, heat of decomposition, activation energy (E_a) and reaction models as well as chemical pathways of thermolysis.[243–247] As mentioned above, CNMs have large SSAs, excellent thermal conductivity and superior electroconductivity. Therefore, they are capable of promoting thermochemical reactions, for example, catalyzing the decomposition of energetic compounds including RDX, HMX and AP. The new nEMs based on functionalized fullerene, CNTs and graphene can either be used as catalysts or main energetic ingredients in explosive charges and propellants.

It was found from the decomposition of HMX/CNT composites that the CNTs reduced the decomposition E_a and the peak temperature (T_p) of HMX.[248] About 1 wt% of CNTs in this mixture reduced the E_a of HMX by more than 70 kJ mol^{-1}, resulting in a higher decomposition rate. However, the heat of decomposition and T_p of HMX decreased as the CNT content increased. Similar research has been carried out for hexanitrohexaazaiso wurtzitane (CL-20) and aminonitrobenzodifuroxan (CL-18) using DSC and TG techniques.[249,250] It was shown that CNTs also bring down the initial thermolysis temperature of these explosives. It was suggested that the reason for this phenomenon is that CNTs promote homolytic scission of the N–NO bond, thereby promoting formation of NO$^{\bullet}$ free radicals. This is also the case for AP-based compositions, where the decomposition rate of AP has been raised above its typical onset temperature.[251]

In fact, the porous structure of CNT bundles, having a very large SSA, can be considered as a combustion catalyst nanocarrier, forming many types of highly-promising composite catalysts. The synergistic effect of the CNTs with the catalysts greatly improves catalytic activity and the agglomeration problem of nano-sized catalysts can also be resolved. For instance, the catalyst Ag/CNTs can change the thermal decomposition mechanism of RDX, where the dominant liquid phase reaction changes to a faster gas-phase reaction, resulting in a lower T_p.[221] The effect is also similar for a PbO–CuO/CNT composite catalyst,[230] which has a greater influence on the thermal decomposition of RDX compared to the parent PbO–CuO. Another two nano-catalysts, CuO/CNTs[231] and SnO_2–Cu_2O/CNTs,[239] were also shown to decrease the T_p of FOX-12 decomposition, meanwhile the heat release and E_a were decreased accordingly. When CNTs are used to encapsulate energetic molecules, such as nitromethane (NM), they form a NM/CNT composite material, which has very different thermal behavior in comparison with the parent NM.[252] It has been shown that a transition state (TS) exists for the thermal decomposition of NM/CNT (5, 5), while there is no TS for dissociation of a C–N bond in the gas phase of a "stand-alone" NM molecule.[253] In fact, SWCNTs can change the molecular structure and electronic charge of the NO_2 and CH_3 groups of NM during its decomposition. The energy barrier of the TS (in the CNT-bound NM) was calculated to be about 198 kJ mol^{-1},

which is 21 kJ mol^{-1} lower than that of the aforementioned C–N dissociation of free NM. Meanwhile, the energy barriers for the nitromethane–methyl nitrite rearrangement and H-migration, as well as C–N homolytic dissociation are significantly decreased.[254,255] This is also the case for nitramide encapsulated in SWCNTs.[256] Regarding some other ingredients of composite propellants, CNTs have little effect on the thermal decomposition of phase-stabilised ammonium nitrate (PSAN) and GAP, while they were shown to stabilize HTPB binder.[257]

The thermal behavior of ADN is greatly affected by CNT-based catalysts. For instance, Fe_2O_3/CNTs and Fe·Cu/CNTs decrease the decomposition T_p of ADN by 12.1 °C and 11.6 °C, respectively, when just 1 wt% of the catalyst is used.[258] These results were observed when a large amount of hematite phase Fe_2O_3 uniformly filled the MWCNTs and the mass fraction of Fe_2O_3 in such a composite was about 25.8 wt%.[204] In the presence of 10 wt% Fe_2O_3/MWCNT composites, the second T_p of AP decreased by 116 °C and the first exothermic peak disappeared with a 200 kJ mol^{-1} decomposition heat increase.

Graphene, a two-dimensional carbon crystal with monoatomic thickness, is considered to be a basic structural unit of CNTs and graphite. It also has a large SSA and can form many complexes with energetic molecules. Ni/graphene nanocomposites were prepared *via* a one-step mixing method and then their catalytic effect on the thermal decomposition of AP was investigated.[259] It was shown that when the content of Ni/graphene composites is about 1% of the mixture, the catalytic effect is the most significant. In this case, the second decomposition peak temperature decreased by 97.3 °C, while the first peak disappeared. Later, these researchers used the same methodology to prepare a complex of Mn_3O_4 nanoparticles with graphene, which also exhibited a significant catalytic effect on AP decomposition.[260] Similarly, two decomposition peaks in the latter AP formulation merged into one peak. Meanwhile, the T_p was reduced by 141.9 °C, as a result of the synergy between Mn_3O_4 and graphene. In contrast to graphene, GO has functional groups on its surface, It is easier to combine with other substances, extending the range of application of GO-based materials. It was reported that CuO/GO nano-composites prepared from a water/isopropanol solvent are very effective in catalyzing AP decomposition and combustion.[261] In addition, when some other groups were introduced to GO, the catalytic activity was significantly improved. For instance, nitrated GO decreased the T_p of AP decomposition by 106 °C,[262] while the heat of decomposition increased from 875 to 3236 J g^{-1}.

The thermal properties of AN oxidizer, frequently used in propellants and emulsion explosives, can also be modified by integration with CNMs.[263,264] When AN was mixed with activated carbon (AC) or CNTs, violent reactions took place upon its melting. However, mixtures of AN with graphite or fullerene showed only mild exothermic peaks (decomposition), similar to those of pure AN. It was also found that the formation of carbon dioxide was more distinct for AN/AC and AN/CNT mixtures than for other mixtures. When BNCP was doped with CB, its T_p decreased from 289.9 to 276.7 °C, while after doping BNCP with CNTs, the T_p was significantly further reduced. There was an obvious endothermic peak and as the nanotube diameter decreased, the decomposition peak for BNCP became narrower and sharper, accompanied by a disappearing shoulder.[52] In order to compare the thermal behavior and catalytic effects of different CNM-based EMs, the thermal decomposition data, as well as the kinetic parameters of all above-mentioned materials are summarized in Table 7.

As shown in Table 7, addition of flake graphite to ε-CL-20 induces slightly earlier decomposition of this explosive with much lower heat release, while the addition of GO or rGO to ε-CL-20 enhanced the decomposition of an ε-CL-20/glue formulation with remarkable improvement in the heat release.[265] However, only rGO additive could improve the thermal stability of ε-CL-20. Catalysts based on fullerene (CBF) reduced the decomposition T_p and apparent E_a and raised the exothermic heat of FOX-12. When the mass ratio of CBF/FOX-12 is 1-to-5, the decomposition T_p of FOX-12 is reduced by 20.3 °C, while the heat release is increased by 332 J g^{-1}. The corresponding values are 18.08 °C and 148 J g^{-1} for pure CBF.[215] Similarly, the catalytic effect of the Ag/CNT nanocomposite on the thermal decomposition of RDX was investigated by DSC. It was indicated that the irregularly globose nano-Ag particles, evenly attached to the surface of the CNTs, form a promising catalyst for RDX, greatly accelerating the decomposition rate of RDX, with a reduced E_a. This is also the case for a PbO·CuO/CNTs catalyst, which can accelerate the decomposition of RDX and reduce the T_p by 14.1 °C.[216] The nDs can also slightly reduce the T_p of RDX.[81] In contrast, when a fullerene-based catalyst (mNPF) is added to RDX, its T_p drops from 240.4 °C to 234.0 °C and the corresponding exothermic heat increases from 499.5 to 891.8 J g^{-1}. There is another fullerene-based catalyst, FED, whose catalytic effect has not yet been studied. It was shown that FED started to decompose at 150 °C with a T_p of 203 °C and an enthalpy of 1037.7 J g^{-1}. The total mass loss of FED in the temperature range 100–800 °C is 49.7%, with intense decomposition of $-N(NO_2)_2$ and partial decomposition of the branched chain.[114] It was further found that FHN can also accelerate the decomposition of RDX and HMX. The peak temperatures of the exothermal decomposition of these nitramines were reduced[117] and the corresponding E_a of RDX was decreased by 17 kJ mol^{-1}, while that of HMX was reduced by more than 20 kJ mol^{-1}. In addition to stabilizing common explosives, CNTs also have a significant influence on the stability of energetic binders. For example, the onset temperature of the CNTs/BAMO-AMMO composition was measured to be 236 °C, which is 7 °C higher than that of the corresponding TME/BAMO-AMMO energetic binders.[195]

It was recently reported that energetic derivatives of C_{60}-fullerene have very unique thermal properties. For instance, MTNBFP has a very high standard molar enthalpy of formation and could be a highly-promising new candidate for primary explosives.[113] The most probable initial dissociation path for MTNBFP is the release of NO_2 according to dynamic dissociation energies, which are 58.5, 172.5 and 239.2 kJ mol^{-1}.

Table 7 A summary of thermal behavior and decomposition kinetic parameters of various CNM-based EMs

	Exothermic peaks (10 K min^{-1})			Kinetic parameters (Kissinger)		
Samples	T_o/°C	T_p/°C	ΔH	E_a	Ln (A)	Contributors
ε-CL-20/glue	231.2	250.5	1495	Na	na	Yu *et al.* (2014)[265]
ε-CL-20/glue/G	233.0	247.7	1027	Na	na	
ε-CL-20/glue/GO	217.2	234.3	1678	Na	na	
ε-CL-20/glue/rGO	234.3	250.6	1613	Na	na	
RDX	216.7	222.6	na	171.7	40.84	Guan *et al.* (2014)[114]
GAP/FHN	112.5	154.9/242.0	na	Na	na	
RDX/FHN	212.6	218.7	na	154.8	36.94	
HMX	277.3	283.8	na	358.2	76.95	
HMX/FHN	279.2	281.6	na	334.7	72.11	
RDX	208.7	240.4	499.5	174.0	36.38	Jin *et al.* (2014)[114]
RDX/mNPF	206.4	234.0	891.8	166.8	35.00	
HMX	276.3	278.1	—	470.6	—	Zeng *et al.* (2012)[248]
HMX/CNTs	273.2	275.9	—	397.6	—	
PF	160.2	189.7/247.0	2017.7	Na	na	Cataldo *et al.* (2013)[113]
FED	150.3	202.9	1037.7	Na	na	Chen *et al.* (2014)[114]
FEN	100.0	172.3/360.5	na	Na	na	
FPL	151.3	243.6/473.2	na	Na	na	Guan *et al.* (2014)[114]
FPL/RDX	189.3	206.1	na	140.8	34.95	
FGAP	100.3	154.9/242.0	na	Na	na	Huang *et al.* (2015)[121]
FPGN	435.2	473.3/615.3	1280	170.9	36.43	Gong *et al.* (2015)[120]
BNCP	269.6	289.9	na	Na	na	Chen *et al.* (2013)[52]
BNCP/CB	260.7	276.8	na		na	
BNCP/CNTs	263.1	280.1[a]/277.8[b]	na	Na	na	
BNCP/SWCNTs	262.2	278.0	na	Na	na	
FOX-12	206.3	218.5	1540	258.3	59.30	Liu *et al.* (2008)[210,211]
FOX-12/CCNT	189.5	198.3	1872	178.6	42.24	
FOX-12/SCCNT	192.4	204.1	1150	181.2	45.62	Zhang *et al.* (2011)[215]
RDX/PCC	208.2	226.9	na	100.7	26.29	Ren *et al.* (2010)[216]
RDX	205.2	240.2/253.3	2546	174.0	36.38	An *et al.* (2012)[221]
RDX/Ag-CNT-1	203.7	241.0/252.1	2451	Na	na	
RDX/Ag-CNT-2	203.2	249.8	2120	Na	na	
AP	263.2	297.0/406.2	621	Na	na	Wang *et al.* (2012)[231]
AP/GA	265.1	322.5	2110	Na	na	
AP/GA/Fe_2O_3	257.8	312/348	1985	Na	na	Lan *et al.* (2015)[158]
AP/HTPB	274.4	335.9/405.8	1940	Na	na	Liu *et al.* (2008)[210]
AP/HTPB/CNTs	266.9	328.5/380.9	2170	Na	na	
AP/HTPB/Cu-CNTs	271.2	353.4	2780	Na	na	
RDX/nD-1	217.9	244.6	894.6	127.5	11.30	Tong *et al.* (2009)[81]
RDX/nD-2	215.1	237.3	625.6	199.9	19.10	

T_o, onset temperature of the peaks; T_p, peak temperature of thermal events; ΔH, heat release in J g^{-1}; E_a, activation energy; A, pre-exponential factor; na, not available; [a]CNTs with diameter of 10–20 nm, while [b]CNTs with diameter of 60–100 nm; Ag-CNT-1 and -2 means the mass ratio of Ag/CNTs is 19 : 1 and 9 : 1, respectively. Nomenclature: CL-20, 2,4,6,8,10,12-hexanitro-2,4,6,8,10,12-hexaazaisowurtzitane; FEN, fullerene ethylenediamine nitrate; FED, fullerene ethylenediamine dinitramide, $H_{12}C_{60}(HNCH_2\ CH_2NH_2{\cdot}HN(NO_2)_2)_{12}$; mNPF, *N*-methyl-2-(3-nitrophenyl) pyrrolidino- [3′,4′:1,2] fullerene; PF, polynitro[60]fullerene, $C_{60}(NO_2)_{14}$; FPGN, [60]fullerene-poly(glycidyl nitrate); FPL, fullerene phenyl-alanine lead salt; FFGAP, functionalized [60]fullerene-glycidyl azide polymer; FPL, fullerene phenylalanine lead salt; FHN, fullerene hydrazine nitrate; FDN, derivative with molar ratio of C_{60}, 2,4-dinitrobenzaldehyde and *N*-methylglycine 1 : 2 : 6; NPF, trinitrophenyl C_{60} derivative; SCCNT, SnO_2–Cu_2O/CNT composites; PCC, PbO·CuO/CNTs; CCNT, CuO-CNTs (8.8 nm, 5%); GA, graphene aerogel; nD-1, nD/RDX = 1 : 8, while it is 1 : 4 for nD-2.

In terms of energetic polymers based on fullerene, it has been shown that C_{60}-PGN is thermally stable up to 200 °C. The decomposition E_a of C_{60}-PGN was measured to be 170.9 3 kJ mol^{-1} (by the Kissinger method) and 168.3 kJ mol^{-1} (by the Ozawa–Doyle method).[120] C_{60}-PGN is more stable than any other known polynitrofullerene. C_{60}-GAP decomposition shows a three-step thermal process,[121] where the first step is due to the reaction of the azide group and fullerene at approximately 150 °C. The second mass loss step is due to the decomposition of the main chain of the remaining GAP and N-heterocyclic at approximately 240 °C. The final decomposition step could be attributed to the burning of amorphous carbon or the carbon fullerene cage at around 600 °C.

Highly energetic polynitro[C_{60}]fullerene (PF) starts to decompose below 160 °C, with two peaks at 189.7 and 247.0 °C, with a combined heat release of 2017.7 J g^{-1}. The energy content is comparable to those of HMX and CL-20. Its total mass loss of 47.3% corresponds to the theoretical value of 47.2%, corresponding to the calculated formula of $C_{60}(NO_2)_{14}$. During decomposition, PF releases a mixture of nitrogen oxides: NO_2 and NO with minor amounts of N_2O. A residue of oxidized carbon was obtained after the main decomposition step. By further release of CO_2 and CO above 700 °C, the residue is reduced to a carbonaceous matter free of oxygenated groups, also showing the presence of a small amount (<10%) of C_{60} fullerene.[114] Theoretical investigation

shows that explosion of PF starts with NO_2 group isomerization into C–O–N–O, followed by emission of NO molecules and formation of CO groups on the buckyball surface.[266] Then, NO oxidizes into NO_2 and the C_{60} structure falls apart, liberating CO_2. As a comparison, FEN decomposes just in two steps: the first-stage with 40.8% mass loss (100–250 °C), due to intense scission of NO_3- and partial decomposition of the branched chain, releasing H_2O, CO_2, CO, N_2O and NO_2. The second-stage has 59.2% of the mass loss (250–580 °C), due to the decomposition of residual branched chains on a carbon cage, releasing CO_2.[115] For comparison of the decomposition processes of different energetic fullerene derivatives, their TG/DTG curves under a heating rate of 10 °C min^{-1} are shown in Fig. 34.

According to Fig. 34, at least two steps are involved in the decomposition of these fullerene derivatives, which started between 100 and 150 °C. In particular, FPL undergoes a four-step exothermic process starting at 135 °C,[117] which can reduce the decomposition T_p of RDX by more than 20 °C and decrease E_a by 30 kJ mol^{-1}. FHN undergoes at least four decomposition steps, under a N_2 atmosphere, starting at around 150 °C, while FEN decomposes in only two steps, as described above. Moreover, FHN decomposed completely in air with a trace amount of residue. FED initially decomposes in one slow step, with a mass loss of 3.3%, followed by a main decomposition step, with a mass loss of around 50%. It can also be seen that F-GAP decomposes in three steps under an air atmosphere. The first stage of thermal degradation appears at 150 °C, with around 10.4% mass loss. The other two onsets of thermolysis appear at 300 °C and 600 °C, with approximately 22.9% and 64.2% total mass losses, respectively. In contrast, GAP decomposes at approximately 200 °C, with the main gaseous products being CO, HCN, HCHO and NH_3.[267–269] It is indicated that the initial thermal degradation of F-GAP is probably due to the scission of the $-N_3$ group *via* the intramolecular or intermolecular cycloaddition of $-N_3$ to the fullerene carbon cage, as well as subsequent nitrogen release. The second step that takes place between 200 and 400 °C is due to decomposition of GAP's main chain and N-heterocyclic decomposition, while the final mass loss step is caused by decomposition of the fullerene cage (Scheme 12).

As shown in Table 7, the decomposition of AP can be greatly affected by CNMs. For instance, the presence of GA, on the one hand, has a catalytic effect on the decomposition of AP. On the other hand, the oxidants produced from AP may react with GA, promoting heat release (Scheme 13).[156] There was only one exothermic peak observed in DSC for AP/GA nanocomposites (in contrast to two peaks observed for pure AP); this is 83.7 °C lower than the second peak of AP, with a total heat release of 2110 J g^{-1}. It has been shown that as-prepared AP/GA nanostructured energetic composites have numerous nanoscale pores and their SSA is about 49.2 m^2 g^{-1}. These properties result in their accelerated decomposition and greater total heat release.[157] Graphene also changes the decomposition mechanism of AP, as shown in Scheme 13. In contrast, the Cu/CNTs catalyst remarkably decreased the second peak of AP, with a higher decomposition heat.[210] The GA/Fe_2O_3 nanostructured catalyst dispersed in AP showed a significant catalytic effect in promoting the thermolysis of AP. In the latter case, only a single decomposition step was observed, with a decreased peak temperature and a large increase in the total heat release. Thus, the as-prepared GA/

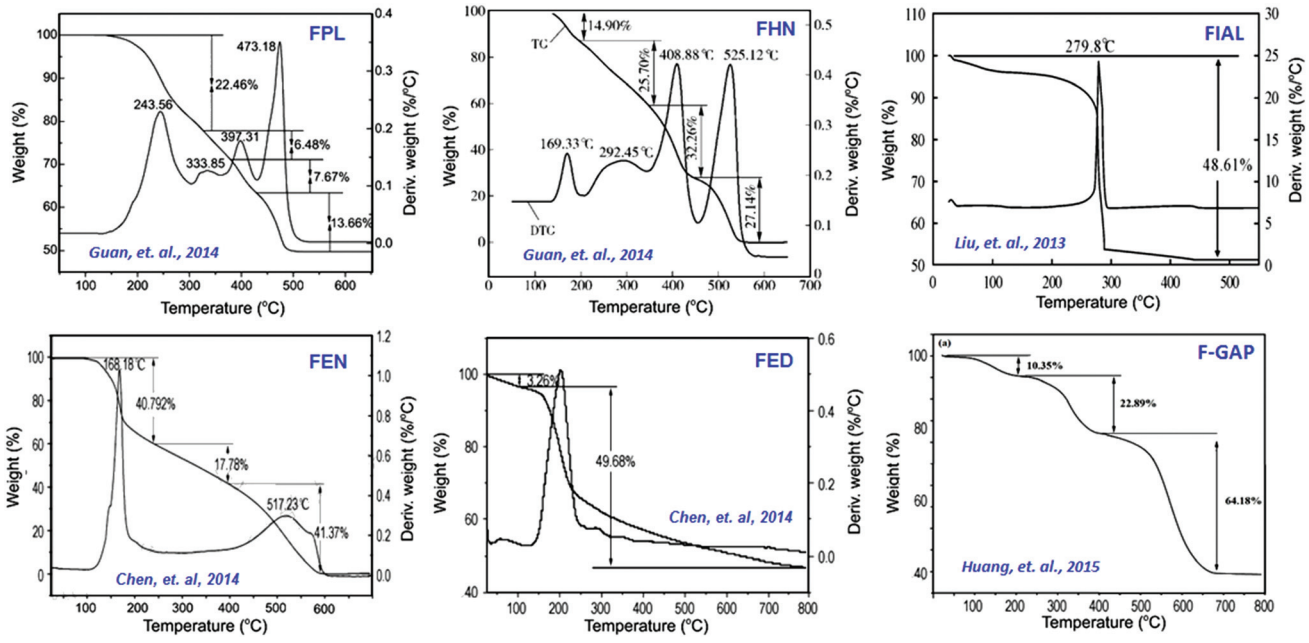

Fig. 34 TG-DTG curves of several energetic fullerene derivatives: FPL (fullerene phenylalanine lead salt), FHN, FIAL (fullerene itaconic acid copolymer lead salt), FEN, FED and F-GAP (C_{60}-GAP). Several figures that appeared in the listed ref. 93, 95, 97 and 101 are recombined with permission.

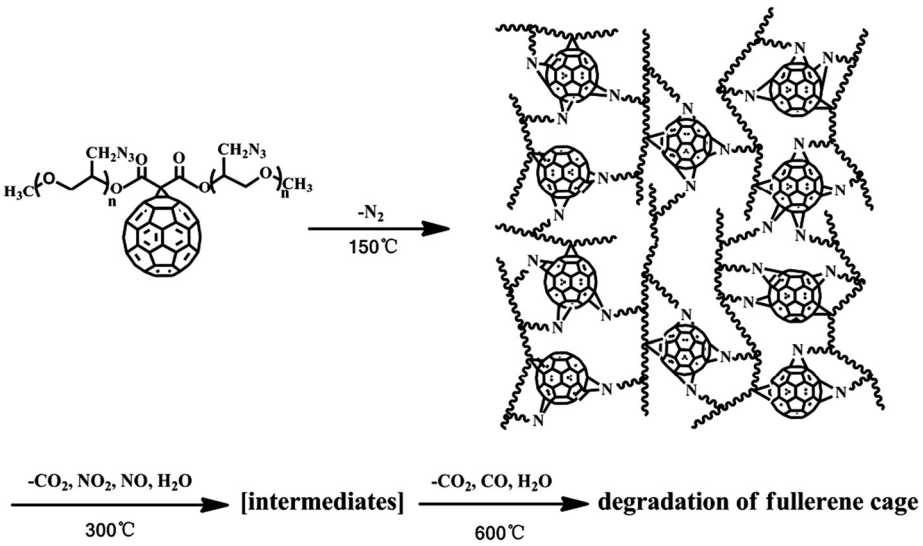

Scheme 12 Thermal decomposition mechanism of C_{60}-GAP under air atmosphere (adapted from Huang *et al.*, *Polymers*, 2015, **7**, 896–908). Reprinted from ref. 229 with permission. Copyright © 2011, American Chemical Society.

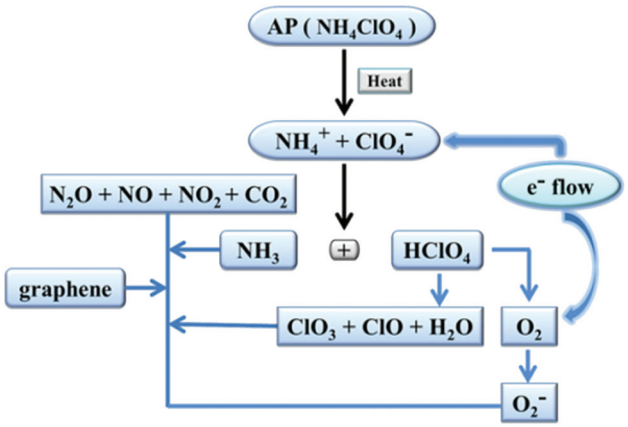

Scheme 13 Thermal decomposition processes of GA/AP nanostructured energetic composite.

Fe_2O_3/AP nanostructured energetic composite could be a promising candidate as a component for solid propellants.[158] GA also has a significant catalytic effect on the decomposition of AN,[159] whose T_p was decreased by 33.7 °C and total heat release was increased by 532.8 J g^{-1}. In comparison to GA and GA/Fe_2O_3, the addition of CoAl-MMO and CoAl-MMO/CNT to AP resulted in decomposition occurring *via* a single exothermic process. For example, in the case of the CoAl-MMO additive, AP shows a maximum peak temperature of 297 °C. Surprisingly, when using CoAl-MMO/CNT, the second peak temperature of AP is significantly decreased to 271 °C, strongly suggesting that this nanocomposite is the most efficient catalyst for promoting the decomposition of AP.[217]

Based on the above-mentioned results, one can see that CNTs and their functionalized analogs have a strong catalytic effect on energetic compounds such as RDX, FOX-12 and AP. In fact, CNTs also have a significant effect on the oxidation of Al, which is a very important ingredient in many propellants and explosives. It was shown that the CNTs can be fully embedded into Al aggregates, forming sea urchin-type Al/CNT particles. This material has the largest exothermic enthalpy at a lower oxidation temperature for both γ-Al_2O_3 and α-Al_2O_3 phases.[222] This was attributed to fast heat transfer into Al particles *via* partially embedded CNTs. The TG curves of Al/CNTs at a heating rate of 5 °C min^{-1} are shown in Fig. 35. The results presented in Fig. 35 show that the exothermic enthalpy of Al oxidation is strongly dependent on the content of CNTs and increases to −188 kJ g^{-1} at 20 wt% of CNTs.[222] Moreover, the oxidation process of pure Al particles takes place in the range 580 to 970 °C (TGA measurements). The first oxidation peak of pure Al at 580 °C is known as γ-Al_2O_3 phase formation, while the second peak, near 970 °C is known as α-Al_2O_3 phase formation. This is in agreement with the typical route of alumina phase transformations: amorphous–Al_2O_3 → γ → (δ) → (θ) → α-Al_2O_3.[270] Typically, amorphous–Al_2O_3 transforms to more thermodynamically stable crystalline polymorphs, as the layer thickness reaches a critical value.[271] Once the formation of the γ-Al_2O_3 phase is completed, the oxide layer thickness reaches a critical thickness to form an α-Al_2O_3 phase near 970 °C. However, the oxidation behavior of the Al/CNT (10 wt%) mixture was found to be very different from pure Al. The weight of the Al/CNT mixture was reduced during the initial stage of oxidation (400–600 °C; Fig. 35b). This phenomenon was explained by the burning of CNTs, which are located on the surface of Al particles.

The weight increase at near 600 °C was due to the formation of a γ-Al_2O_3 layer, which was almost nullified by the weight decrease from burning of the CNTs. The formation temperature of the α-Al_2O_3 phase shifted from 970 to 907 °C, while the weight increase reached 145% (much

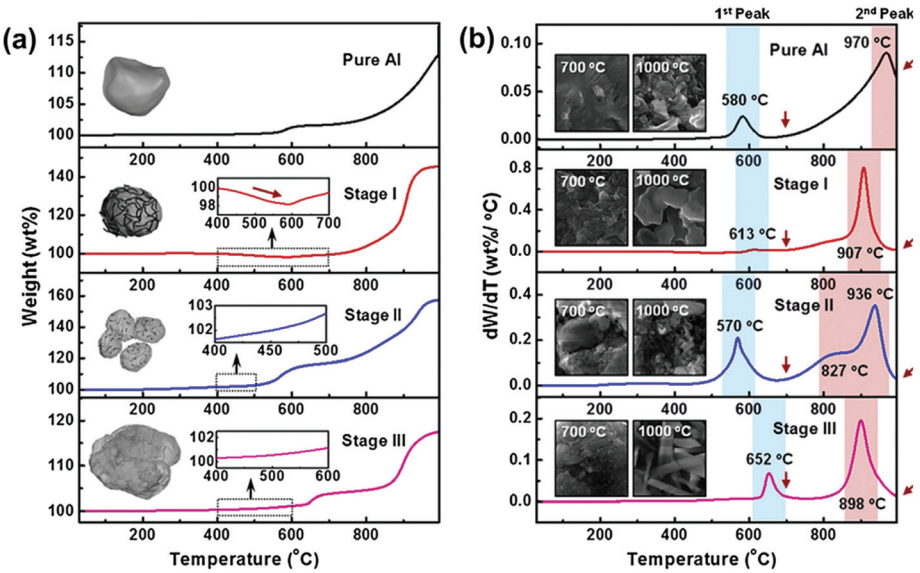

Fig. 35 (a) TGA profile under air, at a ramping rate of 5 °C min^{-1} for different stages: Stage I (60 min), Stage II (120 min), and Stage III (180 min). The inset image shows the schematics of Al/CNTs mixture morphologies and (b) the corresponding DTG; the inset shows SEM images of Al/CNTs mixtures obtained after TGA terminated at 700 and 1000 °C. Note that the scales of the *y*-axes in (b) are different from each other, to allow better visualization of each peak. Reprinted from ref. 222 with permission of Crown copyright © 2013 Published by Elsevier Ltd.

larger than that of pure Al) due to enhanced oxidation in the presence of CNTs. As shown above, although the structure and shape of graphene and CNTs are different, both these nanomaterials are capable of facilitating electron transfer and promoting chemical reactions, as well as catalytic effects. These effects could be further enhanced by addition of other catalysts. GO, CNTs and fullerene CNM-based catalysts have large SSAs and thus high reactivity, especially when these nanomaterials are derivatized with additional functional groups.

Ignition of pyrotechnics and thermites. A pyrotechnic initiator (igniter) is a device that contains a pyrotechnic composition (oxidants and fuels), used primarily to ignite other more difficult-to-ignite materials, *e.g.* thermites, gas generators and solid-fuel rockets.[272,273] The initiator compositions are similar to those of flash powders but they are different in their burning rate. Although the explosion of igniters is not favored, they are responsible for an intentionally high production of hot particles. Commonly used oxidizers are KP and KN, while typical fuels are Ti, titanium(II) hydride, zirconium, zirconium hydride and boron.[274] There are many factors that affect the energy output of these compositions, whose performance can be modified by catalysts or energetic additives.[275] It was found that ignition of BNCP by laser was difficult but the inclusion of just 5 wt% of CNTs or CB significantly decreases both the critical energy for ignition and the ignition delay time.[52] This indicates that the CNMs and their energetic derivatives have a positive effect on the ignition properties of materials containing them. It has been reported that EMs mixed with optically active CNTs can be subject to optical initiation using ordinary light with an intensity of several W cm^{-2}, over a large surface area.[276] These energetic mixtures could be new ideal candidates for safety apparatus, such as the firing of bolts on space shuttle rockets and aircraft exit doors.

It was further shown that the addition of both CNTs and graphene can significantly enhance the thermal transport properties of energetic composites made of Al and Teflon.[277] However, composites containing CNTs are much more sensitive to impact. In contrast, although graphene cannot significantly sensitize energetic composites to ignition, it does induce greater overall reactivity. Increasing the concentration of CNM additives may decrease the overall thermal diffusivity and increase the sites for probable hot spot formation during impact.[278] TEM images of the above-mentioned energetic composites containing CNT, graphene and nano-C are shown in Fig. 36. In fact, the heat conductivity of polymeric materials can be improved by incorporating CNTs[279] and this is also the case for pyrotechnic compositions. According to the aforementioned results, CNTs are more effective than other CNMs in improving the ignition performance of pyrotechnic compositions. In particular, SWCNTs are the best choice for this purpose and it has been demonstrated that the burn rate and pressurization rate of SWCNTs/Al/CuO nanocomposites achieve maximum values of about 240 ms^{-1} and 5.9 ± 0.8 psi μs^{-1}, respectively, when the content of SWCNT is just 1 wt%.[280] The preparation method of SWCNTs/Al/CuO nanocomposites, their morphology and flash irradiation ignition process are shown in Fig. 37. The mixing ratio of fuel and oxidizer was fixed at Al : CuO = 3 : 7 (wt%). Then, the SWCNTs were added to the nEMs precursor solution in mixing ratios of 1, 2, 5 and 10 wt%. The nano-Al particles were firmly attached to the surface of CuO NPs, while the SWCNTs appeared to be homogeneously distributed in an Al and CuO NP-based matrix. As the content of SWCNTs increased to more than 2 wt%,

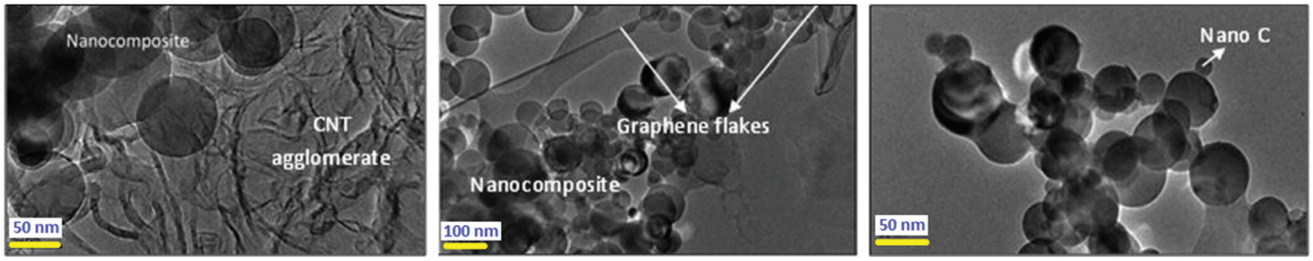

Fig. 36 TEM images of Al/Teflon energetic composites combined with CNTs, graphene flakes and nano carbon. Reprinted from ref. 277 with permission. Copyright © 2012, managed by AIP Publishing LLC.

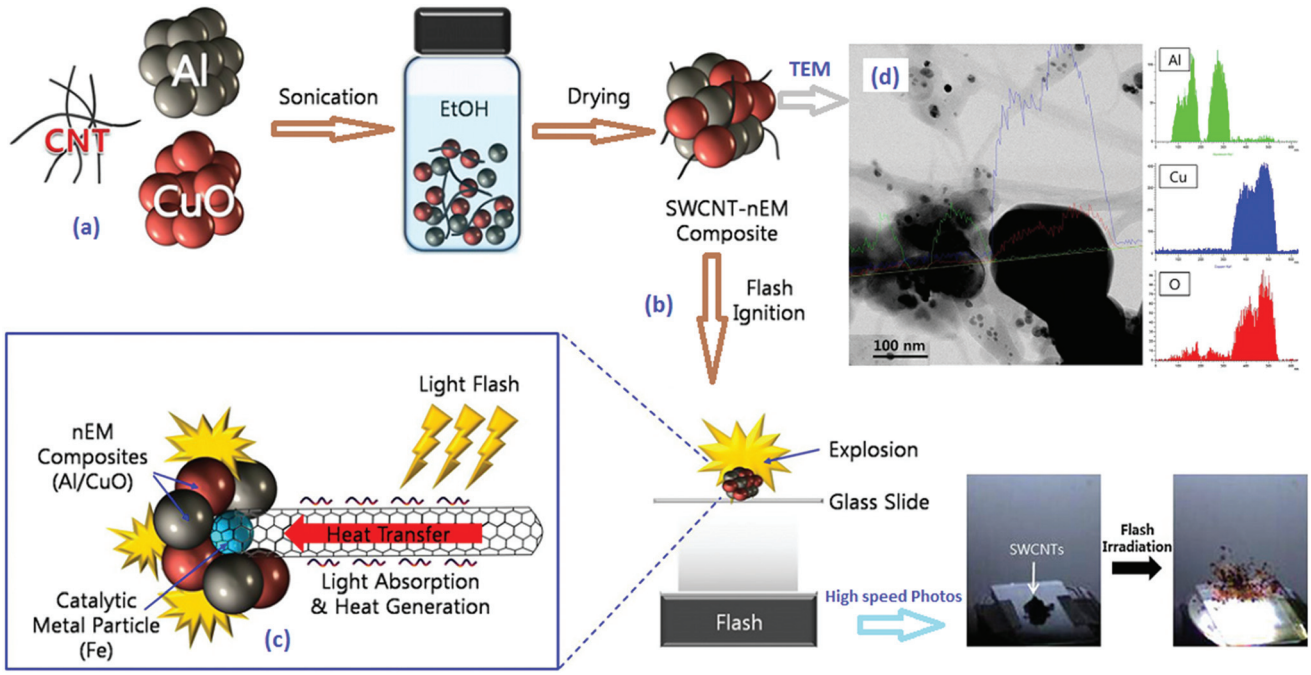

Fig. 37 Schematics of (a) the fabrication of SWCNT-nEM composites, (b) the flash ignition of an SWCNT-nEM composite, (c) the optical ignition mechanism of an SWCNT-nEM composite, and (d) scanning TEM image and line scan analysis of SWCNT/Al/CuO nanocomposites. Recombination of several figures from ref. 280 reprinted with permission. Copyright © 2012 The Combustion Institute. Published by Elsevier Inc.

both the burn rate and the pressurization rate of the as-prepared SWCNT-nEM composites decreased significantly. The researchers believe that this was due to the large amount of SWCNTs in the nEM matrix, which may increase the heat dissipation, resulting in a very limited temperature increase for the SWCNT-nEM composite, thus hindering the oxidation and subsequent ignition of the nEMs. In the latter case, the remote optical ignition and controlled-explosion reactivity of nEMs was achieved by incorporating less than 2 wt% of SWCNTs, as optical ignition agent.

In addition to ignition by irradiation, the ESD ignition properties of pyrotechnics could also be tailored by highly electroconductive nano-fillers, including CNTs, graphene nano platelets (GNP) and their combinations. It has been found that the ignition and the electrical conductivity of a binary composite of Al and polytetrafluoroethylene (PTFE) can be changed significantly.[281] Instead of GNP, a lower volume fraction of CNTs is adequate to create an electrical conductivity percolation threshold. However, a CNT/GNP composite could create a better percolating network. In this way, compositions that are insensitive to ESD ignition become sensitive due to improvement in electrical conductivity. Based on this strategy, flash-ignitable nEMs composed of Al/CuO nanoparticles for underwater explosion were invented using "sea urchin-like" CNTs (SUCNTs, Fig. 38).[282] The underwater ignition of nEMs is a big challenge because water perturbs the reactants prior to ignition and quenches the subsequent combustion. The SUCNTs can absorb the irradiated flash energy and rapidly convert it into thermal energy. Similar to the above-mentioned Al/CuO system, the maximum burn rate was achieved by adding 1 wt% of SUCNTs into the nEM matrix. However, the resulting maximum underwater burn rate was found to be only

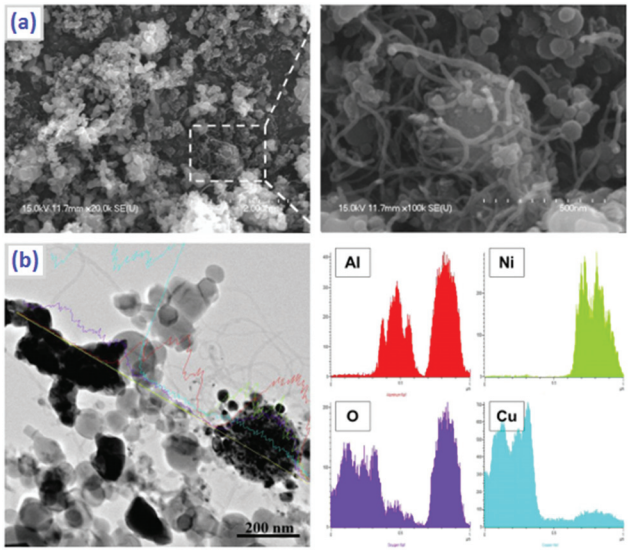

Fig. 38 (a) SEM and (b) scanning TEM images of SUCNT/nEM. Reprinted from ref. 282 with permission. Copyright © 2014 The Combustion Institute and published by Elsevier Inc.

about 34 m s^{-1}, which is much lower than the burning rate of this composition in air (240 m s^{-1}).[280]

Use of CNMs in combustion of propellants. The combustion properties, including burn rate, pressure exponent, combustion wave and flame structure, are the most important parameters for propellants.[283,284] In general, the burn rate should be controllable, while the pressure exponent must be smaller than 0.5, for solid rocket applications, and higher than 1.0, for gun propellants. It is common practice to use burn rate modifiers or combustion catalysts to control the burn rate and pressure exponent of solid propellants. It has been shown that many CNM derivatives can be used as effective combustion catalysts.[285] The coupled energy balances for CNTs with an annular coating of reactive metals are solved, where the thermal transport in the nanotube accelerates reaction in the annulus. In the case of Zr metal, the CNTs increase the reaction front velocity from 530 to 5100 mm s^{-1}, along the axial direction of the nanotube.[286] This remarkable result offers a proof-of-concept for 1-D anisotropic EMs and could find application in novel propellants. Interestingly, there are large temperature differences (>1000 K) between the CNT and the reaction front of the annulus. The directional heat conduction in the CNT makes the interfacial heat conductance a less significant factor affecting the heat distribution.

In addition to CNTs, graphene could also enhance the combustion properties of propellants. A comparative study showed[287] that the ignition temperature was lowered and burning rates were increased for colloidal suspensions of nitromethane with graphene, compared to liquid nitromethane monopropellant alone. It has been further reported[288] that the addition of raw fullerene soot (FS), extracted FS (EFS), pure C_{60} and CB additives to nitroglycerine (NG) markedly accelerated its liquid phase decomposition. The effect of these nanomaterials on the combustion properties of double-base propellants (DB) has been also evaluated. As indicated earlier, CNTs have a strong catalytic effect on the decomposition of AP and they are also a promising combustion catalyst for AP. It was proven that as the CNT content increased, the burning rate of an AP composite also increased with a lower pressure exponent (n).[251] Table 8 lists the burn rate and n of different propellants when using CNMs as burn rate modifiers. Regarding applications of CNM additives as catalysts, in the early 1960s, the USA began using AC in solid propellants, where Bice[289] and Ives[290] found that AC increased the burning rate of AN-based propellants. These researchers also reported that a certain amount of carborane/AC composites increased the burning rate of the same propellant from 5.5 to 9.2 mm s^{-1}. Moreover, they showed that the burn rate of aluminized composite propellants may be increased to 25 mm s^{-1} at 7 MPa by using AC as a modifier.[291]

A combination of AC with iron oxide can make the propellant burn at a speed of 50 mm s^{-1}. However, it has an unacceptably large pressure exponent. Later on, it was proven through the analysis of a flame surface by SEM images,[292] that a hole in the water encapsulated in AC can reduce the melt flow on the burning surface of the propellant, resulting in a higher pressure exponent. Therefore, it is better to use water-free AC. In addition to AC, CNTs also increased the burn rate of HTPB propellant by 20%, while having practically no effect on its pressure exponents.[293] Similar findings were observed for NEPE propellant but the pressure exponent was decreased at low pressures (*e.g.* <10 MPa), while it was increased at higher pressures (15–18 MPa).[294]

As shown in Table 8, Cu/CNTs can markedly increase the burning rate and decrease the pressure exponent for AP/HTPB propellant.[186] A significant amount of work regarding catalytic effects of CNMs on the combustion behavior of solid rocket propellants was done in China by Zhao's group.[295–299] They prepared composite catalysts based on PbO, CuO, Bi_2O_3 and GO, as well as the "Pb–CB" binary catalytic system, to increase the burn rate of DB propellant. It was shown that "mesa burning" could be achieved in the pressure range 8–14 MPa. The PbO–Cu_2O was jointly supported by CB, forming a "Pb–Cu–CB" three-element catalytic system, so that the burning rate of DB propellant at 2 MPa could be elevated from 2.15 to 8.57 mm s^{-1}, with a wider "plateau combustion" pressure range (10–20 MPa).[295]

These researchers also used a combination of Bi_2O_3 and GO to replace PbO/GO, as a green combustion catalyst.[296,297] It was observed that both Bi_2O_3/GO and Cu_2O–Bi_2O_3/GO catalysts significantly increased the burning rate of DB propellants and reduced the pressure exponent (Table 8). Although the "mesa burning" disappeared upon replacement of PbO by Bi_2O_3, the pressure exponents were still found to be acceptable. This was also the case for CNT-based catalysts where the above-mentioned oxides were used. There might be another reason for the enhancement of the combustion of nitrocellulose (NC) by GO. In fact, it was found that the burn rate of NC significantly increased as the GO content increased in GO/NC films.[141] The

Table 8 The effects of CNM combustion modifiers on burning rates of solid rocket propellants (under N_2 atmosphere, 20 °C)

	μ/(mm·s^{-1}) at different pressures						
Propellants	3 MPa	5 MPa	7 MPa	9 MPa	11 MPa	n (3–11 MPa)	Ref.
AP	4.70	6.33	7.39	8.93	10.14	0.586	251
AP/CNT(1%)	7.84	9.46	11.11	12.53	13.26	0.427	
AP/CNT(2%)	9.47	11.51	13.78	14.54	16.28	0.406	
AP/CNT(3%)	10.64	13.63	14.83	16.39	17.86	0.386	
AP/CNT(4%)	13.24	15.02	16.12	17.49	18.30	0.247	
	5 MPa	7 MPa	9 MPa	10 MPa	11 MPa	(5–11 MPa)	206
AP/HTPB	5.75	7.03	7.37	8.58	9.12	0.572	
AP/HTPB/CNT	6.68	7.84	8.90	9.76	10.08	0.538	
AP/HTPB/Cu-CNT	7.93	8.92	10.00	10.48	10.85	0.408	
	2 MPa	4 MPa	6 MPa	8 MPa	12 MPa	(2–8 MPa)	
CMDB	3.71	5.88	7.87	10.23	14.30	0.721	288
CMDB/CB	3.96	6.10	7.82	9.74	13.57	0.642	
CMDB/FS	3.76	5.88	7.82	9.90	13.63	0.692	
CMDB/EFS	3.50	5.76	7.55	9.36	13.52	0.706	
CMDB/C_{60}	3.57	5.72	7.49	9.49	13.46	0.697	
DB	1.22	2.36	4.55	5.93	8.53	1.171	299
DB/PbO–GO	4.68	8.15	10.09	10.99	10.38	0.630	300
DB/Cu_2O–PbO/GO	8.17	11.36	12.96	14.33	16.74	0.405	301
DB/Bi_2O_3/GO	3.01	6.98	10.21	12.37	15.91	1.035	
DB/Cu_2O–Bi_2O_3/GO	8.58	11.44	13.53	15.07	17.27	0.408	
	8 MPa	10 MPa	12 MPa	16 MPa	20 MPa	(16–22 MPa)	291
DBP	6.49	7.81	8.99	10.30	12.24	0.783	
DBP/CuO-CNTs	13.34	15.28	16.49	19.03	20.34	0.384	
DBP/nano-Bi_2O_3	6.86	8.02	8.91	10.62	12.04	0.639	290
DBP/Bi_2O_3-CNTs	9.38	10.66	11.74	13.81	15.21	0.431	

RDX used was a mixture of 80 μm and 50 μm particle sizes, with a weight ratio of 1/1; AP particle sizes were in the range of 120–200 μm; the N content in NC was 12.6%; CMDB, RDX/AP/NC/NG/additives/catalyst with a mass ratio of 20/10/29/32.5/5.0/3.5; FS, was composed of 10% fullerenes and 90% CB; EFS, containing about 80% C_{60} and 20% C_{70}; DBP, double-base propellants containing (NC + NG)/DEP/C_2 with a mass ratio of 89/8.5/2.0, where DEP is diethyl phthalate and C_2 is a stabilizer; the contents of Bi_2O_3 and Bi_2O_3-CNTs are 2.5 wt%.

flame structure as well as the burn rate curves are presented in Fig. 39.

It is shown in Fig. 39 that CNTs, as a carrier, can prevent aggregation of Bi_2O_3 or CuO nanoparticles and improve the catalytic efficiency, resulting in a much higher burning rate and a lower pressure exponent.[298,299] Later on, Liu *et al.* found that carbon-coated Cu–Bi/CNTs powders could function as effective catalysts for DB propellants;[300] plateau combustion was obtained within a pressure of 10–22 MPa, with an exponent of 0.173, which is very promising for solid rocket motors. In fact, nano-Cu/CNT and nano-Ni/CNT composite catalysts have a similar catalytic effect on AP/HTPB propellants.[301,302]

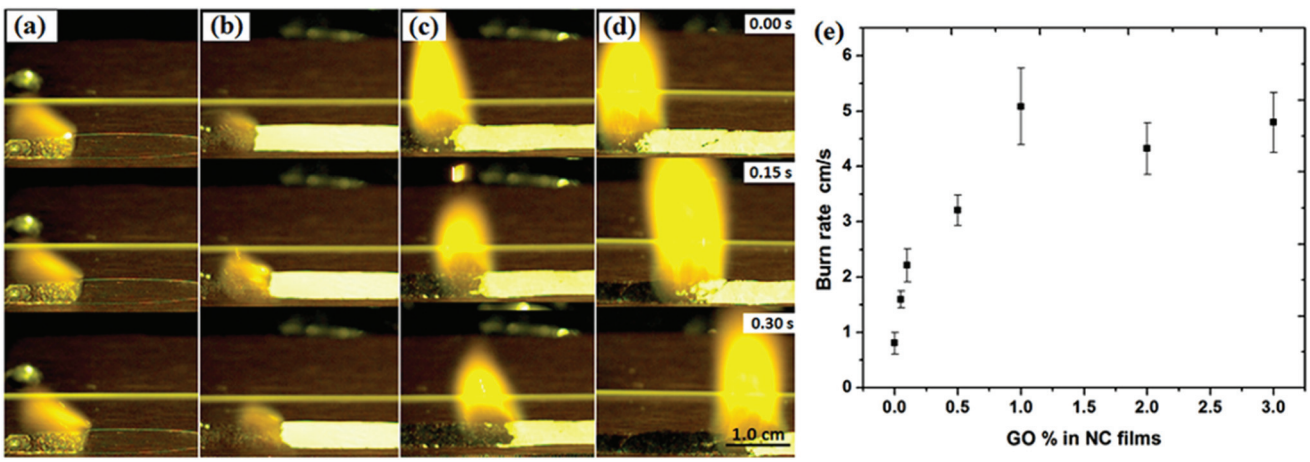

Fig. 39 High-speed images of the combustion process of pure NC films and GO-NC films under ambient conditions: (a) pure NC film; (b) 0.05% GO-NC film; (c) 0.5% GO-NC film; and (d) 1% GO-NC film. (e) Comparison of the burn rates of pure NC films and GO-NC films. Reproduced from ref. 164 with permission from the Royal Society of Chemistry.

It has been stated that when 3 wt% of such catalysts, including nano CNTs, Fe_2O_3/CNTs and Fe·Cu/CNTs, are used, the burn rate of ADN at 4 MPa increases from 30.49 to 50.59, 39.72 and 38.79 mm s^{-1} and the corresponding pressure exponents decrease from 0.81 to 0.36, 0.67 and 0.75, respectively.[258] In general, the use of modified CNMs can improve the combustion properties of propellants.[303] Such modified nanomaterials, which include metal oxides, nanometer-sized rare earth materials and nanometer-sized oxidizers, can increase the burn rates of solid propellants. In addition to increasing the burn rate, the aforementioned CNMs and their derivatives could also improve the energy release rate. For instance, MWCNTs can be used in composition with porous silicon (pSi), impregnated with sodium perchlorate and this makes pSi explode easily.[304]

As well as propellants and explosives, CNMs can be used in nanothermites. Nanothermite formulations that use Al or Mg as reducing agents and Fe_2O_3, MoO_3 or WO_3 as oxidizers, have various applications due to their high energy density and large energy release rate, in comparison to conventional thermites. The addition of boron and CNTs to these nanothermites results in doubling of the gas peak pressure,[305] indicating that the boron–CNT mixtures could be useful for a new generation of propellants, explosives and pyrotechnic systems. Recently, MWCNTs were coupled with iron oxide nanoparticles, to form new pyrophoric compositions prepared on the basis of water-dispersed CNTs.[306]

As mentioned earlier, addition of CNTs to Zr/$KClO_4$ has a significant impact on the light radiation energy of this material. As the CNT content was increased, the combustion rate and exothermic output of these pyrotechnic mixtures were increased correspondingly.[206] Flash-ignitable nEMs for underwater explosions or for other purposes could be achieved by addition of SUCNTs[282] to Al/CuO nanoparticles or by addition of SWCNTs to pentaerythritol tetranitrate (PETN),[307] as an optical sensitizer. The CNMs absorb the irradiated energy and rapidly convert it into thermal energy, greatly improving the ignition and burning properties of the pure parent explosive. The same phenomenon was observed for the case of Zr/oxidant/CNT composites.[308] As well as CNTs, functionalized graphene sheet (FGS) is also a promising additive capable of enhancing fuel/propellant combustion. A series of molecular dynamic simulations based on a reactive force field (ReaxFF) show that the catalytic activity of FGS in the combustion of nitromethane is significant.[309] The derivatives of fullerene have an even better catalytic effect than C_{60} and CB on the combustion of DB propellants containing RDX. As mentioned earlier, mNPF is a typical example for demonstration of this effect. The burn rates of RDX-CMDB propellants were greatly improved by addition of mNPF, increasing with the mNPF content. The maximum burning rate can reach up to 19.6 mm s^{-1} when 1.0 wt% mNPF is used, while the corresponding "plateau combustion" region is in the range from 8 to 22 MPa.[310] The unique structure of CNMs and their energetic derivatives can modify the combustion characteristics of propellants, especially when new functional groups or energetic moieties are introduced to their structures. On the one hand, such a catalytic effect could be due to the special carbon structure allowing facile electron and heat transfer, promoting chemical reactions. On the other hand, the metal oxide catalysts could be dispersed in the inner layer or porous structure of the CNMs. Such dispersion can prevent agglomeration of nanoparticles, resulting in more uniform, catalytically active sites and thus better combustion properties. Moreover, the catalytic efficiency could be further improved by synergistic effects between the CNMs and the carried catalysts.

Stabilization and desensitization of EMs by CNMs

Improvement of thermal stability of EMs. During development of new EMs, many compounds with a high energy content were found not to be sufficiently thermally stable. The stabilization of these EMs is essential for their practical applications. The stabilization of such EMs includes improvement of their molecular stability and crystalline phase stability. There are several strategies for improvement of the thermal stability,[311] including (i) recrystallization, in order to exclude the defects, (ii) cocrystallization of unstable compounds with stable ones, (iii) coating of sensitive crystals with inert materials and (iv) chemical functionalization of crystal surfaces with thermally stable groups or compounds. For instance, AN undergoes a polymorphic phase transition near ambient temperature, affecting the usability of this oxidizer. However, the 1 : 1 energetic co-crystals of AN with benzo-18-crown-6 (AN-B18C6) avoid this problem.[312] Alternatively, in order to achieve both phase and thermal stabilization of AN, a new material, polyvinylpyrrolidone (PVP)-AN glass has been developed, where PVP can separate AN into its ions through an ion–dipole interaction.[313]

It has been reported that ADN could also be stabilized by coating it with other inert materials.[314] Recently, a theoretical investigation showed that the stability of EMs could also be improved by encapsulating them inside CNTs or between graphene layers.[315] Preparations of a variety of energetic compounds have been attempted, including FOX-7, RDX, HMX, 3,6-di(hydrazino)-1,2,4,5-tetrazine (DHT), 3,6-diazido-1,2,4,5-tetrazine (DiAT) and DAAT, as well as five different *N*-oxides of DAAT ($DAATO_n$, with n = 1–5). It was found that all of these EMs could be stabilized by 32–53 kcal mol^{-1} by using CNTs with appropriate diameters. Moreover, FOX-7, RDX and HMX could also be confined between graphene layers, resulting in stabilization by 28–40 kcal mol^{-1}. The stabilization results from dispersion interactions between the molecules and carbon nanostructures, as well as coulombic interactions, due to charge dissipation and intermolecular H-bonding.

In addition to stabilization of normal sensitive energetic compounds, it is also possible to stabilize unstable high-nitrogen compounds using CNTs. Finite temperature simulations demonstrated the stabilization of a polymeric nitrogen (N_8) at ambient pressure and room temperature, by confinement inside a CNT. If proven experimentally viable, it may open a new path towards stabilization of polynitrogen or polymeric nitrogen compounds under ambient conditions.[316,317] An

energy barrier of 1.07 eV was found for the formation of N_8/CNT (5,5) from N_2/CNT (5,5), while the dissociation barrier was 0.2 eV. Reaction pathway snapshots have shown that the transition state is composed of N_2 and N_6 inside a CNT (5,5).[317]

Moreover, the simulation of NM with SWCNTs shows that size-dependent ordered structures of NM with preferred orientations are formed inside the tubular cavities, driven by van der Waals attractions between NM and SWCNT, together with the dipole–dipole interactions of NM, resulting in a higher local mass density than that of bulk NM.[318] On the basis of these calculations, the stabilization of nitrogen clusters has been proposed. It was demonstrated that nitrogen clusters could be stabilized by CNTs under various conditions. A linear chain nitrogen cluster could be formed under plasma conditions and it would probably be stabilized inside the walls of the CNTs that were used as substrates for synthesis.[319] Later on, a N_8 was stabilized on the positively charged sidewalls of MWNTs that were synthesized by cyclic voltammetry (CV) under ambient conditions. It was shown from temperature programmed desorption (TPD) data that MWNT/N_8 is thermally stable up to 400 °C.[320] Furthermore, an experimental study regarding interaction and energy transport of Al/Teflon nanocomposites with nano-carbon, graphene flakes and CNTs,[278] showed that graphene has the greatest influence on the thermal conductivity (increased by 98%), thermal diffusivity and specific heat of the Al/Teflon matrix.

Decreasing the sensitivity of EMs. Sensitivity refers to explosive phenomena caused by external stimuli that are ordinarily insufficient to produce a detonation, where such stimuli include impact, friction, shock, electrostatic charges and heat. Both experimental and empirical methods were established to determine or predict the sensitivity of EMs.[321] In past decades, considerable efforts were made to improve the survivability and safety of munitions, during which many new insensitive energetic compounds, as well as mitigation techniques, were developed.[322–325] As suggested by many researchers, the important factor determining the sensitivity of EMs, the sub-threshold ignition, involves the generation of hot spots.[326] In fact, various mechanisms have been proposed for the formation of such hot spots, including adiabatic compression of trapped gases in voids, friction involving sliding or impacting surfaces, shear band formation due to mechanical failure, sparks, triboluminescence and heating at crack tips. In addition to "hot spot" theory, over the years, various methods based on the bond dissociation energy, electronic structure and energetic transfer rate have been proposed in order to evaluate and interpret the sensitivity of energetic compounds.

Table 9 The mitigation effect of CNMs on the sensitivity of various EMs

Materials	IS/H_{50}	FS/%	ESD	Ref.
BNCP	10.6 cm	24 (swing 70°)	Positive-0.99/negative-1.18	52
BNCP/MWCNTs-1	17.5 cm	36	No fire	
BNCP/MWCNTs-2	24.7 cm	4	No fire	
BNCP/SWCNTs	23.1 cm	54	No fire	
BNCP/CB	27.1 cm	90	Positive-0.49/negative-0.47	
HMX	100%	100%	Note: friction: recorded at 90°, 3.92 MPa; impact: 10 kg hammer, 25 cm, 50 mg; probability out of 30 times	327
HMX/1%_C_{60}-1	100%	100%		
HMX/1%_C_{60}-2	100%	90%		
HMX/1%_C_{60}-3	60%	70%		
WO_3/Al	>50 J	144 N	<0.14 mJ	54
WO_3/Al/V3G	>50 J	252 N	<0.14 mJ	
WO_3/Al/TO	>50 J	64 N	<0.14 mJ	
WO_3/Al/RM	>50 J	>360 N	0.14 mJ	
WO_3/Al/AM	>50 J	>360 N	<0.14 mJ	
MnO_2/Al	31.9 J	>5 N	1.0 mJ	330
MnO_2/Al/CNF (mix)	29.4	>360 N	1800	
MnO_2/Al/CNF	44.2 J	>360 N	35 mJ/5400 mJ (fuel rich)	
ε-CL-20	100%	100%	Note: the drop hammer is 5 kg, 20 cm height; friction sensitivity of the samples was recorded at 66° ± 1°, 2.45 MPa; [robability out of 30 times	265
ε-CL-20/glue	30%	36%		
ε-CL-20/glue/graphene	20%	22%		
ε-CL-20/glue/GO	25%	30%		
ε-CL-20/glue/rGO	22%	28%		
	Laser sensitivity (Sapphire) mJ		Laser sensitivity (K9 glass) mJ	
PETN	271		268	329
PETN/1%CB	61.6		43.3	
PETN/1%CNTs	187.9		266.6	

IS, impact sensitivity; FS, friction sensitivity; F_s, flame sensitivity; C_{60}-1, commercially available; C_{60}-2, crystallized from pellucid purple carbon disulfide solution; C_{60}-3 brown sheet fullerene obtained from pellucid purple carbon disulfide/petroleum ether solution (80 °C, 10 h); (a) V3G, nanometer-sized graphitized carbon black; RM and AM, carbon milling under air and argon atmospheres; TO, Thermally oxidized carbon nanoparticles.

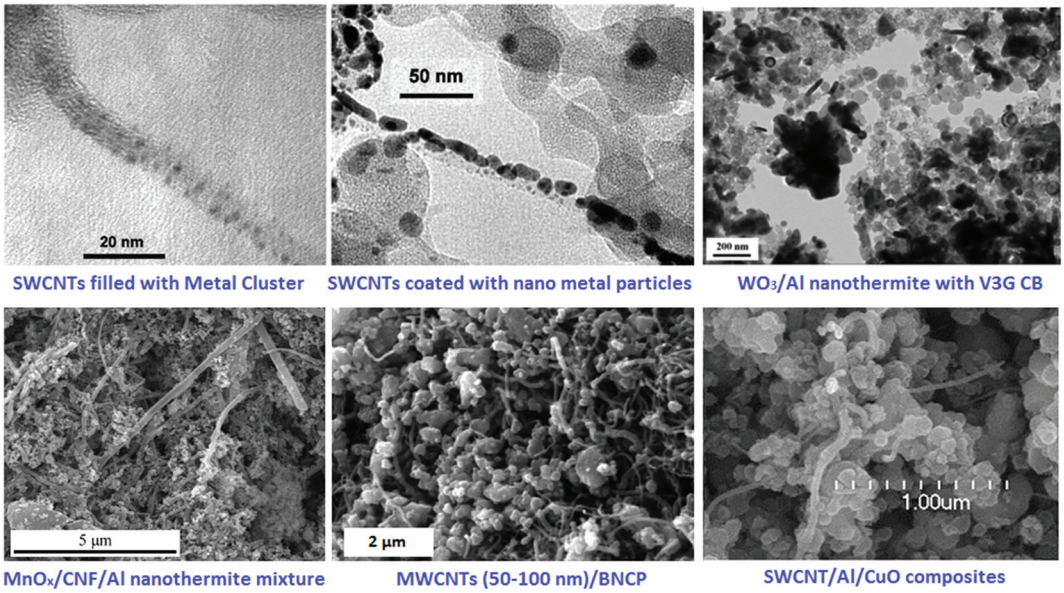

Fig. 40 A comparison of SEM morphologies and TEM images of several MWCNTs and CB-based thermites. This combined figure is reproduced from several figures appearing in ref. 58, 60 and 284 with permission.

One may decrease the sensitivity of a compound by eliminating or preventing hot-spot formation during unwanted stimuli. There are many CNMs and their derivatives capable of decreasing the sensitivity of EMs by suppressing hotspot formation. It was found that the three types of C_{60} derivatives exhibit different thermal stabilities, while the friction and impact sensitivities of HMX can be reduced from 100% to 70% and even to 60%, when 1% of C_{60} is added to HMX (Table 9).[327] For primary explosive, BNCP, its mechanical sensitivity could also be decreased by addition of CNMs and the impact sensitivity decreases in the following order: BNCP > BNCP/CNTs > BNCP/CB. However, MWCNT-2 with a smaller diameter (10–20 nm, Fig. 40) decreased its friction sensitivity.[52] CNMs are good coating materials for Mg and Al particles. In particular, SWCNTs are the most attractive CNM for coating small metal nanoparticles and clusters, forming metalized SWCNTs. In this way, the sensitivity of energetic compositions based on these metals is decreased.[328] However, when RDX and PETN are doped with CB or CNTs, their laser initiation sensitivity is lowered due to an increase in their light absorbance.[329] Although CB increased the photo-sensitivity of RDX and PETN, it decreased the mechanical sensitivity of thermites. As mentioned earlier, the mechanical sensitivity of a WO_3/Al nanothermite (Fig. 40) could be improved by using pristine or chemically modified V3G CB as an additive.[54] All of the prepared energetic composites were found to be insensitive to impact (with threshold >50 J, Table 9).

Unfortunately, the influence of the CNM additives on the electrostatic discharge sensitivity was very limited, due to the low amount of additive used in the preparation of these nanothermites (<5 wt%). This indicates that ESD desensitization is more related to percolation effects than to the intrinsic conductivity of the CB. In addition to CB, "herringbone" carbon nanofibers (CNFs) are another suitable desensitizer for nanothermites (*e.g.*, MnO_2/Al), to allow safer handling.[330] A dramatic decrease in the friction sensitivity (>360 N), compared to pure MnO_2/Al nanothermite (>5 N), was found and the ESD sensitivity was also considerably reduced (from 1.0 to 5300 mJ). Even though some energetic compounds such as 3-nitro-1,2,4-triazol-5-one (NTO) are quite insensitive, it is still useful to add a certain amount of CNMs (*e.g.* 1 wt% of graphene) to increase the processing capability of NTO as an ingredient of PBXs.[331] It was also shown that the mechanical sensitivities of ε-CL-20/glue can be reduced with the incorporation of graphite, GO and rGO in PBX formulations.[265] A later report shows that GO sheets exhibited a better desensitizing effect than C_{60} and CNTs.[166] When 2 wt% GO sheets are added, the impact sensitivity of as-prepared HMX decreases from 100% to 10% and the friction sensitivity reduces from 100% to 32%.

Conclusions and future directions

As summarized in this review, extensive investigations were and are currently being conducted regarding the design, synthesis, characterization and application of various CNMs or functionalized CNMs in EMs. Widely used CNMs include graphene, GO, rGO, CNTs, activated carbon fiber and EG, as well as functionalized graphene and C_{60}-fullerene. Until now, EG had only been used in chemical heat pumps, however, it may have additional uses in the field of EMs, *e.g.*, as an additive in nanothermites and as a promising flame retardant additive in cladding materials for solid propellant charges. In contrast to EG, C_{60}-fullerene can be functionalized with energetic groups, forming a new family of energetic compounds with excellent

thermal stability. However, the variety of energetic moieties used for C_{60}-fullerene functionalization is still limited and more exploration is required in this field. C_{60}-fullerene derivatives can either be used as combustion catalysts, energetic binders or additives, depending on the type of functional groups. Their compatibility with other components of explosives and propellants, as well as their sensitivity, also needs to be systematically investigated with respect to their practical applications. Graphene and its aerogels can usually be combined with either catalysts or oxidizers using a sol–gel method. These novel composite materials are likely to be used as advanced oxidizers and combustion catalysts. Among all the CNMs, only GO and rGO were found to be energetic by themselves. They could also be used as matrices to bind many other energetic compounds, including HMX, NC and FOX-7. The common energetic materials could either be deposited on the surface of GO or their crystals/particles could be coated with thin layers of GO (rGO). It should be mentioned that the development of practically all composite materials based on GO or rGO was reported during the last 3 years. Many other new energetic compounds could be deposited on GO or rGO in order to enhance their performance, as potential combustion catalysts of solid propellants or as additives to propellants and explosives. Similarly to C_{60}-fullerene, many functionalized CNTs were developed as combustion catalysts or energetic additives to propellants. Likewise, some of these nanomaterials were also used in new formulations of thermites and ignitors. The preparation procedures of CNM-containing EMs are well developed and include a broad variety of synthetic techniques such as microemulsion, hydrothermal, reductive deposition, ultrasonic compositing and CVD, as well as chemical reaction methods. Combination of CNTs with highly sensitive EMs could provide a way to improve the sensitivity and performances of these EMs. However, the encapsulation of sensitive or unstable energetic molecules into CNTs is still extremely challenging and will require much more theoretical and experimental work. The desensitization mechanism of CNMs on EMs is still not very clear and more theoretical work is needed to address this issue. Although the use of DnDs has become more and more popular in various areas, its application in EMs is only in its infancy. DnDs can be functionalized with energetic or other functional groups, where one of the most challenging issues will be their surface structure characterization.

In summary, it is very clear from the information presented in this review that use of various CNMs in energetic applications is extremely promising and rewarding, being capable of addressing numerous problems in this field and having tremendous growth opportunities in the near future.

Acknowledgements

The financial support from the Planning and Budgeting Committee (PBC) of the Council for Higher Education in the Israeli government is greatly appreciated. This work was also partially supported by the Center for Nanoscience and Nanotechnology and by the Faculty of Exact Sciences in Tel Aviv University.

References

1 J. P. Agrawal, *High Energy Materials Propellants, Explosives and Pyrotechnics*, Wiley-VCH, 2010, p. 69, ISBN: 978-3-527-32610-5.
2 C. S. David, *The Mother of Gunpowder*, Oxford University Press, 2013.
3 A. K. Sikder and N. Sikder, A review of advanced high performance, insensitive and thermally stable energetic materials emerging for military and space applications, *J. Hazard. Mater.*, 2004, **112**, 1–15.
4 T. M. Klapotke, in *High Energy Density Materials*, ed. T. M. Klapotke, Springer, Heidelberg, 2007, pp. 85–121.
5 J. Ying, X. Guo-gen and W. Xuan-jun, *Application of lightweight carbon materials*, National Defense Industry Press, Beijing, 2013.
6 M. Lulu, H. C. Amelia, S. O. Hart, V. Robert and M. A. Pulickel, Spiers memorial lecture advances of carbon nanomaterials, *Faraday Discuss.*, 2014, **173**, 9.
7 Y. Zhai, Z. Zhu and S. Dong, Carbon-based nanostructures for advanced catalysis, *ChemCatChem*, 2015, **7**(18), 2806–2815.
8 M. Comet, V. Pichot, B. Siegert and D. Spitzer, Use of nanodiamonds as a reducing agent in a chlorate-based energetic composition, *Propellants, Explos., Pyrotech.*, 2009, **34**, 166–173.
9 P. Jiang-feng, Z. Feng-Qi, S. Xiu-duo and Z. Wei, Progress of the application of lightweight carbon materials and their composites in solid rocket propellants, *Chin. J. Explos. Propellants*, 2014, **2**, 1–6.
10 P. Delhaes, *Carbon-based Solids and Materials Carbon-based Solids and Materials*, 2013, pp. 1–640, ISBN: 9781118557617.
11 W. Han, Z. Feng-qi and L. Shang-wen, Function of carbon materials used in solid propellants and their action mechanism, *Chin J. Explos. Propellants*, 2005, **29**, 32–35.
12 W. Ying-lei, Z. Feng-Qi and Y. Jian-hua, New progress of study combustion catalysts used for solid rocket propellants, *Chin. J. Explos. Propellants*, 2012, **35**, 1–8.
13 V. D. Heijden, R. H. B. Bouma, A. C. Van Der Steen and H. R. Fischer, Application and characterization of nanomaterials in energetic compositions, *Mater. Res. Soc. Symp. Proc.*, 2003, **800**, 191–208.
14 Synthesis, characterization and properties of energetic/reactive nanomaterials, Materials Research Society Symposium - Proceedings, 2003, vol. 800, p. 392.
15 V. V. Pokropivny and A. L. Ivanovskii, New nanoforms of carbon and boron nitride, *Russ. Chem. Rev.*, 2008, **77**, 837–873.
16 X. Han and S. Li, Advances in catalytic function of fullerene materials, *Prog. Chem.*, 2006, **18**, 715–720.
17 Y.-F. Lan, X.-Y. Li and Y.-J. Luo, Research progress on application of graphene in energetic materials, *Chin. J. Explos. Propellants*, 2015, **38**, 1–7.

18 C. K. Law, Fuel options for next-generation chemical propulsion, *AIAA J.*, 2012, **50**, 19–36.
19 C. Ren, X.-J. Wang, Y.-X. Li, J.-L. Wang and D.-L. Cao, Research and application of graphene composites, *Mod. Chem. Industry*, 2015, **35**, 32–35.
20 P. M. Ajayan and T. W. Ebbesen, Nanometre-size tubes of carbon, *Rep. Prog. Phys.*, 1997, **60**, 1025–1062.
21 P. C. Eklund, A. M. Rao, P. Zhou, Y. Wang and J. M. Holden, Photochemical transformation of C_{60} and C_{70} films, *Thin Solid Films*, 1995, **257**(2), 185–203.
22 M. F. L. De Volder, S. H. Tawfick, R. H. Baughman and A. J. Hart, Carbon Nanotubes Present and Future Commercial Applications, *Science*, 2013, **339**, 535–539.
23 M. Zhang, S. Fang, A. A. Zakhidov, S. B. Lee, A. E. Aliev, C. D. Williams, K. R. Atkinson and R. H. Baughman, Strong, Transparent, Multifunctional, Carbon Nanotube Sheets, *Science*, 2005, **309**, 1215–1219.
24 S. Wu, R. Ge, M. Lu, R. Xu and Z. Zhang, Graphene-based nano-materials for lithium-sulfur battery and sodium-ion battery, *Nano Energy*, 2015, **15**, 379–405.
25 D. Geng, H. Wang and G. Yu, Graphene single crystals Size and morphology engineering, *Adv. Mater.*, 2015, **27**, 2821–2837.
26 D. Tománek, Interfacing graphene and related, 2D materials with the 3D world, *J. Phys.: Condens. Matter*, 2015, **27**, 133203.
27 S. Ge, F. Lan, F. Yu and J. Yu, Applications of graphene and related nanomaterials in analytical chemistry, *New J. Chem.*, 2015, **39**, 2380–2395.
28 Y. Li, H. Dong, Y. Li and D. Shi, Graphene-based nanovehicles for photodynamic medical therapy, *Int. J. Nanomed.*, 2015, **10**, 2451–2459.
29 W.-B. Ding, L. Wang, Q. Yang, W.-D. Xiang, J.-M. Gao and W. A. Amer, Recent research progress on polymer grafted carbon black and its novel applications, *Int. Polym. Process.*, 2013, **28**, 132–142.
30 T. Novakov and H. Rosen, The black carbon story Early history and new perspectives, *Ambio*, 2013, **42**, 840–851.
31 X. Li, Z. Li and Y. Xia, Test and calculation of the carbon black reinforcement effect on the hyper-elastic properties of tire rubbers, *Rubber Chem. Technol.*, 2015, **88**, 98–116.
32 M. Jacobsson, F. Wang, P. Cameron, J. Neilsen, L. Nikiel and W. Wampler, Improvements in carcass carbon blacks to enhance compound performance, *Rubber World*, 2015, **251**, 30–34.
33 V. M. Shopin, Separation of the desired product from aerosol flows in the manufacture of carbon black a review, *Solid Fuel Chem.*, 2014, **48**(3), 180–197.
34 L. Wang, X. Wang, B. Zou, X. Ma, Y. Qu, C. Rong, Y. Li, Y. Su and Z. Wang, Preparation of carbon black from rice husk by hydrolysis, carbonization and pyrolysis, *Bioresour. Technol.*, 2011, **102**, 8220–8224.
35 K.-H. Kuo, Y.-H. Peng, W.-Y. Chiu and T.-M. Don, A novel dispersant for preparation of high loading and photosensitive CB dispersion, Inc, *J. Polym. Sci., Part A: Polym. Chem.*, 2008, **46**, 6185–6197.
36 C. M. Karbiwnyk and K. E. Miller, A review of current analytical applications employing graphitized carbon black, *Carbon Black Product., Proper. Uses*, 2011, 69–92.
37 L. Li, W. Li, D. Qin, S. Jiang and F. Liu, Application of graphitized carbon black to the quechers method for pesticide multiresidue analysis in Spinach, *J. AOAC Int.*, 2009, **92**, 538–547.
38 T. Horikawa, Y. Zeng, D. D. Do, K.-I. Sotow and J. R. Alcántara Avila, On the isosteric heat of adsorption of non-polar and polar fluids on highly graphitized carbon black, *J. Colloid Interface Sci.*, 2015, **439**, 1–6.
39 X.-Q. Yang, B. Wang, S.-E. Liu and X.-J. Guo, Effect of carbon black on burning properties of modified nitramine double base propellant, *Energ. Mater.*, 2004, **12**, 408.
40 E. Papirer, E. Brendle, F. Ozil and H. Balard, Comparison of the surface properties of graphite, CB and fullerene samples, measured by inverse gas chromatography, *Carbon*, 1999, **37**, 1265–1274.
41 M. Kruk, Z. Li, M. Jaroniec and W. R. Betz, Nitrogen Adsorption Study of Surface Properties of Graphitized Carbon Blacks, *Langmuir*, 1999, **15**, 1435–1441.
42 S.-P. Rwei, F.-H. Ku and K.-C. Cheng, Dispersion of CB in a continuous phase Electrical, rheological, and morphological studies, *Colloid Polym. Sci.*, 2002, **280**, 1110–1115.
43 Y.-F. Shih and R.-J. Jeng, Carbon black containing interpenetrating polymer networks based on unsaturated polyester/epoxy. I. Dynamic mechanical properties, thermal analysis, and morphology, *J. Appl. Polym. Sci.*, 2002, **86**, 1904–1910.
44 G. Wu, S. Asai, M. Sumita and H. Yui, Entropy penalty-induced self-assembly in carbon black or carbon fiber filled polymer blends, *Macromolecules*, 2002, **35**, 945–951.
45 P. Kowalczyk, K. Kaneko, A. P. Terzyk, H. Tanaka, H. Kanoh and P. A. Gauden, The evaluation of the surface heterogeneity of carbon blacks from the lattice density functional theory, *Carbon*, 2004, **42**, 1813–1823.
46 A. Schröder, M. Klüppel and R. H. Schuster, Characterisation of surface activity of carbon black and its relation to polymer-filler interaction, *Macromol. Mater. Eng.*, 2007, **292**, 885–916.
47 T. Mathew, R. N. Datta, W. K. Dierkes, J. W. M. Noordermeer and W. J. Van Ooij, A comparative investigation of surface modification of CB and silica by plasma polymerization, *Rubber Chem. Technol.*, 2008, **81**, 209–226.
48 T. Mathew, R. N. Datta, W. K. Dierkes, W. J. van Ooij, J. W. M. Noordermeer, T. M. Gruenberger and N. Probst, Importance of fullerenic active sites in surface modification of carbon black by plasma polymerization, *Carbon*, 2009, **47**, 1231–1238.
49 Q.-L. Yan, S. Zeman and A. Elbeih, Recent advances in thermal analysis and stability evaluation of insensitive plastic bonded explosives PBXs, *Thermochim. Acta*, 2012, **537**, 1–12.
50 Y.-L. Duan, Y. Tong, Y. Cao and F.-L. Huang, Phase transition of carbon black shocked by explosion, *Acta Armamentarii*, 2013, **34**, 169–174.

51 E. M. Zhazaeva, A. G. Pshikhachev, T. A. Gubzhev, A. A. Kashirgov, Z. M. Gekkieva and R. B. Tkhakakhov, Surface energetic and strength characteristics of heat treated composites based on butadiene-acrylonitrile elastomer modified with CB, *Inter. Polym. Sci. Tech.*, 2013, **40**, T33–T37.

52 L.-K. Chen, D.-L. Sheng, B. Yang, Y.-H. Zhu, M.-H. Xu, Y.-L. Pu and Z.-X. Li, Effects of carbon nanotubes and carbon black on sensitivity performances of BNCP, *Chin. J. Energet. Mater.*, 2013, **21**, 35–38.

53 B. Yang, D.-L. Sheng, L.-K. Chen, H.-S. Xu, Y.-Y. Men and Y.-H. Zhu, Performance of carbon black/potassium nitrate propellant for blasting valve, *Chin. J. Energet. Mater.*, 2014, **22**, 397–400.

54 A. Bach, P. Gibot, L. Vidal, R. Gadiou and D. Spitzer, Modulation of the Reactivity of a WO_3/Al Energetic Material with Graphitized CB as Additive, *J. Energ. Mater.*, 2015, **33**, 260–276.

55 O. Shenderova, A. M. Panich, S. Moseenkov, S. C. Hens, V. Kuznetsov and H.-M. Vieth, Hydroxylated detonation nanodiamond FTIR, XPS, and NMR studies, *J. Phys. Chem. C*, 2011, **115**, 19005–19011.

56 G. Amaratunga, A. Putnis, K. Clay and W. Milne, Crystalline diamond growth in thin films deposited from a CH_4/Arrf plasma, *Appl. Phys. Lett.*, 1989, **55**, 634–635.

57 B. Wen, J. J. Zhao and T. J. Li, Synthesis and crystal structure of n-diamond, *Int. Mater. Rev.*, 2007, **52**, 131–151.

58 A. Krishnan, E. Dujardin, M. M. J. Treacy, J. Hugdahl, S. Lynum and T. W. Ebbesen, Graphitic cones and the nucleation of curved carbon surfaces, *Nature*, 1997, **388**, 451–454.

59 S. Lijima, P. M. Ajayan and T. Ichihashi, Growth model for carbon nanotubes, *Phys. Rev. Lett.*, 1992, **69**, 3100–3103.

60 H. W. Kroto, J. R. Heath, S. C. O'Brien, R. F. Curl and R. E. Smalley, C_{60} buckminsterfullerene, *Nature*, 1985, **318**, 162–163.

61 J. B. Howard, J. T. McKinnon, Y. Makarovsky, A. L. Lafleur and M. E. Johnson, Fullerenes C_{60} and C_{70} in flames, *Nature*, 1991, **352**, 139–141.

62 M. T. Yin and M. L. Cohen, Will diamond transform under megabar pressures?, *Phys. Rev. Lett.*, 1983, **50**, 2006–2009.

63 M. Frenklach, R. Kematick, D. Huang, W. Howard, K. E. Spear, A. W. Phelps and R. Koba, Homogeneous nucleation of diamond powder in the gas phase, *J. Appl. Phys.*, 1989, **66**, 395–399.

64 E. Papirer, E. Brendle, F. Ozil and H. Balard, Comparison of the surface properties of graphite, CB and fullerene samples, measured by inverse gas chromatography, *Carbon*, 1999, **37**, 1265–1274.

65 H. Hirai and K.-I. Kondo, Modified phases of diamond formed under shock compression and rapid quenching, *Science*, 1991, **253**, 772–774.

66 J. B. Howard, K. D. Chowdhury and J. B. Vander Sande, Carbon shells in flames, *Nature*, 1994, **370**, 603.

67 F. Cataldo, The impact of a fullerene-like concept in carbon black science, *Carbon*, 2002, **40**, 157–162.

68 C. Mailhiot and A. K. McMahan, Atmospheric-pressure stability of energetic phases of carbon, *Phys. Rev. B: Condens. Matter*, 1991, **44**, 11578–11591.

69 C. S. Yoo, W. J. Nellis, M. L. Sattler and R. G. Musket, Diamond like metastable carbon phases from shock-compressed C_{60} films, *Appl. Phys. Lett.*, 1992, **61**, 273–275.

70 J. L. Peng, L. A. Bursill, B. Jiang, J. O. Orwa and S. Prawer, Growth of c-diamond, n-diamond and i-carbon nanophases in carbon-ion-implanted fused quartz, Philosophical Magazine B Physics of Condensed Matter; Statistical Mechanics, Electronic, *Opt. Magnet. Proper.*, 2001, **81**, 2071–2087.

71 B. Wen, T. Li, C. Dong, X. Zhang, S. Yao, Z. Cao, D. Wang, S. Ji and J. Jin, Preparation of diamond nanocrystals from catalysed carbon black in a high magnetic field, *J. Phys.: Condens. Matter*, 2003, **15**, 8049–8054.

72 B. Wen, J. Zhao, T. Li, C. Dong and J. Jin, n-diamond from catalysed carbon nanotubes synthesis and crystal structure, *J. Phys.: Condens. Matter*, 2005, **17**, L513–L519.

73 E. Mironov, E. Petrov and A. Koretz, Chemical aspect of ultradispersed diamond formation, *Diamond Relat. Mater.*, 2003, **12**, 1472–1476.

74 G. V. Sakovich, A. S. Zharkov and E. A. Petrov, Results of research into the physicochemical processes of detonation synthesis and nanodiamond applications, *Nanotechnol. Russ.*, 2013, **8**, 581–591.

75 A. A. Gromov, S. A. Vorozhtsov, V. F. Komarov, G. V. Sakovich, Y. I. Pautova and M. Offermann, Ageing of nanodiamond powder Physical characterization of the material, *Mater. Lett.*, 2013, **91**, 198–201.

76 V. Y. Dolmatov, V. Myllymäki and A. Vehanen, A possible mechanism of nanodiamond formation during detonation synthesis, *J. Sup. Hard Mater.*, 2013, **35**, 143–150.

77 R. K. Barton and A. J. Barratt, Observations on the Reactivity of Pyrotechnic Compositions Containing Potassium Chlorate and Thiourea, *Propellants, Explos., Pyrotech.*, 1993, **18**, 77.

78 M. Comet, L. Schreyeck and H. Fuzellier, An efficient composition for bengal lights, *J. Chem. Educ.*, 2002, **79**, 70.

79 M. Comet, V. Pichot, B. Siegert, D. Spitzer, J.-P. Moeglin and Y. Boehrer, Use of nanodiamonds as a reducing agent in a chlorate-based energetic composition, *Propellants, Explos., Pyrotech.*, 2009, **34**, 166–173.

80 M. Comet, V. Pichot, F. Schnell and D. Spitzer, Oxidation of detonation n-D in a reactive formulation, *Diamond Relat. Mater.*, 2014, **47**, 35–39.

81 Y. Tong, R. Liu and T. Zhang, The effect of a detonation nanodiamond coating on the thermal decomposition properties of RDX explosives, *Phys. Chem. Chem. Phys.*, 2014, **16**, 17648–17657.

82 M.-Y. Shen, K.-Y. Li, C.-F. Kuan, H.-C. Kuan, C.-H. Chen, M.-C. Yip, H.-W. Chou and C.-L. Chiang, Preparation of expandable graphite via ozone-hydrothermal process and

flame-retardant properties of high-density polyethylene composites, *High Perform. Polym.*, 2014, **26**, 34–42.

83 X.-Y. Pang, M.-W. Duan, Y. Tian and M. Zhai, Preparation of expandable graphite with phosphoric acid as ancillary intercalation reagent and its antiflame property for linear low density polyethylene, *Asian J. Chem.*, 2013, **25**, 5390–5394.

84 C.-F. Kuan, K.-C. Tsai, C.-H. Chen, H.-C. Kuan, T.-Y. Liu and C.-L. Chiang, Preparation of expandable graphite via H_2O_2-hydrothermal process and its effect on properties of high-density polyethylene composites, *Polym. Composit.*, 2012, **33**, 872–880.

85 W. Meiling, Z. Jinjiang, G. Yunqiao, Y. Xiongbo, G. Yajun and Z. Jianwei, Electrochemical Determination of Sunset Yellow Based on an Expanded Graphite Paste Electrode, *J. Electrochem. Soc.*, 2013, **160**(8), H459–H462.

86 Y. Wen, K. He, Y. Zhu, F. Han, Y. Xu, I. Matsuda, Y. Ishii, J. Cumings and C. Wang, Expanded graphite as superior anode for sodium-ion batteries, *Nat. Commun.*, 2014, **5**, 4033.

87 L. Ji-hui, F. Li-li and J. Zhi-xin, Preparation of expanded graphite with 160 μm mesh of fine flake graphite, *Mater. Lett.*, 2006, **60**, 746–749.

88 S. Ba, C. Jiang, K. Sun and Z. Sun, Prepared and infrared extinction characteristics of micron expanded graphite, *Adv. Mater. Res.*, 2011, **308–310**, 710–714.

89 L. Gao, Y.-X. Gong and L. Ma, Effect of expansion time on the microstructure of an expanded natural flake graphite, *New Carbon Mater.*, 2006, **21**, 139–143.

90 M. Balat and B. Spinner, Optimization of a chemical heat pump Energetic density and power, *Heat Recovery Syst. CHP*, 1993, **13**, 277–285.

91 M. Zamengo, J. Ryu and Y. Kato, Thermochemical performance of magnesium hydroxide-expanded graphite pellets for chemical heat pump, *Appl. Therm. Eng.*, 2014, **64**, 339–347.

92 X. Wu, L. Wang, C. Wu, G. Wang and P. Jiang, Flammability of EVA/IFR APP/PER/ZB system, and EVA/IFR/synergist $CaCO_3$, NG, and EG, composites, *J. Appl. Polym. Sci.*, 2012, **126**, 1917–1927.

93 Q. Zhang, J. Yan, T.-P. Li and J. Wang, Preparation of magnetic expanded graphite by Sol-gel method and its electromagnetic properties, *Adv. Mater. Res.*, 2011, **295-297**, 93–97.

94 P. R. Birkett, Fullerene chemistry, *Annu. Rep. Prog. Chem., Sect. A: Inorg. Chem.*, 1999, **95**, 431–451.

95 P. Maurizio, Fullerene chemistry for materials science applications, *J. Mater. Chem.*, 1997, **7**, 1097–1109.

96 I. Kenichiro, Molecular Catalysis for Fullerene Functionalization, *Chem. Rec. MBLA Spec. Is.*, 2011, **11**(5), 226–235.

97 M. Nazario, S. Nathalie and N. Jean-François, Advances in Molecular and Supramolecular Fullerene Chemistry, *Electrochem. Soc. Interface*, 2006, 29–33.

98 K. Li, D. I. Schuster, D. M. Guldi, M. A. Herranz and L. Echegoyen, Convergent Synthesis and Photophysics of [60]Fullerene/Porphyrin-Based Rotaxanes, *J. Am. Chem. Soc.*, 2004, **126**, 3388.

99 Y. Nakamura, S. Minami, K. Iizuka and J. Nishimura, Preparation of Neutral [60]Fullerene-Based [2]Catenanes and [2]Rotaxanes Bearing an Electron-Deficient Aromatic Diimide Moiety, *Angew. Chem., Int. Ed.*, 2003, **42**, 3158.

100 F. Cardinali, H. Mamlouk, Y. Rio, N. Armaroli and J.-F. Nierengarten, Fullerohelicates: a new class of fullerene-containing supermolecules, *Chem. Commun.*, 2004, 1582.

101 D. Felder, B. Heinrich, D. Guillon, J.-F. Nicoud and J.-F. Nierengarten, A Liquid Crystalline Supramolecular Complex of C_{60} with a Cyclotriveratrylene Derivative, *Chem. – Eur. J.*, 2000, **6**, 3501.

102 D. M. Guldi and N. Martin, Fullerene architectures made to order; biomimetic motifs — design and features, *J. Mater. Chem.*, 2002, **12**, 1978.

103 U. Hahn, M. Elhabiri, A. Trabolsi, H. Herschbach, E. Leize, A. van Dorsselaer, *et al.*, Supramolecular click chemistry with a bisammonium-C_{60} substrate and a ditopic crown ether host, *Angew. Chem., Int. Ed.*, 2005, **44**, 5338.

104 S. Delia and S. Roberto, Coordination Modes and Different Hapticities for Fullerene Organometallic Complexes, *Molecules*, 2012, **17**, 7151–7168.

105 S. Osuna, M. Swart and M. Solà, The reactivity of endohedral fullerenes. What can be learnt from computational studies?, *Phys. Chem. Chem. Phys.*, 2011, **13**, 3585–3603.

106 S. Yang, F. Liu, C. Chen, M. Jiao and T. Wei, Fullerenes encaging metal clusters-Clusterfullerenes, *Chem. Commun.*, 2011, **47**, 11822–11839.

107 Y. Matsuo, K. Kanaizuka, K. Matsuo, Y.-W. Zhong, T. Nakae and E. Nakamura, Photocurrent-Generating Properties of Organometallic Fullerene Molecules on an Electrode, *J. Am. Chem. Soc.*, 2008, **130**, 5016–5017.

108 N. Wang, J. Li and G. Ji, Synthesis of trinitrophenyl C_{60} derivative, *Propellants, Explos., Pyrotech.*, 1996, **21**, 317–319.

109 B. Jin, R.-F. Peng, Y.-J. Shu, F.-C. Zhong and S.-J. Chu, Study on the synthesis of new energetic fullerene derivative, Chinese, *J. High Pressure Phys.*, 2006, **20**, 220–224.

110 B. Jin, R.-F. Peng, B.-S. Tan, Y.-M. Huang, Y.-J. Shu, S.-J. Chu and Y.-B. Fu, Synthesis and characterization of nitro fulleropyrrolidine derivatives, *Chin. J. Energet. Mater.*, 2009, **17**, 287–292.

111 W. Tingting and Z. Heping, Synthesis, charge-separated state characterization of N-methyl-2-4′-N-ethylcarbozole,-3-fulleropyrrolidine and its derivatives, *Frontiers Chem. China*, 2006, **1**, 161–169.

112 B. Tan, R. Peng, H. Li, B. O. Jin, S. Chu and X. Long, Theoretical investigation of an energetic fullerene derivative, *J. Comput. Chem.*, 2010, **31**, 2233–2237.

113 F. Cataldo, O. Ursini and G. Angelini, Synthesis and explosive decomposition of polynitro[60]fullerene, *Carbon*, 2013, **62**, 413–421.

114 B.-L. Chen, B. Jin, R.-F. Peng, F.-Q. Zhao, J.-H. Yi, W.-J. Han, H.-J. Guan and S.-J. Chu, Synthesis and

characterization of fullerene-ethylenediamine nitrate, *Chin. J. Energet. Mater.*, 2014, **22**, 186–191.

115 Q.-Q. Liu, B. Jin, R.-F. Peng, F.-Q. Zhao, S.-Y. Xu and S.-J. Chu, Preparation and characterization of fullerene itaconic acid copolymer lead salt, *Chin. J. Explos. Propellants*, 2013, **36**, 64–69.

116 B.-L. Chen, B. Jin, R.-F. Peng, F.-Q. Zhao, J.-H. Yi, H.-J. Guan, X.-B. Bu and S.-J. Chu, Synthesis, characterization and thermal decomposition of fullerene-ethylenediamine dinitramide, *Chin. J. Energet. Mater.*, 2014, **22**, 467–472.

117 H.-J. Guan, R.-F. Peng, B. Jin, H. Liang, F.-Q. Zhao, X.-B. Bu, W.-J. Han and S.-J. Chu, Preparation and thermal performance of fullerene-based lead salt, *Bull. Korean Chem. Soc.*, 2014, **35**, 2257–2262.

118 Z. Hu, C. H. Zhang, Y. D. Huang, S. F. Sun, W. C. Guan and Y. H. Yao, Photodynamic anticancer activities of water-soluble C_{60} derivatives and their biological consequences in a HeLa cell line, *Chem. – Biol. Interact.*, 2012, **195**, 86–94.

119 H.-J. Guan, B. Jin, R.-F. Peng, F.-Q. Zhao, W.-J. Han, B.-L. Chen and S.-J. Chu, The preparation and thermal decomposition performance of fullerene hydrazine nitrate, *Acta Armamentarii*, 2014, **35**, 1756–1764.

120 W. Gong, B. Jin, R. Peng, N. Deng, R. Zheng and S. Chu, Synthesis and Characterization of [60]Fullerene-Polyglycidyl nitrate, and Its Thermal Decomposition, *Ind. Eng. Chem. Res.*, 2015, **54**, 2613–2618.

121 T. Huang, B. Jin, R. F. Peng, C. D. Chen, R. Z. Zheng, Y. He and S. J. Chu, Synthesis and characterization of [60]fullerene-glycidyl azide polymer and its thermal decomposition, *Polymers*, 2015, **7**, 896–908.

122 K. S. Novoselov, A. K. Geim, S. V. Morozov, D. Jiang, Y. Zhang, S. V. Dubonos, *et al.*, Electric field effect in atomically thin carbon films, *Science*, 2004, **306**, 666–669.

123 M. J. Allen, V. C. Tung and R. B. Kaner, Honeycomb Carbon: A review of graphene, *Chem. Rev.*, 2010, **110**, 132–145.

124 Q. Tang, Z. Zhou and Z. Chen, Graphene-related nanomaterials tuning properties by functionalization, *Nanoscale*, 2013, **5**, 4541–4583.

125 X. Li, W. Cai, J. An, S. Kim, J. Nah, D. Yang, R. Piner, A. Velamakanni, I. Jung, E. Tutuc, S. K. Banerjee, L. Colombo and R. R. Ruoff, Large-area synthesis of high-quality and uniform graphene films on copper foils, *Science*, 2009, **324**, 1312–1314.

126 C. Mattevi, H. Kima and M. Chhowalla, A review of chemical vapour deposition of graphene on copper, *J. Mater. Chem.*, 2011, **21**, 3324–3334.

127 C. Vallés, C. Drummond, H. Saadaoui, C. A. Furtado, M. He, O. Roubeau, L. Ortolani, *et al.*, Solutions of negatively charged graphene sheets and ribbons, *J. Am. Chem. Soc.*, 2008, **130**(47), 15802–15804.

128 T. Morishita, A. J. Clancy and M. S. P. Shaffer, Optimised exfoliation conditions enhance isolation and solubility of grafted graphenes from graphite intercalation compounds, *J. Mater. Chem. A*, 2014, **2**(36), 15022–15028.

129 O. C. Compton and S. T. Nguyen, Graphene Oxide, Highly reduced graphene oxide, and graphene versatile building blocks for carbon-based materials, *Small*, 2010, **6**, 711–723.

130 D. Chen, H. Feng and J. Li, Graphene oxide Preparation, functionalization, and electrochemical applications, *Chem. Rev.*, 2012, **112**, 6027–6053.

131 D. R. Dreyer, S. Park, C. W. Bielawski and R. S. Ruoff, The chemistry of graphene oxide, *Chem. Soc. Rev.*, 2010, **39**, 228–240.

132 S. Gilje, W. Han, M. Wang, K. L. Wang and R. B. Kaner, A Chemical route to graphene for device applications, *Nano Lett.*, 2007, **7**, 3394–3398.

133 J. Pyun, Graphene Oxide as Catalyst Application of Carbon Materials beyond Nanotechnology, *Angew. Chem., Int. Ed.*, 2011, **50**, 46–48.

134 T.-F. Yeh, J.-M. Syu, C. Cheng, T.-H. Chang and H. Teng, Graphite Oxide as a Photocatalyst for Hydrogen Production from Water, *Adv. Funct. Mater.*, 2010, **20**, 2255–2262.

135 D. R. Dreyer, H.-P. Jia and C. W. Bielawski, Graphene Oxide: A Convenient Carbocatalyst for Facilitating Oxidation and Hydration Reactions, *Angew. Chem., Int. Ed.*, 2010, **49**, 6813–6816.

136 Y. J. Song, Y. Chen, L. Y. Feng, J. S. Ren and X. G. Qu, Selective and quantitative cancer cell detection using target-directed functionalized graphene and its synergetic peroxidase-like activity, *Chem. Commun.*, 2011, **47**, 4436–4438.

137 Y. J. Guo, L. Deng, J. Li, S. J. Guo, E. K. Wang and S. J. Dong, Hemin–Graphene Hybrid Nanosheets with Intrinsic Peroxidase-like Activity for Label-free Colorimetric Detection of Single-Nucleotide Polymorphism, *ACS Nano*, 2011, **5**, 1282–1290.

138 Y. Wang, Z. Li, J. Wang, J. Li and Y. Lin, Graphene and Graphene Oxide biofunctionalization and applications in biotechnology, *Trends Biotechnol.*, 2011, **29**, 205–212.

139 V. C. Sanchez, A. Jachak, R. H. Hurt and A. B. Kane, Biological Interactions of Graphene-Family Nanomaterials: An Interdisciplinary Review, *Chem. Res. Toxicol.*, 2012, **25**, 15–34.

140 J. Kim, L. J. Cote, F. Franklin Kim, W. Yuan, K. R. Shull and J. Huang, Graphene oxide sheets at interfaces, *J. Am. Chem. Soc.*, 2010, **132**, 8180–8186.

141 J. Sha, X. Lin-sheng, M. Yu-lu, H. Jing-jie, X. Zhang, Z. Guo-xun, D. Shu-mei and W. Yan-yun, Low-temperature expanded graphite for preparation of graphene sheets by liquid-phase method, *J. Phys.: Conf. Ser.*, 2009, **188**, 012040.

142 D. Yongqiang, C. Congqiang, Z. Xinting, G. Lili, C. Zhiming, Y. Hongbin, G. Chunxian, C. Yuwu and L. Chang-Ming, One-step and high yield simultaneous preparation of single- and multi-layer graphene quantum

dots from CX-72 carbon black, *J. Mater. Chem.*, 2012, **22**, 8764–8766.
143 B. C. Brodie, On the atomic weight of graphite, *Philos. Trans. R. Soc. London*, 1859, **14**, 249–259.
144 W. S. Hummers and R. E. Offeman, Preparation of graphitic oxide, *J. Am. Chem. Soc.*, 1958, **80**, 1339.
145 D. C. Marcano, D. V. Kosynkin, J. M. Berlin, A. Sinitskii, Z. Sun, A. Slesarev, *et al.*, Improved synthesis of graphene oxide, *ACS Nano*, 2010, **4**, 4806–4814.
146 J. Chen, Y. Li, L. Huang, C. Li and G. Shi, High-yield preparation of graphene oxide from small graphite flakes via an improved Hummers method with a simple purification process, *Carbon*, 2015, **81**, 826–834.
147 P. S. V. Jimenez, Thermal Decomposition of Graphite Oxidation Products DSC Studies of Internal Combustion of Graphite Oxide, *Mater. Res. Bull.*, 1987, **22**, 601–608.
148 C. H. A. Wong, O. Jankovský, Z. Sofer and M. Pumera, Vacuum-assisted microwave reduction/exfoliation of graphite oxide and the influence of precursor graphite oxide, *Carbon*, 2014, **77**, 508–517.
149 D. Krishnan, F. Kim, J. Luo, R. Cruz-Silva, L. J. Cote, H. D. Jang and J. Huang, Energetic graphene oxide challenges and opportunities, *Nano Today*, 2012, **7**, 137–152.
150 J. C. Garcia, D. B. de Lima, L. V. C. Assali and J. F. Justo, Group IV graphene- and graphane-like nanosheets, *J. Phys. Chem. C*, 2011, **115**, 13242–13246.
151 Y. Yamada, M. Miyauchi, K. Jungpil, *et al.*, Exfoliated graphene ligands stabilizing copper cations, *Carbon*, 2011, **49**, 3375–3378.
152 Y. Yamada, Y. Suzuki, H. Yasuda, S. Uchizawa, K. Hirose-Takai, Y. Sato, K. Suenaga and S. Sato, Functionalized graphene sheets coordinating metal cations, *Carbon*, 2014, **75**, 81–94.
153 C. Zhang, X. Cao and B. Xiang, Sandwich complex of TATB/graphene: An approach to molecular monolayers of explosives, *J. Phys. Chem. C*, 2010, **114**, 22684–22687.
154 Z.-M. Li, M.-R. Zhou, T.-L. Zhang, J.-G. Zhang, L. Yang and Z.-N. Zhou, The facile synthesis of graphene nanoplatelet-lead styphnate composites and their depressed electrostatic hazards, *J. Mater. Chem. A*, 2013, **1**, 12710–12714.
155 R. Liu, W. Zhao, T. Zhang, L. Yang, Z. Zhou and J. Zhang, Particle refinement and graphene doping effects on thermal properties of potassium picrate, *J. Therm. Anal. Calorim.*, 2014, **118**, 561–569.
156 X.-B. Wang, J.-Q. Li and Y.-J. Luo, Preparation and thermal decomposition behaviour of ammonium perchlorate/graphene aerogel nanocomposites, *Chin. J. Explos. Propellants*, 2012, **35**, 76–80.
157 X.-B. Wang, J.-Q. Li, Y.-J. Luo and M. Huang, A Novel ammonium perchlorate/graphene aerogel nanostructured energetic composite preparation and thermal decomposition, *Sci. Adv. Mater.*, 2014, **6**, 530–537.
158 Y. Lan, M. Jin and Y. Luo, Preparation and characterization of graphene aerogel/Fe_2O_3/ammonium perchlorate nanostructured energetic composite, *J. Sol-Gel Sci. Technol.*, 2015, **74**, 161–167.
159 S. Yang, X. Feng and K. Mullen, Sandwich-like, graphene-based titania nanosheets with high surface area for fast lithium storage, *Adv. Mater.*, 2011, **2331**, 3575–3579.
160 Y.-F. Lan and Y.-J. Luo, Preparation and characterization of graphene aerogel/ammonium nitrate nano composite energetic materials, *Chin. J. Explos. Propellants*, 2015, **38**, 15–18.
161 R. Thiruvengadathan, S. W. Chung, S. Basuray, B. Balasubramanian, C. S. Staley, K. Gangopadhyay and S. Gangopadhyay, A versatile self-assembly approach toward high performance nanoenergetic composite using functionalized graphene, *Langmuir*, 2014, **30**(22), 6556–6564.
162 Y. Wang, H. Liu, H. Cheng, M. Zu and J. Wang, Corrosion behavior of pyrocarbon coatings exposed to Al_2O_3-SiO_2 gels containing ammonium nitrate, *Corros. Sci.*, 2015, **94**, 401–410.
163 H. Cai, L. Tian, B. Huang, G. Yang, D. Guan and H. Huang, 1,1-Diamino-2,2-dintroethene FOX-7, nanocrystals embedded in mesoporous carbon FDU-15, *Microporous Mesoporous Mater.*, 2013, **170**, 20–25.
164 A. C. Ferrari, F. Bonaccorso, V. Fal'ko, *et al.*, Science and technology roadmap for graphene, related two-dimensional crystals, and hybrid systems, *Nanoscale*, 2015, **7**, 4598–4810.
165 X. Zhang, W. M. Hikal, Y. Zhang, S. K. Bhattacharia, L. Li, S. Panditrao, S. Wang and B. L. Weeks, Direct laser initiation and improved thermal stability of nitrocellulose/graphene oxide nanocomposites, *Appl. Phys. Lett.*, 2013, **102**, 141905.
166 P. D. McCrary, P. A. Beasley, S. A. Alaniz, C. S. Griggs, R. M. Frazier and R. D. Rogers, Graphene and graphene oxide can "lubricate" ionic liquids based on specific surface interactions leading to improved low-temperature hypergolic performance, *Angew. Chem., Int. Ed.*, 2012, **51**, 9784–9787.
167 Y. Zhang, Z. Shao, K. Gao, X. Wu and Y. Liu, Tensile properties of nitrate glycerol ether cellulose/graphene oxide nanocomposites, *Integr. Ferroelectr.*, 2014, **154**, 147–153.
168 R. Li, J. Wang, J. P. Shen, C. Hua and G. C. Yang, Preparation and characterization of insensitive HMX/graphene oxide composites, *Propellants, Explos., Pyrotech.*, 2013, **38**, 798–804.
169 Y. Li, V. Alain-Rizzo, L. Galmiche, P. Audebert, F. Miomandre, G. Louarn, M. Bozlar, M. A. Pope, D. M. Dabbs and I. A. Aksay, Functionalization of Graphene Oxide by Tetrazine Derivatives: A Versatile Approach toward Covalent Bridges between Graphene Sheets, *Chem. Mater.*, 2015, **27**, 4298–4310.
170 M. Endo, H. Takuya and K. Yoong-Ahm, Large-scale production of carbon nanotubes and their applications, *Pure Appl. Chem.*, 2006, **78**, 1703–1713.
171 W. Z. Li, S. S. Xie, L. X. Qian, B. H. Chang, B. S. Zou, W. Y. Zhou, *et al.*, Large-Scale Synthesis of Aligned Carbon Nanotubes, *Science*, 1996, **274**, 1701–1703.
172 Z. F. Ren, Z. P. Huang, J. W. Xu, J. H. Wang, P. Bush, M. P. Siegal and P. N. Provencio, Synthesis of Large Arrays

of Well-Aligned Carbon Nanotubes on Glass, *Science*, 1998, **282**, 1105–1107.

173 S. Fan, M. G. Chapline, N. R. Franklin, T. W. Tombler, A. M. Cassell and H. Dai, Self-Oriented Regular Arrays of Carbon Nanotubes and Their Field Emission Properties, *Science*, 1999, **283**, 512–514.

174 B. Zheng, C. Lu, G. Gu, A. Makarovski, G. Finkelstein and J. Liu, Efficient CVD Growth of Single-Walled Carbon Nanotubes on Surfaces Using Carbon Monoxide Precursor, *Nano Lett.*, 2002, **2**, 895–898.

175 K. Hata, D. N. Futaba, K. Mizuno, T. Namai, M. Yumura and S. Iijima, Water-Assisted Highly Efficient Synthesis of Impurity-Free Single-Walled Carbon Nanotubes, *Science*, 2004, **306**, 1362–1364.

176 M. Terrones, N. Grobert, J. Olivares, J. P. Zhang, H. Terrones, K. Kordatos, W. K. Hsu, J. P. Hare, P. D. Townsend, K. Prassides, A. K. Cheetham, H. W. Kroto and D. R. M. Walton, Controlled production of aligned-nanotube bundles, *Nature*, 1997, **388**, 52–55.

177 A. Cao, B. Wei, Y. Jung, R. Vajtai, P. M. Ajayan and G. Ramanath, Growth of aligned carbon nanotubes on self-similar macroscopic templates, *Appl. Phys. Lett.*, 2002, **81**, 1297–1299.

178 B. Q. Wei, R. Vajtai, Y. Jung, J. Ward, R. Zhang, G. Ramanath and P. M. Ajayan, Microfabrication technology Organized assembly of carbon nanotubes, *Nature*, 2002, **416**, 495–496.

179 Y. J. Jung, B. Wei, R. Vajtai, P. M. Ajayan, Y. Homma, K. Prabhakaran and T. Ogino, Mechanism of Selective Growth of Carbon Nanotubes on SiO_2/Si Patterns, *Nano Lett.*, 2003, **3**, 561–564.

180 A. Cao, P. L. Dickrell, W. G. Sawyer, M. N. Ghasemi-Nejhad and P. M. Ajayan, Super-Compressible Foamlike Carbon Nanotube Films, *Science*, 2005, **310**, 1307–1310.

181 A. Cao, V. P. Veedu, X. Li, Z. Yao, M. N. Ghasemi-Nejhad and P. M. Ajayan, Multifunctional brushes made from carbon nanotubes, *Nat. Mater.*, 2005, **4**, 540–545.

182 C. R. Dean, A. F. Young, I. Meric, C. Lee, L. Wang, S. Sorgenfrei, K. Watanabe, T. Taniguchi, P. Kim, K. L. Shepard and J. Hone, Boron nitride substrates for high-quality graphene electronics, *Nat. Nanotechnol.*, 2010, **5**, 722–726.

183 M. S. Arnold, A. A. Green, J. F. Hulvat, S. I. Stupp and M. C. Hersam, Sorting carbon nanotubes by electronic structure using density differentiation, *Nat. Nanotechnol.*, 2006, **1**, 60–65.

184 Y.-M. Lin, C. Dimitrakopoulos, K. A. Jenkins, D. B. Farmer, H.-Y. Chiu, A. Grill and Ph. Avouris, 100-GHz transistors from wafer-scale epitaxial graphene, *Science*, 2010, **327**, 662.

185 K. S. Novoselov, V. I. Fal'Ko, L. Colombo, P. R. Gellert, M. G. Schwab and K. Kim, A roadmap for graphene, *Nature*, 2012, **490**, 192–200.

186 S. V. Morozov, K. S. Novoselov, M. I. Katsnelson, F. Schedin, D. C. Elias, J. A. Jaszczak and A. K. Geim, Giant intrinsic carrier mobilities in graphene and its bilayer, *Phys. Rev. Lett.*, 2008, **100**, 016602.

187 P. W. Sutter, J.-I. Flege and E. A. Sutter, Epitaxial graphene on ruthenium, *Nat. Mater.*, 2008, **7**, 406–411.

188 T. Utschig, M. Schwarz, G. Miehe and E. Kroke, Synthesis of carbon nanotubes by detonation of, 2,4,6-triazido-1,3,5-triazine in the presence of transition metals, *Carbon*, 2004, **42**, 823–828.

189 E. Kroke, M. Schwarz, V. Buschmann, G. Miehe, H. Fuess and R. Riedel, Nanotubes formed by detonation of C/N precursors, *Adv. Mater.*, 1999, **11**, 158–161.

190 S. J. Shearer, G. C. Turrell, J. I. Beyant and R. L. Brooks III, Vibrational spectra of cyanuric triazide, *J. Chem. Phys.*, 1968, **48**, 1138–1144.

191 C. Ye, H. Gao, J. A. Boatz, G. W. Drake, B. Twamley and J. M. Shreeve, Polyazidopyrimidines High-energy compounds and precursors to carbon nanotubes, *Angew. Chem., Int. Ed.*, 2006, **45**, 7262–7265.

192 E.-C. Koch, Metal/fluorocarbon pyrolants VI. Combustion behaviour and radiation properties of magnesium/polycarbon monofluoride, pyrolant, *Propellants, Explos., Pyrotech.*, 2005, **30**, 209–215.

193 G. Ćirić-Marjanovic, I. Pašti and S. Mentus, One-dimensional nitrogen-containing carbon nanostructures, *Prog. Mater. Sci.*, 2014, **69**, 61–182.

194 C. Zhang, J. Li, Y. Luo, X. Zhang and B. Zhai, Preparation and properties of carbon nanotubes modified glycidyl azide polymer binder film, *Polym. Mater. Sci. Eng.*, 2013, **29**, 105–108.

195 C. Zhang, J. Li, Y.-J. Li and Z. B. Zhang, Preparation and property studies of carbon nanotubes covalent modified BAMO-AMMO energetic binders, *J.Energet Mater*, 2015, **33**, 305–314.

196 Q.-L. Yan, S. Zeman and A. Elbeih, Thermal behavior and decomposition kinetics of Viton A bonded explosives containing attractive cyclic nitramines, *Thermochim. Acta*, 2013, **562**, 56–64.

197 Q.-L. Yan, S. Zeman, T.-L. Zhang and A. Elbeih, Non-isothermal decomposition behavior of Fluorel bonded explosives containing attractive cyclic nitramines, *Thermochim. Acta*, 2013, **574**, 10–18.

198 C.-M. Lin, J.-H. Liu, S.-J. Liu, Z. Huang, Y.-B. Li and J.-H. Zhang, Characterization viscoelastic properties of multi-walled carbon Nanotubes/F2314 composites using DMA method, *Chin. J. Energet. Mater.*, 2015, **23**, 140–145.

199 X.-M. Qian, N. Deng, S.-F. Wei and Z.-Y. Li, Catalytic effect of carbon nanotubes on pyrotechnics, *Chin. J. Energet. Mater.*, 2009, **17**, 603–607.

200 R. Guo, Y. Hu, R. Shen, Y. Ye and L. Wu, A micro initiator realized by integrating KNO_3/CNTs nanoenergetic materials with a Cu microbridge, *Chem. Eng. J.*, 2012, **211-212**, 31–36.

201 H. Yan, G. Rui, Y. Yinghua, S. Ruiqi, W. Lizhi and Z. Peng, Fabrication and electro-explosive performance of carbon nanotube energetic igniter, *Sci. Technol. Energ. Mater.*, 2012, **73**, 116–123.

202 R. Guo, Y. Hu, R. Shen and Y. Ye, Electro-explosion performance of KNO_3-filled carbon nanotubes initiator, *J. Appl. Phys.*, 2014, **115**, 174901.

203 L. J. Currano, W. Churaman, C. Becker, C. J. Morris, L. M. Reddy, A. Ihnen, P. Ajayan and W. Y. Lee, Energetic materials for integration on chip, Proceedings - 14th International Detonation Symposium, IDS, 2010, pp. 30–36.

204 V. Pelletier, S. Bhattacharyya, I. Knoke, F. Forohar, M. Bichay and Y. Gogotsi, Copper azide confined inside templated carbon nanotubes, *Adv. Funct. Mater.*, 2010, **20**, 3168–3174.

205 W. Choi, S. Hong, J. T. Abrahamson, J.-H. Han, C. Song, N. Nair, S. Baik and M. S. Strano, Chemically driven carbon-nanotube- guided thermopower waves, *Nat. Mater.*, 2010, **9**, 423–429.

206 L.-M. Liu, X.-L. Kang, Y. Yi, H.-F. Zhang, J.-S. Luo and Y.-J. Tang, Influence of CNTs on thermal behavior and light radiation properties of $Zr/KClO_4$ pyrotechnics, *Chin. J. Energet. Mater.*, 2014, **22**, 75–79.

207 N. Labhsetwar, P. Doggali, S. Rayalu, R. Yadav, T. Mistuhashi and H. Haneda, Ceramics in environmental catalysis Applications and possibilities, *Chin. J. Catalyst.*, 2012, **33**, 1611–1621.

208 X.-F. Dong, Y. Li, X.-F. Xiong and D.-L. Cao, Preparation and performance of copper-lead-carbon composite burning rate catalyst, *Chin. J. Explos. Propellants*, 2011, **34**, 69–73.

209 B. Van Devener, J. P. L. Perez, J. Jankovich and S. L. Anderson, Oxide-free, catalyst-coated, fuel-soluble, air-stable boron nanopowder as combined combustion catalyst and high energy density fuel, *Energy Fuels*, 2009, **23**, 6111–6120.

210 Y. Liu, W. Jiang, J.-X. Liu, Y. Wang, G.-P. Liu and F.-S. Li, Study of catalyzing thermal decomposition and combustion of AP/HTPB propellant with nano Cu/CNTs, *Acta Armamentarii*, 2008, **29**, 1029–1033.

211 X. Liu, W.-L. Hong, F.-Q. Zhao, D.-Y. Tian, J.-X. Zhang and Q.-S. Li, Synthesis of CuO/CNTs composites and its catalysis on thermal decomposition of FOX-12, *J. Solid Rocket Technol.*, 2008, **31**, 508–511.

212 I. G. Assovskiy and A. A. Berlin, Metallized carbon nanotubes, *Int. J. Energ. Mater. Chem. Propul.*, 2009, **8**, 281–289.

213 F. Wang, S. Arai and M. Endo, Metallization of multi-walled carbon nanotubes with copper by an electroless deposition process, *Electrochem. Commun.*, 2004, **6**, 1042–1044.

214 R. Wang, Z. Li, Y. Ma, F. Zhao and C. Pei, Preparation of high filling ratio Fe_2O_3/MWCNTs composite particles and catalytic performance on thermal decomposition of ammonium perchlorate, *Micro. Nano Lett.*, 2014, **9**, 787–791.

215 J.-X. Zhang, W.-L. Hong, F.-Q. Zhao, J.-H. Liu, D.-Y. Tian, X.-Y. Zhu and Y.-Q. Ma, Synthesis of SnO_2-Cu_2O/CNTs catalyst and its catalytic effect on thermal decomposition of FOX-12, *Chin. J. Explos. Propellants*, 2011, **34**, 47–51.

216 H. Ren, Y.-Y. Liu, Q.-J. Jiao, X.-F. Fu and T.-T. Yang, Preparation of nanocomposite PbO·CuO/CNTs via microemulsion process and its catalysis on thermal decomposition of RDX, *J. Phys. Chem. Solids*, 2010, **71**, 149–152.

217 G. Fan, H. Wang, X. Xiang and F. Li, Co-Al mixed metal oxides/carbon nanotubes nanocomposite prepared via a precursor route and enhanced catalytic property, *J. Solid State Chem.*, 2013, **197**, 14–22.

218 W. Pang, X. Fan, F. Zhao, H. Xu, W. Zhang, H. Yu, Y. Li, F. Liu, W. Xie and N. Yan, Effects of different metal fuels on the characteristics for HTPB-based fuel rich solid propellants, Propellants, *Explos. Pyrotech.*, 2013, **386**, 852–859.

219 Q.-L. Yan, X.-G. Wu, X. Guo, X.-F. Qi, X.-J. Li and K.-Q. Wang, Combustion efficiency and pyrochemical properties of micron-sized metal particles as the components of modified double-base propellant, *Acta Astro.*, 2011, **687–8**, 1098–1112.

220 D. Sylvain, B. Patric, G. Nicole, C. Sebastien and T. Serge, Flash-ignitable energetic material, *US Patent*, 20040040637A1, Mar 4, 2004.

221 T. An, H.-Q. Cao, F.-Q. Zhao, X.-N. Ren, D.-Y. Tian, S.-Y. Xu, H.-X. Gao, Y. Tan and L.-B. Xiao, Preparation and characterization of Ag/CNTs nanocomposite and its effect on thermal decomposition of cyclotrimethylene trinitramine, *Acta Physo.–Chim. Sin.*, 2012, **28**, 2202–2208.

222 H. Y. Jeong, K. P. So, J. J. Bae, S. H. Chae, T. H. Ly, T. H. Kim, D. H. Keum, C. K. Kim, J. S. Hwang, Y. J. Choi and Y. H. Lee, Tailoring oxidation of Al particles morphologically controlled by carbon nanotubes, *Energy*, 2013, **55**, 1143–1151.

223 A. Rai, D. Lee, K. Park and M. R. Zachariah, Importance of phase change of aluminum in oxidation of aluminum nanoparticles, *J. Phys. Chem. B*, 2004, **108**, 14793–14795.

224 K. J. Blobaum, M. E. Reiss, J. M. Plitzko Lawrence and T. P. Weihs, Deposition and characterization of a self-propagating CuO_x/Al thermite reaction in a multilayer foil geometry, *J. Appl. Phys.*, 2003, **94**, 2915–2922.

225 A. M. K. Esawi, K. Morsi, A. Sayed, M. Taher and S. Lanka, Effect of carbon nanotube CNT, content on the mechanical properties of CNT-reinforced aluminium composites, *Compos. Sci. Tech.*, 2010, **70**, 2237–2241.

226 Y. Wang, S. Malhotra and Z. Iqbal, Nanoscale energetics with carbon nanotubes, *Mater. Res. Soc. Symp. Proc.*, 2003, **800**, 351–359.

227 F. Forohar, C. M. Whitaker, I. C. Uber and V. Bellitto, Synthesis and Characterization of Nitro-Functionalized Single-Walled Carbon Nanotubes, *J. Energet. Mater.*, 2012, **30**, 55–71.

228 X.-T. Ji, J.-H. Bu, Z.-X. Ge, T.-Q. Li, H.-P. Su, Q. Liu, Y. Zhu and X. Xiao, Preparation and characterization of tetrazolyl-functionalized single walled carbon nanotubes, *Chin. J. Energet. Mater.*, 2015, **23**, 99–102.

229 J. T. Abrahamson, C. Song, J. H. Hu, J. M. Forman, S. G. Mahajan, N. Nair, W. Choi, E.-J. Lee and M. S. Strano, Synthesis and energy release of nitro-

benzene-functionalized single-walled carbon nanotubes, *Chem. Mater.*, 2011, **23**, 4557–4562.

230 L. Wang, C. Yi, H. Zou, H. Gan, J. Xu and W. Xu, Adsorption of the insensitive explosive TATB on single-walled carbon nanotubes, *Mol. Phys.*, 2011, **109**, 1841–1849.

231 L. Wang, J. Wu, C. Yi, H. Zou, H. Gan and S. Li, Assemblies of energetic 3,3′-diamino-4,4′-azofurazan on single-walled carbon nanotubes, *Comput. Theor. Chem.*, 2012, **982**, 66–73.

232 Y. Zhong, M. Jaidann, Y. Zhang, G. Zhang, H. Liu, M. Ioan Ionescu, R. Li, X. Sun, H. Abou-Rachid and L.-S. Lussier, Synthesis of high nitrogen doping of carbon nanotubes and modeling the stabilization of filled DAATO/CNTs 10,10, for nanoenergetic materials, *J. Phys. Chem. Solids*, 2010, **71**, 134–139.

233 M. A. Hiskey, D. E. Chavez and D. Naud, Preparation of 3,3′-azobis6-amino-1,2,4,5-tetrazine, *US Patent*, 6342589, 2002, United States Department of Energy, USA.

234 C. C. Tang, Y. Bando, D. Golberg and F. F. Xu, Structure and nitrogen incorporation of carbon nanotubes synthesized by catalytic pyrolysis of dimethylformamide, *Carbon*, 2004, **42**, 2625–2633.

235 K. Huang, S. Pisharath and S.-C. Ng, Preparation of polyurethane-carbon nanotube composites using 'click' chemistry, *Tetrahedron Lett.*, 2015, **56**, 577–580.

236 K. A. Jiang, L. S. Eitan, P. M. Schadler, R. W. Ajayan, N. Siegel, Grobert, *et al.*, Selective attachment of gold nanoparticles to nitrogen-doped carbon nanotubes, *Nano Lett.*, 2003, **3**, 275–277.

237 H. Abou-Rachid, A. Hu, V. Timoshevskii, Y. Song and L.-S. Lussier, Nanoscale high energetic materials A polymeric nitrogen chain N8 confined inside a carbon nanotube, *Phys. Rev. Lett.*, 2008, **100**, 196401.

238 G.-Q. Zhang, X.-B. Liu and M. Huang, Review on energetic nitroguanidine derivatives, *Chin. J. Energet. Mater.*, 2013, **21**, 668–674.

239 H. Gao and J. M. Shreeve, Azole-based energetic salts, *Chem. Rev.*, 2011, **111**, 7377–7436.

240 U. R. Nair, S. N. Asthana, A. S. Rao and B. R. Gandhe, Advances in high energy materials, *Defense Sci. J.*, 2010, **60**, 137–151.

241 V. P. Sinditskii, V. Y. Egorshev, V. V. Serushkin, A. I. Levshenkov, M. V. Berezin, S. A. Filatov and S. P. Smirnov, Evaluation of decomposition kinetics of energetic materials in the combustion wave, *Thermochim. Acta*, 2009, **496**, 1–12.

242 M. B. Talawar, R. Sivabalan, T. Mukundan, H. Muthurajan, A. K. Sikder, B. R. Gandhe and A. S. Rao, Environmentally compatible next generation green energetic materials GEMs, *J. Hazard. Mater.*, 2009, **161**, 589–607.

243 O. P. Korobeinichev, A. A. Paletskii and E. N. Volkov, Flame structure and combustion chemistry of energetic materials, *Russ. J. Phys. Chem. B*, 2008, **2**, 206–228.

244 M. W. Beckstead, K. Puduppakkam, P. Thakre and V. Yang, Modeling of combustion and ignition of solid-propellant ingredients, *Prog. Energy Combust. Sci.*, 2007, **33**, 497–551.

245 S. Zeman, Q.-L. Yan and M. Vlcek, Recent advances in the study of the initiation of energetic materials using characteristics of their thermal decomposition, Part I. cyclic nitramines, *Cent. Eur. J. Energ. Mater.*, 2014, **112**, 173–189.

246 S. Zeman, Q.-L. Yan and A. Elbeih, Recent Advances in the study of the initiation of energetic materials using the characteristics of their thermal decomposition, Part II. Using simple differential thermal analysis, *Cent. Eur. J. Energ. Mater.*, 2014, **113**, 285–294.

247 Q.-L. Yan, S. Zeman, J.-G. Zhang, P. He, T. Musil and M. Bartošková, Multi-stage decomposition of 5-aminotetrazole derivatives kinetics and reaction channels for the rate-limiting steps, *Phys. Chem. Chem. Phys.*, 2014, **16**, 24282–24291.

248 G.-Y. Zeng, C.-M. Lin and J.-H. Zhou, Influences of Carbon Nanotubes on the Thermal Decomposition Behavior of HMX, *Chin. J. Explos. Propellants*, 2012, **356**, 55–57.

249 Yu Xian-feng, The effect of carbon nanotubes on the thermal decomposition of CL-20, *Chin. J. Explos. Propellants*, 2004, **273**, 78–80.

250 W. Zhang, M.-M. Li and J. Li, Effect of carbon nanotubes on thermal decomposition of aminomitrobenzodifuroxan, *J. Combus.t Sci. Tech.*, 2004, **101**, 92–95.

251 K.-Z. Gu, X.-D. Li and R.-J. Yang, Catalytic action on combustion and thermal decomposition of AP with CNTs, *Chin. J. Explos. Propellants*, 2006, **291**, 48–51.

252 L.-X. Wang, Z.-B. Wu, X.-L. Tuo, H.-T. Zou, J. Xu, C.-H. Yi and W.-L. Xu, Theoretical study on thermal decomposition of nitromethane confined inside an armchair 5, 5, single-wall carbon nanotube, *Chin. J. Energet. Mater.*, 2009, **17**(5), 518–522.

253 L. Wang, J. Xu, C. Yi, H. Zou and W. Xu, Theoretical study on the thermal decomposition of nitromethane encapsulated inside single-walled carbon nanotubes, *J. Mol. Struct.: THEOCHEM*, 2010, **940**, 76–81.

254 L. Wang, C. Yi, H. Zou, J. Xu and W. Xu, Rearrangement and thermal decomposition of nitromethane confined inside an armchair 5, 5, single-walled carbon nanotube, *Chem. Phys.*, 2010, **367**, 120–126.

255 L. Wang, H. Zou, C. Yi, J. Xu and W. Xu, Finite-Length Effect of Carbon Nanotubes on the Encapsulation and Decomposition of Nitromethane ONIOM Calculation, *Curr. Nanosci.*, 2011, **7**, 1054–1060.

256 L. Wang, C. Yi, H. Zou, J. Xu and W. Xu, On the isomerization and dissociation of nitramide encapsulated inside an armchair 5,5, single-walled carbon nanotube, *Mater. Chem. Phys.*, 2011, **127**, 232–238.

257 S. Reshmi, K. B. Catherine and C. P. Reghunadhan Nair, Effect of carbon nanotube on the thermal decomposition characteristics of selected propellant binders and oxidisers, *Int. J. Nanotechnol.*, 2011, **8**, 979–987.

258 X.-D. Li and R.-J. Yang, Combustion and thermal decomposition of ammonium dinitramide catalyzed by carbon nanotubes, *New Carbon Mater.*, 2010, **25**, 444–448.

259 N. Li, M. Cao and Q. Wu, A facile one-step method to produce Ni/graphenenanocomposites and their application to the thermal decomposition of ammonium perchlorate, *CrystEngComm*, 2012, **142**, 428–434.
260 N. Li, Z. Geng and M. Cao, Well-dispersed ultrafine Mn_3O_4 nanoparticles on graphene as a promising catalyst for the thermal decomposition of ammonium perchlorate, *Carbon*, 2013, **54**, 124–132.
261 J. Zhu, G. Zeng and F. Nie, Decorating graphene oxide with CuO nanoparticles in a water-isopropanol system, *Nanoscale*, 2010, **26**, 988–994.
262 W. Zhang, Q. Luo, X. Duan, *et al.*, Nitrated graphene oxide and its catalytic activity in thermal decomposition of ammonium perchlorate, *Mater. Res. Bull.*, 2014, **50**, 73–78.
263 Y.-I. Izato, A. Miyake and H. Echigoya, Influence of the physical properties of carbon on the thermal decomposition behavior of ammonium nitrate and carbon mixtures, *Sci. Technol. Energ. Mater.*, 2009, **70**, 101–104.
264 A. Miyake and Y.-I. Izato, Thermal decomposition behaviors of ammonium nitrate and carbon mixtures, *Int. J. Energ. Mater. Chem. Propul.*, 2010, **9**, 523–531.
265 L. Yu, H. Ren, X.-Y. Guo, X.-B. Jiang and Q.-J. Jiao, A novel ε-HNIW-based insensitive high explosive incorporated with reduced graphene oxide, *J.Therm Anal Calorim*, 2014, **117**, 1187–1199.
266 V. V. Chaban, E. E. Fileti and O. V. Prezhdo, Buckybom, reactive molecular dynamics simulation, *J. Phys. Chem. Lett.*, 2015, **6**, 913–917.
267 H. Fazhoğlu and J. Hacaloğlu, The effect of triethanolamine on thermal decomposition of GAP, *J. Macromol. Sci., Part A: Pure Appl.Chem.*, 2002, **7**, 759–768.
268 H. Fazlıoğlu and J. Hacaloğlu, Thermal decomposition of glycidyl azide polymer by direct insertion probe mass spectrometry, *J. Anal. Appl. Pyrolysis*, 2002, **2**, 327–338.
269 B. Jin, J. Shen, R. F. Peng, Y. J. Shu, B. S. Tan, S. J. Chu and H. S. Dong, Synthesis, characterization, thermal stability and sensitivity properties of the new energetic polymer through the azidoacetylation of polyvinyl alcohol, *Polym. Degrad. Stab.*, 2012, **4**, 473–480.
270 I. Levin and D. Brandon, Thermodynamic stability of Metastable alumina polymorphs crystal structures and transition sequences, *J. Am. Ceram. Soc.*, 1998, **81**, 1995–2012.
271 L. Jeurgens, W. Sloof, F. Tichelaar and E. Mittemeijer, Amorphous oxidefilms on metals application to aluminum oxide films on aluminum substrates, *Phys. Rev. B: Condens. Matter*, 2000, **62**, 4707–4719.
272 L. Ren, E. Chu, G. Zhang, Y. Bai, C. Shi and L. Sun, Development discussion on metrology of initiators and pyrotechnics, Proceedings - 4th International Conference on Computational and Information Sciences, ICCIS, 2012, 6300819, pp. 1120–1122.
273 P. Zhu, X. Zhou, R.-Q. Shen, Y.-H. Ye and Y. Hu, Electrical-explosion performance of dielectric structure pyrotechnic initiators prepared by Al/CuO reactive multilayer films, *Chin. J. Energet. Mater.*, 2011, **19**, 366–369.
274 P. Zhu, R. Shen, N. N. Fiadosenka, Y. Ye and Y. Hu, Dielectric structure pyrotechnic initiator realized by integrating Ti/CuO-based reactive multilayer films, *J. Appl. Phys.*, 2011, **109**, 084523.
275 T. J. Hinkel and F. Salazar, Material properties effects on pyrotechnic initiator output, 44th AIAA/ASME/SAE/ASEE Joint Propulsion Conference and Exhibit, 2008.
276 M. R. Manaa, A. R. Mitchell, P. G. Garza, P. F. Pagoria and B. E. Watkins, Flash ignition and initiation of explosives-nanotubes mixture, *J. Am. Chem. Soc.*, 2005, **127**, 13786–13787.
277 K. Kappagantula, M. L. Pantoy and E. M. Hunt, Impact ignition of aluminum-teflon based energetic materials impregnated with nano-structured carbon additives, *J. Appl. Phys.*, 2012, **112**, 024902.
278 K. Kappagantula and M. L. Pantoya, Experimentally measured thermal transport properties of aluminum-polytetrafluoroethylene nanocomposites with graphene and carbon nanotube additives, *Int. J. Heat Mass Transfer*, 2012, **55**, 817–824.
279 W. Hong and N. Tai, Investigations on the thermal conductivity of composites reinforced with carbon nanotubes, *Diamond Relat. Mater.*, 2008, **17**, 1577–1581.
280 J. H. Kim, J. Y. Ahn, H. S. Park and S. H. Kim, Optical ignition of nanoenergetic materials: the role of single-walled carbon nanotubes as potential optical igniters, *Combust. Flame*, 2013, **160**, 830–834.
281 E. S. Collins, B. R. Skelton, M. L. Pantoya, F. Irin, M. J. Green and M. A. Daniels, Ignition sensitivity and electrical conductivity of an aluminum fluoropolymer reactive material with carbon nanofillers, *Combust. Flame*, 2015, **162**, 1417–1421.
282 J. H. Kim, S. B. Kim, M. G. Choi, D. H. Kim, K. T. Kim, H. M. Lee, H. W. Lee, J. M. Kim and S. H. Kim, Flash-ignitable nanoenergetic materials with tunable underwater explosion reactivity: the role of sea urchin-like carbon nanotubes, *Combust. Flame*, 2015, **162**, 1448–1454.
283 Y.-L. Wang, Z.-X. Wei and L. Kang, Progress on combustion catalysts of solid propellant, *Chin. J. Energet. Mater.*, 2015, **23**, 89–98.
284 Y.-P. Chai and T.-L. Zhang, Advances on burning rate catalyzer of composite solid propellant at home and abroad, *J. Solid Rocket Technol.*, 2007, **30**, 44–47.
285 X. Han and S. Li, Advances in catalytic function of fullerene materials, *Prog. Chem.*, 2006, **18**, 715–720.
286 J. T. Abrahamson, N. Nair and M. S. Strano, Modelling the increase in anisotropic reaction rates in metal nanoparticle oxidation using carbon nanotubes as thermal conduits, *Nanotechnol.*, 2008, **19**, 195701.
287 J. L. Sabourin, D. M. Dabbs, R. A. Yetter, F. L. Dryer and I. A. Aksay, Functionalized graphene sheet colloids for enhanced fuel/propellant combustion, *ACS Nano*, 2009, **3**, 3945–3954.

288 X. Han, T. F. Wang, Z. K. Lin, D. L. Han, S. F. Li, F. Q. Zhao and L. Y. Zhang, RDX/AP-CMDB Propellants Containing Fullerenes and Carbon Black Additives, *Def. Sci. J.*, 2009, **59**, 284–293.

289 C. Bice Charles, Propellants with improved burning rate, *US patent*, US3018204A, 1962.

290 K. Ives Edwin, Catalyzed propellant compositions of high burning rate, *US patent*, US3240640A, 1966.

291 S. Verma and P. A. Ramakrishna, Activated charcoal A novel burn rate enhancer of aluminized composite propellants, *Combust. Flame*, 2010, **157**, 1202–1210.

292 S. Verma and P. A. Ramakrishna, Investigations on activated charcoal, a burn-rate enhancer in composite solid propellant, *J. Propul. Power*, 2013, **295**, 1214–1219.

293 X. D. Li, R.-J. Yang and X.-X. Li, The functional additveis CNTs, conference paper in Propellants Explos. Proced., Xi'an Modern Chemistry Research Institute, 2004, pp. 228–231.

294 R.-Z. Hu; Y. Wang; and J. Zheng, The application of nanosized materials in solid propellants, The, 24th annual conference in Professional Committee of solid rocket propellant of Chinese Society of Astronautics, Xiang Fan, China, 2003, pp. 144–149.

295 F.-Q. Zhao and J.-H. Yi, Preparation method of Cu_2O-PbO/GO composites, *Chinese patent*, CN1003007947A, 2013.

296 Q.-L. Tan, W.-L. Hong and X.-B. Xiao, Preparation of Bi_2O_3/GO and its combustion catalytic performance on double-base propellant, *Nanosci. Nanotechnol.*, 2013, **106**, 22–27.

297 W.-L. Hong, H.-B. Shi and F.-Q. Zhao, Preparation method of Cu_2O-Bi_2O_3/GO composites, *Chinese patent*, CN102895979A, 2013.

298 W.-L. Hong, Y.-F. Xue and F.-Q. Zhao, Preparation of Bi_2O_3/CNTs Composite and Its Combustion Catalytic Effecton Double-base Propellant, *Chin. J. Explos. Propellants*, 2012, **6**, 7–11.

299 W.-L. Hong, X.-Y. Zhu and F.-Q. Zhao, Preparation of CuO/CNTs and its combustion catalytic activity on double-base propellant, *Chin. J. Explos. Propellants*, 2010, **336**, 83–86.

300 J.-H. Liu, W. L. Hong and X.-Y. Zhu, A preparation method for Cu-Bi/CNTs composite coated by carbon particles, *Chinese patent*, CN101757927A, 2010.

301 Y. Liu, W. Jiang and J.-X. Liu, A study of catalyzing thermal decomposition and combustion of AP/HTPB propellant with nano Cu/CNTs, *Acta Armamentarii*, 2008, **299**, 1029–1033.

302 X.-J. Zhang, W. Jiang, D. Song and J.-X. Liu, Preparation and catalytic activity of Ni/CNTs nanocomposites using microwave irradiation heating method, *Mater. Lett.*, 2008, **621**, 2343–2346.

303 F. Li, W. Jiang, X. Guo, L. Liu, M. Li, W. Chen and S. Wu, Application of nanometer materials for solid propellants, *Int. J. Energ. Mater. Chem. Propul.*, 2011, **10**, 67–83.

304 C. D. Malec, N. H. Voelcker, J. G. Shapter and A. V. Ellis, Carbon nanotubes initiate the explosion of porous silicon, *Mater. Lett.*, 2010, **64**, 2517–2519.

305 K. S. Martirosyan, L. Wang and D. Luss, Tuning the gas pressure discharge of nanoenergetic materials by boron and carbon nanotubes additives, Technical Proceedings of the, 2011 NSTI Nanotechnology Conference and Expo, *NSTI-Nanotech*, 2011, **1**, 323–326.

306 Z. Doorenbos, L. Groven, C. Haines, D. Kapoor and J. Puszynski, Novel pyrophoric substrates with a tunable energetic output, AIChE Annual Meeting, Conference Proceedings, 2010.

307 M. R. Manaa, A. R. Mitchell, P. G. Garza, P. F. Pagoria and B. E. Watkins, Flash ignition and initiation of explosives-nanotubes mixture, *J. Am. Chem. Soc.*, 2005, **127**, 13786.

308 C. Zhang, Y. Wen and X. Xue, Self-enhanced catalytic activities of functionalized graphene sheets in the combustion of nitromethane Molecular dynamic simulations by molecular reactive force field, *ACS Appl. Mater. Interfaces*, 2014, **6**, 12235.

309 X. Xiang, S.-B. Xiang, Z. Wang, X. Wang and G. Hua, Photo-responsive behaviors and structural evolution of carbon-nanotube-supported energetic materials under a photoflash, *Mater. Lett.*, 2012, **88**, 27–29.

310 B. Jin, R. Peng, F. Zhao, J. Yi, S. Xu, S. Wang and S. Chu, Combustion effects of nitrofulleropyrrolidine on RDX-CMDB propellants, *Propellants, Explos., Pyrotech.*, 2014, **39**, 874–880.

311 M. Huagn and B.-S. Tan, Some strategies on the stabilization of high-energy explosives, *Chin. J. Energet. Mater.*, 2014, **22**, 134–135.

312 T. Lee, J. W. Chen, H. L. Lee, T. Y. Lin, Y. C. Tsai, S.-L. Cheng, S.-W. Lee, J.-C. Hu and L.-T. Chen, Stabilization and spheroidization of ammonium nitrate Co-crystallization with crown ethers and spherical crystallization by solvent screening, *Chem. Eng. J.*, 2013, **225**, 809–817.

313 A. J. Lang and S. Vyazovkin, Phase and thermal stabilization of ammonium nitrate in the form of PVP-AN glass, *Mater. Lett.*, 2008, **62**, 1757–1760.

314 Z. Zhang, B. Wang, Y. Ji, Z. Liu and Q. Liu, Thermal Stabilization of Ammonium Dinitramide ADN, Proceedings of the, International Autumn Seminar on Propellants, Explosives and Pyrotechnics, IASPEP, *Theory Practice Energet. Mater.*, 2003, **5**, 259–262.

315 M. Smeu, F. Zahid, W. Ji, H. Guo, M. Jaidann and H. Abou-Rachid, Energetic molecules encapsulated inside carbon nanotubes and between graphene layers DFT calculations, *J. Phys. Chem. C*, 2011, **115**, 10985–10989.

316 H. Abou-Rachid, A. Hu, V. Timoshevskii, Y. Song and L.-S. Lussier, Nanoscale high energetic materials: A polymeric nitrogen chain N_8 confined inside a carbon nanotube, *Phys. Rev. Lett.*, 2008, **100**, 196401.

317 W. Ji, V. Timoshevskii, H. Guo, H. Abou-Rachid and L. Lussier, Thermal stability and formation barrier of a high-energetic material N_8 polymer nitrogen encapsulated in 5,5, carbon nanotube, *Appl. Phys. Lett.*, 2009, **95**, 021904.

318 Y. Liu, W. Lai, T. Yu, Z. Ge and Y. Kang, Structural characteristics of liquid nitromethane at the nanoscale confinement in carbon nanotubes, *J. Mol. Model.*, 2014, **20**, 8.

319 E. M. Benchafia, C. Yu, M. Sosnowski, N. M. Ravindra and Z. Iqbal, Plasma synthesis of nitrogen clusters on carbon nanotube sheets, *JOM*, 2014, **66**, 608–615.

320 Z. Wu, E. M. Benchafia, Z. Iqbal and X. Wang, N_8 polynitrogen stabilized on multi-wall carbon nanotubes for oxygen-reduction reactions at ambient conditions, *Angew. Chem., Int. Ed.*, 2014, **53**, 12555–12559.

321 Q.-L. Yan and S. Zeman, Theoretical evaluation of sensitivity and thermal stability for high explosives based on quantum chemistry methods a brief review, *Int. J. Quantum Chem.*, 2013, **113**, 1049–1061.

322 A. K. Pandey, Damage prediction of RC containment shell under impact and blast loading, *Struct. Eng. Mech.*, 2010, **366**, 729–744.

323 P. A. Urtiew and C. M. Tarver, Shock initiation of energetic materials at different initial temperatures review, *Combust., Explos. Shock Waves*, 2005, **416**, 766–776.

324 M. H. Keshavarz, Overview on theoretical prediction of 3,6-bis-3,5-dinitro-1,2,4-triazolyl'-1,2,4,5-tetrazine as a high performance explosive, *Chin. J. Energet. Mater.*, 2007, **155**, 551–554.

325 S. M. Walley, J. E. Field and M. W. Greenaway, Crystal sensitivities of energetic materials a review, *Mater. Sci. Technol.*, 2006, **22**, 402–413.

326 C. J. Wu, T. Piggott, J. Yoh and J. Reaugh, Numerical Modeling of Impact Initiation of High Explosives, UCRL-TR-221760, June 1, 2006.

327 B. Jin, R. Peng, S. Chu, Y. Huang and R. Wang, Study of the desensitizing effect of different [60]fullerene crystals on cyclotetramethylene tetranitramine HMX, *Propellants, Explos., Pyrotech.*, 2008, **33**, 454–458.

328 I. G. Assovskiy, Metallized SWCNT-promising way to low sensitive high energetic nanocomposites, *Propellants, Explos., Pyrotech.*, 2008, **33**, 51–54.

329 J. Xu, L.-Z. Wu, R.-Q. Shen, Y.-H. Ye and Y. Hu, Effects of dopants and confined windows on laser initiation sensitivity of explosives, *Chin. J. Explos. Propellants*, 2011, **34**, 77–79.

330 B. Siegert, M. Comet, O. Muller, G. Pourroy and D. Spitzer, Reduced-sensitivity nanothermites containing manganese oxide filled carbon nanofibers, *J. Phys. Chem. C*, 2010, **114**, 19562–19568.

331 T. Zecheru, T. Rotariu, L.-C. Matache, A.-C. Sava, R.-M. Lungu, A. Voicu and L. Cosereanu, Synthesis and applications of 3-nitro-1,2,4-triazol-5-one based hybrid energetic compositions, *Rev. Chim.*, 2014, **65**, 1186–1189.

332 H. Xu, J. Guo and K. S. Suslick, Porous carbon spheres from energetic carbon precursors using ultrasonic spray pyrolysis, *Adv. Materials*, 2012, **24**, 6028–6033.